COMPARISON OF DIRECT AND SUPERPOSITION METHODS OF THE COUPLED HORIZONTAL AND ROCKING VIBRATION OF BLOCK MACHINE FOUNDATIONS

By:

Sofonias Mekdememariam Awlachew

2019

Addis Ababa, Ethiopia

ADDIS ABABA UNIVERSITY
ADDIS ABABA INSTITUTE OF TECHNOLOGY
SCHOOL OF CIVIL AND ENVIRONMENTAL ENGINEERING

COMPARISON OF DIRECT AND SUPERPOSITION METHODS OF THE COUPLED HORIZONTAL AND ROCKING VIBRATION OF BLOCK MACHINE FOUNDATIONS

By:

Sofonias Mekdememariam Awlachew

Advisor: **Dr.-Ing Asrat Worku**

A Thesis Submitted to Addis Ababa Institute of Technology in partial fulfillment of the requirements for the Degree of Master of Science in Geotechnical Engineering

2019

Addis Ababa, Ethiopia

The undersigned have examined the thesis entitled '**Comparison of Direct and Superposition Methods of the Coupled Horizontal and Rocking Vibration of Block Machine Foundations**' presented by **Sofonias Mekdememariam**, a candidate for the degree of Master of Science and hereby certify that it is worthy of acceptance.

_____	_____	_____
Advisor	Signature	Date
_____	_____	_____
External Examiner	Signature	Date
_____	_____	_____
Internal Examiner	Signature	Date
_____	_____	_____
Chairman	Signature	Date

DECLARATION

I hereby declare that the research work titled **"Comparison of Direct and Superposition Methods of the Coupled Horizontal and Rocking Vibration of Block Machine Foundations**" is my own work. The work has not been presented elsewhere for assessment. Where material has been used from other sources, it has been properly acknowledged. Due references have been provided on all supporting literatures and resources.

Name: Sofonias M/Mariam

Signature: _____

Advisor: Asrat Worku (Dr-Ing)

Signature: _____

ACKNOWLEDGEMENT

I would like to express my gratitude to my advisor, Dr-Ing. Asrat Worku for the useful comments, remarks and engagement through the learning process of this thesis. He consistently allowed this paper to be my own work, but steered me in the right direction whenever he thought I needed it.

Secondly, I would like to give thanks Ethiopian Roads Authority (ERA) scholarship support in Master's program in Addis Ababa Institute of Technology.

Finally, I must express my very profound gratitude to my family and friends especially to my mother Negedework Shenkut for providing me with unfailing support and continuous encouragement throughout my years of study and through the process of researching and writing this thesis. This accomplishment would not have been possible without them. Thank you

TABLE OF CONTENTS

LIST OF FIGURES

LIST OF TABLES

LIST OF SYMBOLS AND ABBREVATION

a_o=dimensionless frequency factor

ß=internal damping

2B=width of footing base

C_h=damping coefficient of base in sliding

C_r=damping coefficient of base in rocking

d=effective contact height

e=eccentricity of rotating mass, void ratio

eW_e =eccentric moment

Exp=experimental value

ξ = Damping ratio

G_{max}=dynamic shear modulus

g= acceleration of gravity

g_o=w_e= weight of rotating mass

H=height of footing

I_x, Iy, Iz= mass moment of inertia about x, y, z axes respectively

K_h=stiffness coefficient of base in sliding

K_r=stiffness coefficient of base in rocking

2L=length of the footing base

m=total mass of footing and machine.

OCR=over consolidation Ratio

θo =Angular amplitude

Uo=Horizontal amplitude

ω_n =natural circular frequency

$\bar{\omega}$=excitation circular frequency

V_{La} =Lysmer's analog wave velocity

Vs=shear wave velocity

ω/ω_n = frequency ratio

ABSTRACT

The analysis and design of machine foundation requires more attention since it involves both the static loads and the dynamic loads caused by the machine. The response of such foundation under machine induced vibration depends on several parameters such as the shape and size of the foundation, depth of embedment, static load, dynamic excitation frequency, and other geotechnical parameters.

The main objective of this study focuses on the sensitivity and comparative study of coupled horizontal and rocking vibration of block machine foundation by applying a direct approach which directly considers the combined effect of force and moment without simplifications. This direct approach is compared with a superposition method which uses simple superposition of the separate action of the force and the moment. In both methods impedance functions are utilized by making use of compiled closed form expressions and dimensionless graphs for the purpose of determining frequency dependent dynamic stiffness and dashpot coefficients.

Theoretical results are also validated by comparing results from existing experimental investigations on field test. The comparison showed an encouraging agreement in the case of surface foundation for prediction of natural frequency. Furthermore, a sensitivity study has been conducted on reciprocating compressors based on the dynamic response of surface and embedded block foundations for different aspect ratio under coupled mode of vibration for different embedment ratio for clay, gravel and sand. The results indicate that as the embedment depth increases, the resonant amplitude decreases and resonant frequency increases. In the case of the damped natural frequency when the aspect ratio increases horizontal and angular amplitude increase and damping ratio decreases. On the other hand, in the case of the undamped natural frequency horizontal amplitude, angular amplitude and frequency ratio decrease.

1 INTRODUCTION

1.1 BACKGROUND

Machine foundations are structures below a machine, which are used to support, protect, and guarantee the functionality of the machine from any disturbances. These special types of foundations are required for machines, machine tools and heavy equipment that have wide range of speeds, loads and operating conditions. Thus, these foundations are designed considering the shocks and vibrations (dynamic forces) resulting from operation of machines.

Two types of loads must be considered in the analysis of such foundations namely: dynamic and static. Static loads are principally a function of the weights of the foundation, machine and all its auxiliary equipment. Dynamic loads, which occur during the operation of the machine, result from forces generated by unbalance, inertia of moving parts, or both, and by the flow of fluid and gases for some machines. The magnitude of these dynamic loads primarily depends upon the machine's operating speed and the type, size, weight, and arrangement (position) of moving parts within the casing.

The basic goal in the design of a machine foundation is to limit its motion to amplitudes that neither endanger the satisfactory operation of the machine nor disturb people working in the immediate vicinity (Gazetas G. , 1983).

Satisfactory design of a machine foundation needs information on soil profile, depth of different layers, physical properties of soil and ground water level. Geotechnical properties, such as Poisson's ratio, dynamic shear modulus, and damping, are generally required. The values are usually obtained either from field and laboratory tests or from theoretical correlation with other engineering soil parameters. (ACI, 2011)

Design methods ranging from simple to complex, have been suggested to solve the problem of vibrating foundations. Selecting which method to use for analysis and design of machine foundations requires good understanding of their dynamic behaviour.

Allowable amplitudes depend on the speed, location, and criticality or function of the machine. Other limiting dynamic criteria affecting the design may include avoiding resonance and excessive transmissibility to the supporting soil or structure. Thus, a key ingredient to a successful design is the careful engineering analysis of the soil-foundation response to dynamic loads from the machine operation.

In general a block foundation has six degrees of freedom (three translational, and three rotational) and a set of six simultaneous equations is required for the complete analysis of the response of the foundation. The vertical vibration and rotation about a vertical axis (torsion) are uncoupled motions, while horizontal translation and rotation about a horizontal axis (rocking) usually occur as a coupled motion. For pure horizontal translation and pure rocking to occur, the existence of constraints is implicitly assumed thus eliminating other components of the motion; and it is to be noted that the vibrations of a very flat footing excited horizontally may approximate to pure horizontal translation and the vibration of a very tall footing excited horizontally may approximate to pure rocking (Beredugo, 1971) Most of the time coupled horizontal and rocking vibration occur concurrently.

1.2 OBJECTIVE

1.2.1 General Objective

The main objective of this study focuses on the sensitivity and comparative study of coupled horizontal and rocking vibration of block machine foundation to estimate angular and horizontal amplitudes by applying direct method (Worku, 2016) which directly considers the combined effect of the horizontal force and moment without simplifications. The direct method is compared with a superposition approach (Prakash and Kumar, 1995) which uses simple superposition of the separate action of the force and the moment. Moreover, a sensitivity study is conducted to study which parameter affect the block machine foundation response the most.

1.2.2 Specific Objective

The specific objective of this paper is to compare coupled horizontal and rocking vibration of block machine foundation in different scenarios. These include

i. The foundation is with or without embedment,
ii. Foundation having different aspect ratio.

1.3 SCOPE OF THE STUDY

The study is limited to the investigation of coupled horizontal and rocking vibration of block machine foundation in response to harmonic loading. The soil is considered to be a homogenous, isotropic, linearly elastic semi-infinite medium (the elastic half space).

2 REVIEW OF LITERATURE

2.1 MACHINE FOUNDATIONS

In the past, machine foundations were frequently designed by rules of thumb without any analysis of the expected vibration amplitudes. For instance, one such design rule called for a massive concrete foundation of a total weight equal to at least three to five times the weight of the supported machine(s). Although such a proposition may at first glance seem logical, it is in fact an obsolete one since it ignores the effect on the motion of all the other variables of the problem (e.g. Type of excitation, nature of supporting soil, and so on). For one thing, increasing the mass of a foundation decreases the resonant frequency of the system and, perhaps more importantly, reduces its effective damping. Obviously, this is not what those applying the rule had in mind (Gazetas G. , 1983). Modern methods of analysis of foundation oscillations attempt to rationally account for the dynamic interaction between the foundation and the supporting soil.

The vibrations of block foundations on a flexible soils is a typical dynamic soil-structure-interaction problem, the study of which underwent a remarkable historical development.

Lamb (1904) analyzed the problem of vibration of a single vibrating force acting at a point on the surface of an elastic half-space. His work is also the cornerstone of theoretical solutions developed from the assumption of an oscillator resting on elastic half space. The study included cases in which the oscillating force Q acts in the vertical and horizontal direction, as shown in Figure 2.1 it is generally referred to as the *dynamic Boussinesq problem*.

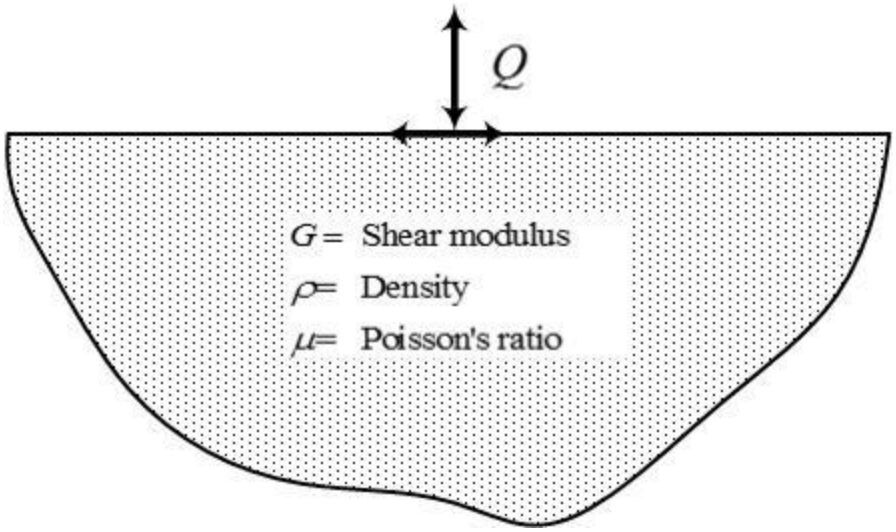

Figure 2.1 Vibrating force Q acting in vertical and horizontal direction on the surface of an elastic half-space

The Deutsche Forschungsgeselschaft fiir Bodenmechanik (DEGEBO) (1930s) carried out experimental studies to investigate the dynamic soil properties by using mechanical oscillators.

Reissner (1936) studied the problem of vibration of a uniformly loaded flexible circular area resting on an elastic half-space. The solution was obtained by integration of Lamb's solution for a point load. Based on Reissner's work, the vertical displacement at the center of the flexible loaded area in Figure 2.2 can be given by:

$$z(t)=\frac{Q_o e^{i\omega t}}{Gr_o}(f_1+if_2) \qquad (2.1)$$

Where, Q_o = amplitude of the exciting force acting on the foundation

$z(t)$ = vertical displacement at the center of the loaded area at time t

ω = circular frequency of the applied load

r_o = radius of the loaded area

G = shear modulus of the soil

Q = exciting force, with the amplitude of Q_o

f_1, f_2 = Reissner's displacement functions

The displacement functions f_1 and f_2 are related to the Poisson's ratio of the medium and the frequency of the exciting force.

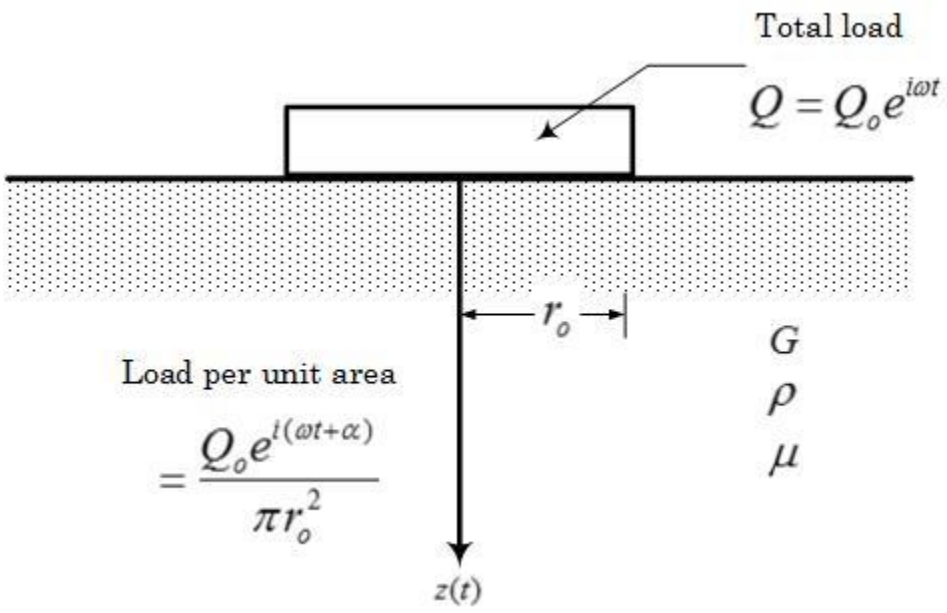

Figure 2.2 Vibration of a uniformly loaded circular flexible area

Using the displacement relation given above and solving the equation of equilibrium of force, Reissner obtained the following relationships:

$$A_z = \frac{Q_o}{Gr_o} * Z \tag{2.2}$$

Where A_z = the amplitude of the vibration

Z = dimensionless amplitude = $\sqrt[2]{\frac{f_1^2 + f_2^2}{(1 - ba_o f_1)^2 + (ba_o^2 f_2)^2}}$

$$b = \frac{m}{\rho r_o^3} = (\frac{W}{g})\left[\frac{1}{(\frac{\gamma}{g}) * r_o^3}\right] = \frac{W}{\gamma r_o^3}$$

b = dimensionless mass ratio

ρ = density of the elastic material

g = unit weight of the elastic material (for this problem, it is soil)

$$a_o = \omega r_o \sqrt{\frac{\rho}{G}} = \frac{\omega r_o}{v_s}$$

a_o = dimensionless frequency parameter

v_s= velocity of shear waves in the elastic material on which the foundation is resting

Reissner's theory established the basis for further analytical studies of oscillating forces on the surface of a half space. His theory, however was not accepted immediately because it did not completely agree with the results from field tests, especially of the DEGEBO experimental studies. Some of the reasons for the disagreement were (Richart et al., 1970)

1) Permanent settlements developed during the tests, violate the assumption of an elastic medium;
2) The assumption of uniformly distributed soil pressure was not realistic; and
3) There was a sign error in Reissner's original derivation, which affected the calculation of f_2 and the computed values of the displacement amplitude. Nevertheless, his contribution has become a classic in the field of soil dynamics.

The work of Reissner was further extended by Quinlan (1953) and Sung (1953). As mentioned before, Reissner's work related only to the case of flexible circular foundations where the soil reaction is uniform over the entire area. Both Quinlan and Sung considered the effects of changes in pressure distribution over the circular area of contact on the surface of the half-space. Quinlan established the equations for oscillating contact pressures which vary across a diameter of the contact area with a parabolic distribution, with a uniform distribution, and with the distribution corresponding to a rigid base. He developed solutions only for the rigid-base case. Sung also established the basic equations for the three pressure distributions and presented solutions for each case.

The distribution of contact pressure q for all three cases may be expressed as follows.

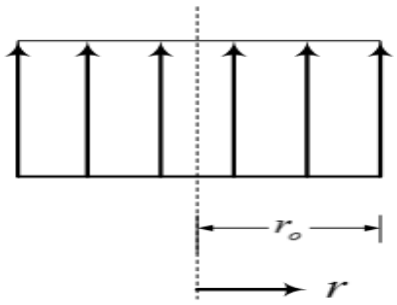

(a) Uniform pressure distribution

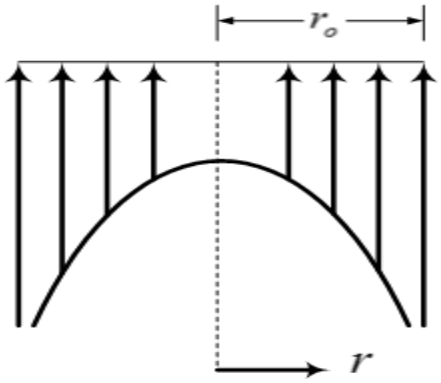

(b) Pressure distribution under rigid foundation

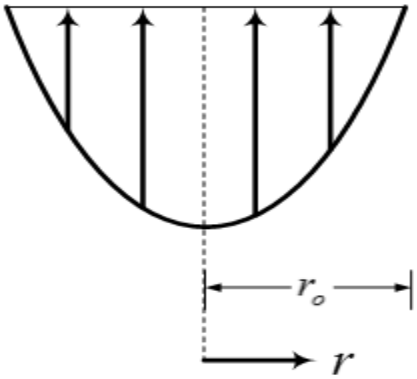

(c) Parabolic pressure distribution

Figure 2.3 Contact pressure distribution under a circular foundation of radius r_0

Where q = contact pressure at a distance r measured from the center of the foundation.

For flexible circular foundations

$$q = \frac{Q_o e^{i(\omega t+\alpha)}}{\pi r_o^{\,2}} (for\ \mathrm{r} \le \mathrm{r_o}) \tag{2.3}$$

For rigid circular foundations

$$q = \frac{Q_o e^{i(\omega t+\alpha)}}{2\pi r_o \sqrt{r_o^{\,2} - r^2}} (for\ \mathrm{r} \le \mathrm{r_o}) \tag{2.4}$$

For foundations with parabolic contact pressure distribution

$$q = \frac{2(r_o^{\,2} - r^2) Q_o e^{i(\omega t+\alpha)}}{\pi r_o^{\,4}} (for\ \mathrm{r} \le \mathrm{r_o}) \tag{2.5}$$

Quinlan derived the equations only for rigid circular foundations, however sung presented the solutions for all the three class described. In Sung's original study, it was assumed that the contact pressure distribution remains the same throughout the range of frequency considered; however, for dynamic loading conditions, the rigid-base pressure distribution does not produce uniform displacement under the foundation.

Bycroft (1956) determined the weighted average of the displacements under a foundation and established improved displacement functions. Also theoretical solutions for foundations subjected to rocking vibration have been presented by Arnold, Bycroft, and Wart burton (1955) and Bycroft (1956). For *rigid circular foundations* (Figure 2.4), the contact pressure can be described by the equation (2.6)

$$q = \frac{3M_{\mathrm{x}} r \cos\alpha}{2\pi r_o^{\,3} \sqrt{r_o^{\,2} - r^2}} e^{i\omega t} \tag{2.6}$$

Where, q = pressure at any point defined by point P on the contact surface

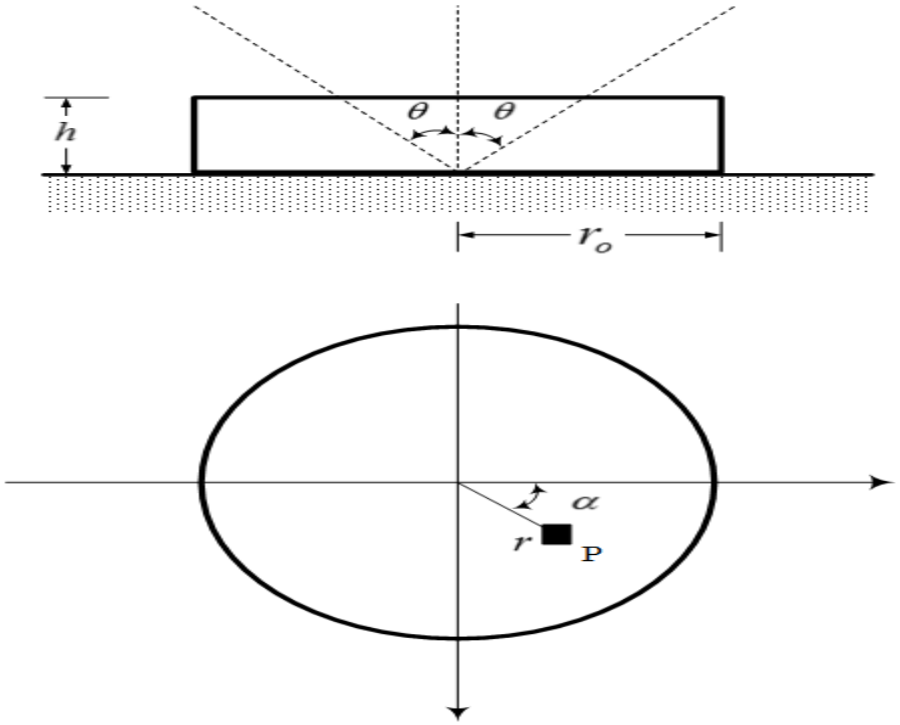

Figure 2.4 Rocking vibration of rigid circular foundation

Hsieh (1962) attempted to modify the original solution of Reissner in order to develop an equation similar to that for damped vibrations of single-degree freedom system. He considered a rigid circular weightless disc on the surface of an elastic half space. The disc is subjected to a vertical vibration by a force $Q = Q_o e^{i\omega t}$.

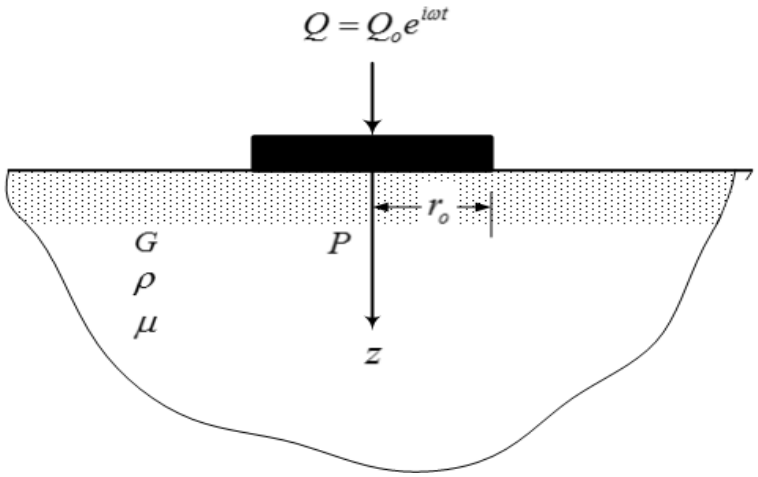

(a)

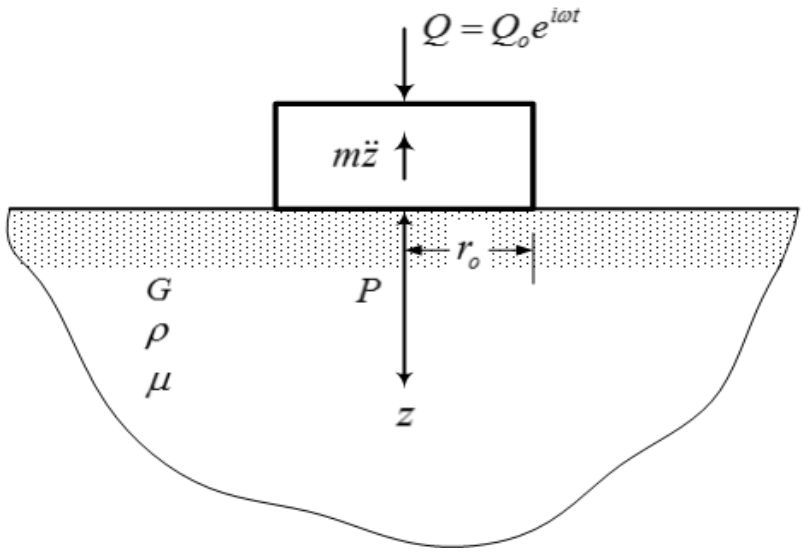

(b)

Figure 2.5 Hsieh's analog

Hsieh also included in his study a description of the frequency dependent damping and spring functions for horizontal oscillation, rocking, and torsional oscillations and showed their use in establishing equations for coupled oscillations.

A simplified model was proposed by Lysmer and Richart (1966), in which the expressions for K_z and C_z were frequency independent. They also redefined the displacement functions in the form

$$F = \frac{f}{\left[\frac{1-\mu}{4}\right]} = \frac{f_1 + if_2}{\left[\frac{1-\mu}{4}\right]} = F_1 + iF_2 \qquad (2.7)$$

Barkan (1962) carried out several field tests to determine soil elastic properties using plate load tests. Barkan used test results to establish charts from which design soil parameters are obtained and used in the dynamic Winkler model to estimate dynamic behavior of the foundation system. The method by Barkan is known as the dynamic subgrade or dynamic Winkler model.

Richart (1962) compiled guidelines for allowable vertical vibration amplitude for a particular frequency of vibration. The procedure for transforming areas of any shape

to an equivalent circle of the same area gives good results in the evaluation of foundation response.

Fry (1963) reported a series of field tests carried out by the U.S Army Corps of Engineers, Waterways Experimental Station, and Vicksburg. The test series included one embedded and other surface footings. The results indicate that embedment decreased the amplitudes and increased the resonant frequencies.

Toshkov (1963) considered the effect of embedment on a forging hammer foundation by assuming it to be hemispherical. He then expressed the radial displacement at any distance from the hemisphere as a simple function of a certain function and the distance. No steady state vibration was considered.

Kaldjian (1967) solved the elasticity problem using the finite element method and showed that embedment increased the vertical spring constant. Kaldjian (1971) later used a similar method to obtain the torsional spring constants of embedded footings.

Baranov (1967) developed a theory for the vibration of an embedded footing under steady state conditions. He formed approximate formulas for dynamic stiffness and damping parameters for use in computing the side reactions due to an embedment in the vertical, horizontal and rocking modes of vibration for a rigid, cylindrical body embedded in an elastic medium.

Hall (1967) developed a mass-spring-dashpot model for rigid circular foundations in the same manner as Lysmer and Richart developed for vertical vibration. According to Hall, the equation of motion for a rocking vibration can be given as in equation 2.8

$$I_o\ddot{\theta}+C_\theta\dot{\theta}+K_\theta\theta = M_x e^{i\omega t} \qquad (2.8)$$

θ =rotation of the vertical axis of the foundation at any time t

I_o = mass moment of inertia about the x axis (through its base)

$$I_o = \frac{W_o}{g}\left(\frac{r_o^2}{4} + \frac{h^2}{3}\right)$$

Where W_o = weight of the foundation

g = acceleration due to gravity

h = height of the foundation

K_θ = static spring constant $= \dfrac{8Gr_o^3}{3(1-\mu)}$

C_θ=dashpot coefficient $= \dfrac{0.8r_o^4\sqrt{G}}{(1-\mu)(1+B_\theta)}$

B_θ=inertia ratio $= \dfrac{3(1\text{-}\mu)I_o}{8\rho r_o^5}$

Chae (1971) carried out small scale model tests of steel footings of various sizes and shapes, embedded in sand. He concluded that embedment reduced the resonant amplitudes but had no effect on the resonant frequencies of vertically excited footings.

Beredugo and Novak (1972) have presented approximate formulas for vertical, horizontal, and rocking vibrations and also developed analytical solutions for embedded footings which predicts the coupled response of embedded footings better than surface footings and they compared theoretical response curves with field experiments. Based on their analysis, they give equation for frequency independent spring constant and dashpot coefficient.

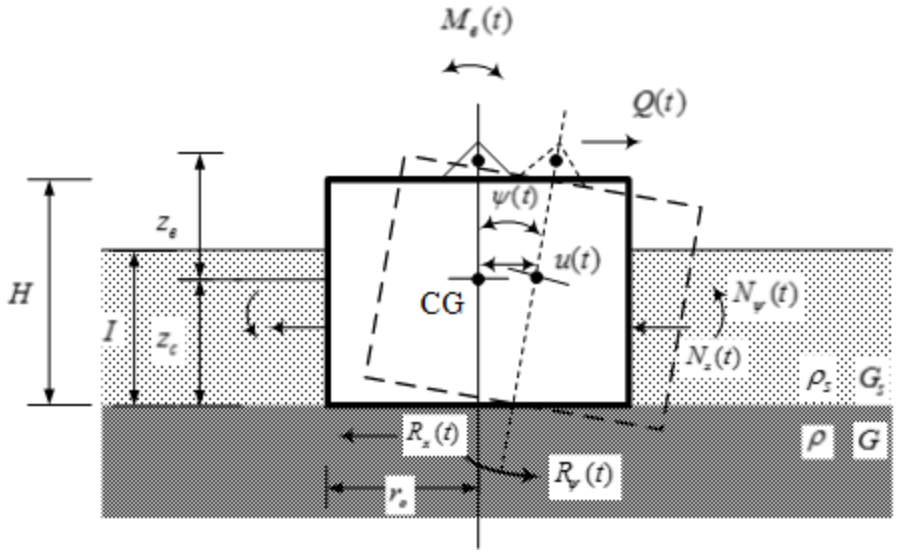

Figure 2.6 Embedded footing in coupled motion (Beredugo and Novak, 1972)

Veletsos and Verbic (1973) developed approximate solutions for the steady state response of a massless, rigid disk, which is supported at the surface of a linear viscoelastic half space and is excited by a harmonically varying horizontal or vertical force, or by a harmonically varying moment. The solution for the massless disk is then applied to the analysis of foundations with mass, and for each mode of excitation, numerical data are presented to illustrate the effects of viscoelastic action on the response of both the massless disk and of foundations with mass by using mathematically equivalent representation of the elastically supported massless disk as a spring-dashpot combination without mass. It is shown that the effective stiffness of the spring may become negative over significant ranges of the exciting frequency, and they recommended that it is preferable to model the disk half-space system as an oscillator with mass, taking its spring constant equal to the static stiffness of the original system.

Dobry, Gazetas and stokoe (1986) conducted experimental verification on twenty one free vibration tests on surface model footings on moist sand having different base shapes and different aspect ratio. The experimental results were obtained from Erden and stoke conducted in 1974 and 1985. Vertical, torsional and coupled swaying and rocking oscillations are considered. Close agreement is found between predicted and

measured frequencies in vertical, torsional and coupled swaying and rocking and also between damping ratios in vertical and torsional vibration. However the analytical method over predicts the measured swaying-rocking damping ratios.

Nii (1987) carried out laboratory experimental tests to determine dynamic stiffness for surface and embedded footings on a half-space made from silicon rubber. The footings, both circular and rectangular, were forced into vertical vibration, and the dynamic stiffnesses were measured by use of a mechanical impedance measurement technique. The dynamic stiffness and damping coefficient obtained from the experimental test data indicated that dynamic stiffness and damping coefficients are frequency dependent.

Gazetas and stokoe (1991) executed comparative studies between theory and experiment for measuring frequency and damping in embedded footings. The experimental results were obtained from Erden and stokoe in 1974 and 1985. Fifty four free vibration tests on model footings embedded at various depths in sand which have different base shapes (circular, rectangular and square).Good agreement is found between theory and experiment for vertical oscillations (in both frequency and damping values) and for swaying and rocking values close value is found only in frequency but measured damping value averages only half the theoretical estimates.

Manyando and Prakash (1991) reanalyzed the data on circular footings they obtained from an experimental result from Fry (1963). They developed a computer program to predict the footing response in vertical, torsional and coupled rocking and sliding vibrations. Their analysis is essentially based on the concept of elastic-half space analogs with modifications made for nonlinearity of soil. Prediction of vertical and coupled rocking and sliding vibrations closely matched the measured data when the material damping is neglected.

Prakash and puri (1988, 2006) and Prakash and Kumar (1995) developed methods of analysis for determining the response of foundations subjected to harmonic vibratory loads with frequency independent foundation parameters using Lysmer analog They developed equations for vibration amplitudes when the force and the moment are acting independently using simple superposition.

Prakash and Nampoothiri (1998) comparative study between theory and experiment for coupled horizontal and rocking response of block foundations have been compared with that from an experimental study carried out by Novak and Beredugo (Beredugo, and Novak, 1972). The computed values do not match the measured response.

Mandal et al.,(2012) conducted experimental investigations to study the effect of 132 model block vibrations tests for different layering and load combination on the dynamic behavior of foundations excited by vertical mode. They recommended that radiation damping of the foundations resting on any two-layered soil underlain by rigid layer can be assumed zero and the resonance frequency of the foundations increases with the increase in thickness of stiff layer at the top, and it decreases with the increase in thickness of soft layer at the top. Resonant frequency increases due to change of position of the stiff layer from the bottom to the top, when total thickness and individual layer thickness being constant.

2.2 MATERIALS PROPERTIES

Foundations that support vibrating equipment experience rigid body displacements. Under the action of unbalanced forces, the rigid block undergoes vertical, lateral, longitudinal, rocking, pitching and yawing oscillations. The cyclic displacement of a foundation can have six possible modes. They are

1. Translation in the vertical direction,
2. Translation in the longitudinal direction,
3. Translation in the lateral direction,
4. Rotation about the vertical axis (that is, yawing or torsion),

5. Rotation about the longitudinal axis (that is, rocking), and

6. Rotation about the lateral axis (that is, pitching).

Translation along the Z axis and rotation about the Z axis occur independently of any other motion. However, translation about the X axis (or Y axis) and rotation about the Y axis (or X axis) are generally coupled motions. The modes of vibration of a rigid block foundation is shown in Figure 2.7.

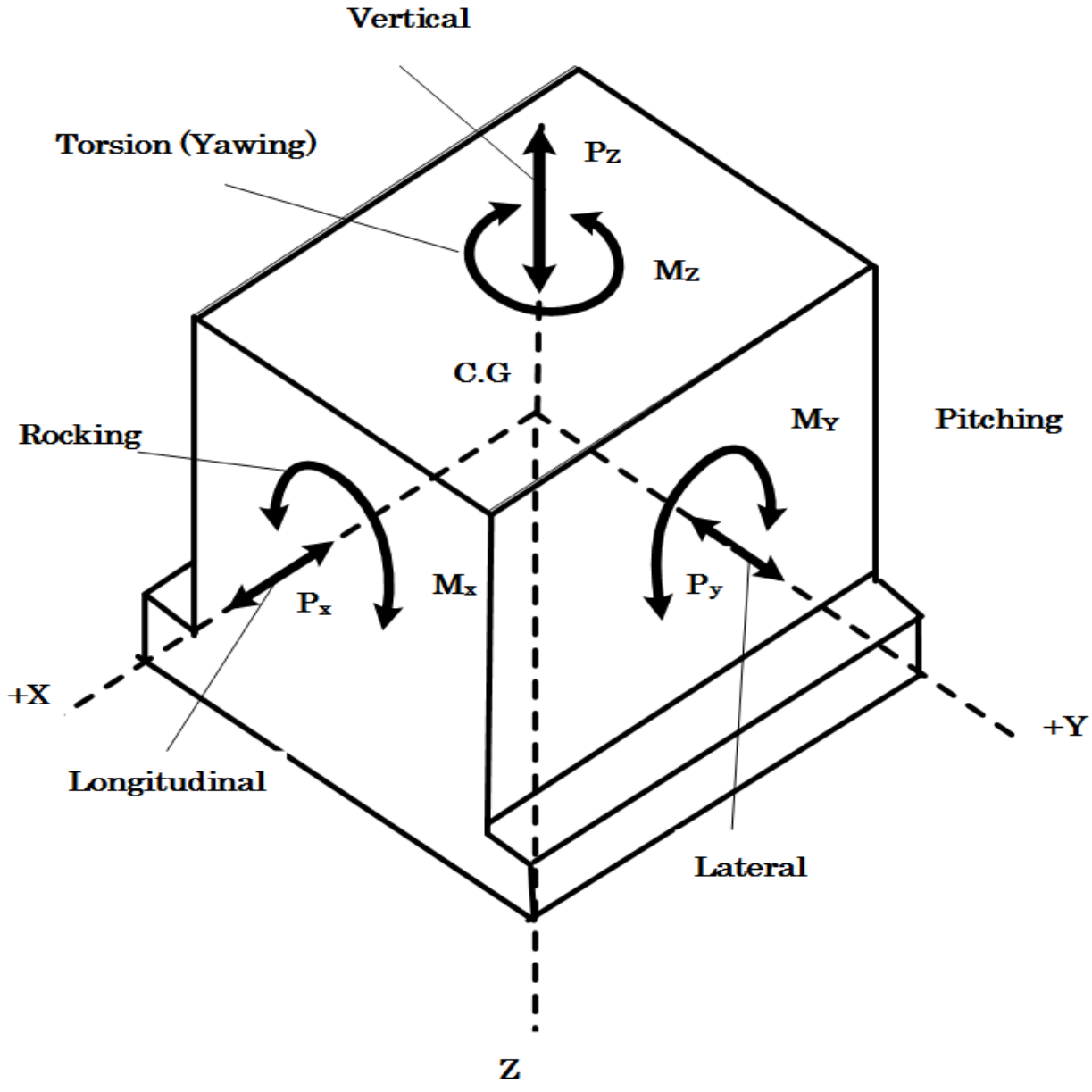

Figure 2.7 Modes of vibration of a rigid block foundation

2.2.1 Dynamic soil properties

For the dynamic analysis of machine foundations, soil properties, such as dynamic shear modulus, Poisson's ratio, density and damping of soil, are generally required. In general, problems involving the dynamic properties of soils are divided into small and large strain amplitude responses. For machine foundations, the amplitudes of dynamic motion, and consequently the strains in the soil, are usually low (strains less than10^{-3} %) (ACI, 2011). However a foundation that is subjected to an earthquake or blast loading is likely to undergo large deformations and, therefore, induce large strains in the soil.

2.2.1.1 Dynamic shear modulus

Dynamic shear modulus is the most important soil parameter influencing the dynamic behavior of the soil-foundation interaction. The dynamic modulus is the ratio of stress to strain under vibratory conditions (calculated from data obtained from either free or forced vibration tests, in shear, compression or elongation), the so called low strain modulus. The shear modulus describes the material's response to shear stress. The shear strains developed in the supporting soil medium caused by the dynamic loading from machine foundations are usually of a much smaller magnitude than the strains produced by static loading. Most soils respond with a combination of elastic and plastic strain. For that reason, plotting shear stress versus shear strain results in a curve not a straight line. The value of G varies based on the strain considered. Thus, the value of the shear modulus for natural soils depends very much on the magnitude of the shear strains. For very small strains the shear modulus may be a factor of 10 or even 100 larger than it is for large strains. The value of the soil shear modulus at smaller strains (G_{max}) is much higher than its corresponding value at larger strains. For this reason, the soil shear modulus used for the computation of the foundation impedances should be evaluated from small strain tests.

Figure 2.8 represents stress–strain behavior of soils and variation of shear modulus with strain level for a typical soil, most soils exhibits a nonlinear hysteretic behavior

when loaded cyclically under high strains. This behavior is characterized by a backbone or initial loading curve (branch *OB* in Figure 2.8) and unloading (branches *BC* and *DE* in Figure 2.8) and reloading branches CD and EF in Figure 2.8) curves that form hysteresis loops. It may be observed, thus, that, in general, the shear modulus *G* of a given soil is not constant but it changes with strain level. It exhibits maximum value at a very low shear strain (i.e, $G=G_{max}$ when the strain is close to zero) and decreases with an increasing strain level. Most seismic geophysical tests induce low shear strains and the measured shear wave velocity can be used to compute the maximum shear modulus of the soil. Generally the shear modulus may be determined from laboratory tests, a field test or correlation with other properties.

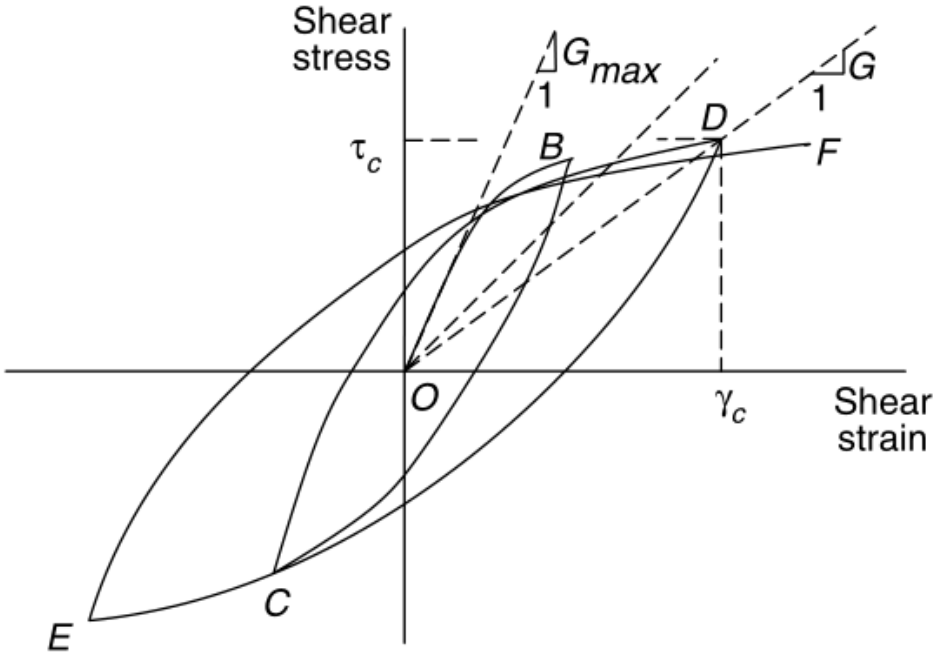

Figure 2.8 Typical stress–strain behavior of soils and variation of shear modulus with strain level (Villaverde, 2009)

Laboratory determination—Laboratory tests are considered less accurate than field measurements due to the possibility of sample disturbance among other factors. Sometimes laboratory tests are used to validate field measurements when a high level of accuracy is required. The most common laboratory test is the resonant column

tests, where a cylindrical sample of soil is placed in a device capable of generating forced vibrations. The soil sample is excited at different frequencies until the resonant frequency is determined. The dynamic soil modulus can be calculated based on the frequency, the length of the soil sample, the end conditions of the soil sample, and the density of the soil sample.

Field determination-Field measurements are the most common method for determining the dynamic shear modulus of a given soil. These methods involve measuring the soil characteristics, in-place, as close as possible to the actual foundation location. Because field determinations are an indirect determination of shear modulus, the specific property measured is the shear wave velocity. There are three different types of stress waves that can be transmitted through soil or any other elastic body.

- Compression (primary P) waves;
- Shear (secondary S) waves; and
- Rayleigh (surface) waves.

Compression waves are transmitted through soil by a volume change associated with compressive and tensile stresses. Compression waves are the fastest of the three stress waves.

Shear waves are transmitted through soil by distortion associated with shear stresses in the soil and are slower than compression waves. No volume change occurs in the soil.

Rayleigh waves occur at the free surface of an elastic body; in geotechnical media typically, this is the ground surface. Rayleigh waves have components that are both perpendicular to the free surface and parallel to the free surface and are slightly slower than shear waves.

Several methods are available for measuring wave velocities of the in-place soil:

- The cross-hole method;
- The down-hole method;
- The up-hole method;

- Steady-State Vibration of the Free Surface and
- Seismic reflection (or refraction).

In the cross-hole method, two vertical boreholes are drilled. A signal generator is placed in one hole and a sensor is placed in the other hole. An impulse signal is generated in one hole, and then the time the shear wave takes to travel from the signal generator to the sensor is measured. The travel time divided by the distance yields the shear wave velocity. This is probably the best geotechnical method for determining the variation with depth of in-situ low strain S-wave velocity, $V_{s,\,max.}$ Apparently, cross hole would not be classified among the most economical in-situ tests, but it is one of the most reliable in-situ tests.

In the down-hole method, only one vertical borehole is drilled. A signal generator is placed at the ground surface some distance away from the borehole, and a sensor is placed in the bottom of the borehole. An impulse signal is generated, and then the time the shear wave takes to travel from the signal generator to the sensor is measured. The travel time divided by the distance yields the shear wave velocity. This method can be run several different times, with the signal generator located at different distances from the borehole each time. This permits the measuring of soil properties at several different locations, which can then be averaged to determine an average shear wave velocity. An effective and economic S-wave source consists of a steel-jacketed rigid beam weighted down the ground and struck horizontally with a sledge hammer. However, if the source is placed too close to the borehole; parasitic waves are created and S-wave arrivals cannot be easily identified; if it is placed too far from the source, the direct wave path may not be a straight line. These problems are largely avoided with cross-hole testing. Down-hole is the economic alternative to cross-hole testing.

The up-hole method is similar to the down-hole method. The difference is that the signal generator is placed in the borehole and the sensor is placed at the ground surface.

The Steady-State Vibration of the Free Surface method, requiring no boreholes, is based on the fact that a circular footing vertically oscillating with frequency f generates along the free surface primarily Rayleigh (R) waves. Their wavelength, λ_R is the distance between any two successive crests or (troughs) of the vibrating surface and their velocity C_R is calculated from: $C_R = f\lambda_R$.Measurement of λ_R is made by moving a seismic geophone away from the vibrator and locating at points that are moving in phase. The insensitivity of S-wave and R-wave to the water table represents a distinct advantages for steady-state techniques.

Dynamic shear modulus and measured-in-field shear wave velocity in an elastic medium are related as follows;

$$G = \rho v_s \tag{2.9}$$

Correlation with other soil properties –existing correlation are another alternative for estimating dynamic soils properties. These are generally the least-accurate methods. Hardin and Richart (1963) determined that soil void ratio e and the probable confining pressure σ_o had the most impact on the dynamic shear modulus.

Hardin and Black (1968) developed the following relationships at low strain amplitudes ($\leq 10^{-4}$). The shear modulus was found dependent on the void ratio at a certain confining pressure.

For round-grained sands with $e < 0.8$, dynamic shear modulus can be estimated from

$$G = \frac{6908(2.17 - e_v)^2\sqrt{\sigma_o}}{(1+e)} \qquad (kPa) \tag{2.10}$$

For angular-grained materials with $e > 0.6$ and normally consolidated clays with low surface activity, dynamic shear modulus can be estimated from

$$G = \frac{3230(2.97 - e)^2\sqrt{\sigma_o}}{(1+e)} \qquad (kPa) \tag{2.11}$$

e =void ratio

$\sigma_o = Mean\ effective\ stress = \frac{(\sigma_1 + \sigma_2 + \sigma_3)}{3}$ *for laboratory samples*

$= \frac{(\sigma'_v + 2\sigma'_v(1 - sin\phi')}{3}$ *in the field* (kPa)

σ'_v =vertical effective stress at a certain point in a soil mass

ϕ' =drained friction angle

Hardin and Drnevich (1972) and Hardin (1978) for all types of soils the following empirical formula:

$$G_{\max} = \frac{625}{0.3 + 0.7e^2}(OCR)^k(\sigma'_o)^n(P_a)^{1-n} \tag{2.12}$$

Where P_a is atmospheric pressure, e is the void ratio, OCR is the over consolidation ratio, σ'_o is the mean effective normal stress, k and n are OCR and stress exponents. In 1991 Jamiolkoski suggested:

$$G_{\max} = \frac{625}{e^{1.3}}(OCR)^k(\sigma'_M)^n(P_a)^{1-n} \tag{2.13}$$

The stress exponent *n* is usually taken equal to 0.5 but can be computed for individual soils from the results of laboratory tests at different confining pressures, and The OCR component k is given in Table 2.1

Table 2.1 over consolidation ratio exponent, k (After Hardin and Drnevich 1972; (Kramer, 1996))

Plasticity Index	k
0	0
20	0.18
40	0.3
60	0.41
80	0.48
≥100	0.5

In 1970 Seed and Idris proposed the maximum shear modulus of sand. Estimated as;

$$G = 6920 k_2 \sqrt{\sigma_o} \quad (N/m^2) \tag{2.14}$$

k_2 is a parameter that depends on void ratio and relative density (Table 2.2).

Table 2.2 Estimation of k_2, max (After seed and Idris (1970) (Kramer, 1996))

e	k_2	D_r (%)	k_2
0.9	34	90	70
0.8	39	75	59
0.7	44	60	52
0.6	51	45	43
0.5	60	40	40
0.4	70	30	34

Common ranges of Gmax and Vs are suggested by Briaud (2013) are provided in Table 2.3. They may be used by preliminary analysis purposes.

Table 2.3 Common values of G_{max} for different soils based on shear wave velocity (Briaud, 2013)

Type of soil	Small strain shear wave velocity, v_s (m/s)	Initial shear modulus, G_{max} (MPa)
Soft clay	40-90	3-14
Firm clay	65-140	7-36
Loose sand	125-270	29-144
Dense sand and gravel	270-400	72-360

2.2.1.2 Poisson's ratio and soil density

Poisson's ratio (v) is the ratio of the strain in the direction perpendicular to loading to the strain in the direction of loading and used to calculate both the soil stiffness

and damping. Poisson's ratio (v) Shows little sensitivity to soil type, confining pressure, and void ratio, but depends very much on the degree of saturation and the drainage conditions. The dynamic behavior of foundations is less sensitive to the values of v *and* ρ. However, the dynamic impedance becomes highly frequency dependent for Poisson's ratios near 0.5 (Arya et al., 1984)

It must be noted that the soil mass density should always be calculated from the total unit weight rather than the submerged unit weight. Total weights are used in dynamic problems because both solid and liquid phases vibrate.

Common values of the poisson's ratio of soils are given in Table 2.4.

Table 2.4 Typical values for Poisson's Ratio after (Arya et al., 1984)

Soil Type	v
Saturated clay	0.45-0.50
Partially saturated clay	0.35-0.45
Dense sand or Gravel	0.40-0.50
Medium dense sand or Gravel	0.30-0.40
Silt	0.30-0.40

2.2.1.3 Damping of soil

Damping is an inherent property of soil and its influence on Forced Vibration Response is significant but during resonance or near resonance conditions. Different soils exhibit different damping properties depending upon their soil composition and other characteristic parameters. In case of embedded foundations, the depth of embedment also influences damping properties.

Soil Damping comprises of a) Geometrical Damping and b) Material Damping. Whereas Geometrical Damping represents energy radiated away from the foundation, whereas Material Damping represents the energy lost within the soil due to hysteresis effects or it is measure of energy lost from friction between soil particles during the dynamic loading. The material damping ratio can be obtained from resonant column testing, the spectral analysis of seismic wave's procedure (SASW) or

multi-channel analysis of surface waves (MASW). The soil material damping, at low strain, is typically 2% to 3% for sand and saturated clay. (Hongchun, 2018).

Damping in the soil has been observed to be both strain and frequency dependent. Same soil exhibits different damping characteristics at different strain levels and similar is the variation for the frequency of excitation. In other words, soil damping not only depends upon stress/strain/contact pressure distribution but also on frequency of vibration.

3 ANALYSIS APPROACH

In this paper two types of analytical approaches are used to obtain horizontal and rotational amplitude of a block foundation using impedance function. The methods considered are:

1. Direct method (Worku, 2016)
2. Superposition (simplified) approach (Prakash and Kumar, 1995)

3.1 DIRECT APPROACH

A rigid block has in general, six degrees of freedom. Three of them are translations along the three principal axis and the other three are rotations about these axes. From the six modes, translation along the vertical axis and rotation around z axis can occur independently of the other motion and are called decoupled modes. However the horizontal motion along the y-axis and the rotational motion around the x-axis are coupled through the off-diagonal terms K_{yrx} and C_{yrx}. Similarly are coupled the horizontal motion along the x– direction and the rotational motion around the y-axis through K_{xry} and C_{xry}. This is evident from the equilibrium equations for the model in either the xz-plane or the yz–plane obtained as shown below: (Worku, 2016)

For equilibrium of the system in Figure 3.1 (c)

$$F_I + F_D + F_S = P \tag{3.1}$$

$$M_I + M_D + M_S - f_D h - f_s h = M \tag{3.2}$$

The various terms in the pair of equations are

$$\left.\begin{array}{lll} F_I = m\ddot{u}, & F_D = C_h(\dot{u} - h\dot{\theta}), & F_S = K_h(u - h\theta) \\ M_I = I\ddot{\theta}, & M_D = c_r\dot{\theta}, & M_S = K_r\theta \end{array}\right\} \tag{3.3}$$

Where u is the horizontal amplitude and θ is the angular amplitude.

substituting 3.3 in equation 3.1 and 3.2 we get

$$\left.\begin{array}{l} m\ddot{u} + C_h(\dot{u} - h\dot{\theta}) + K_h(u - h\theta) = P \\ I\ddot{\theta} + c_r\dot{\theta} + K_r\theta - hC_h(\dot{u} - h\dot{\theta}) - hK_h(u - h\theta) = M \end{array}\right\} \tag{3.4a}$$

rewriting equation 3.4a in the matrix form

$$[m]\{\ddot{u}\}+[C]\{\dot{u}\}+[K]\{u\}=\{F\}$$

$$Where,[m]=\begin{bmatrix} m & 0 \\ 0 & I \end{bmatrix};\quad [C]=\begin{bmatrix} C_h & -hC_h \\ -hC_h & h^2C_h+C_r \end{bmatrix}; \tag{3.4b}$$

$$[K]=\begin{bmatrix} k_h & -hK_h \\ -hK_h & h^2K_h+K_r \end{bmatrix};\quad \{U\}=\begin{Bmatrix} u_o \\ \theta_o \end{Bmatrix},\quad \{F\}=\begin{Bmatrix} P_o \\ M_o \end{Bmatrix}$$

In general we can write equation 3.4b

$$[m]=\begin{bmatrix} m & 0 \\ 0 & I \end{bmatrix};\quad [C]=\begin{bmatrix} C_{11} & C_{12} \\ C_{21} & C_{22} \end{bmatrix};\quad [K]=\begin{bmatrix} K_{11} & K_{12} \\ K_{21} & K_{22} \end{bmatrix} \tag{3.4c}$$

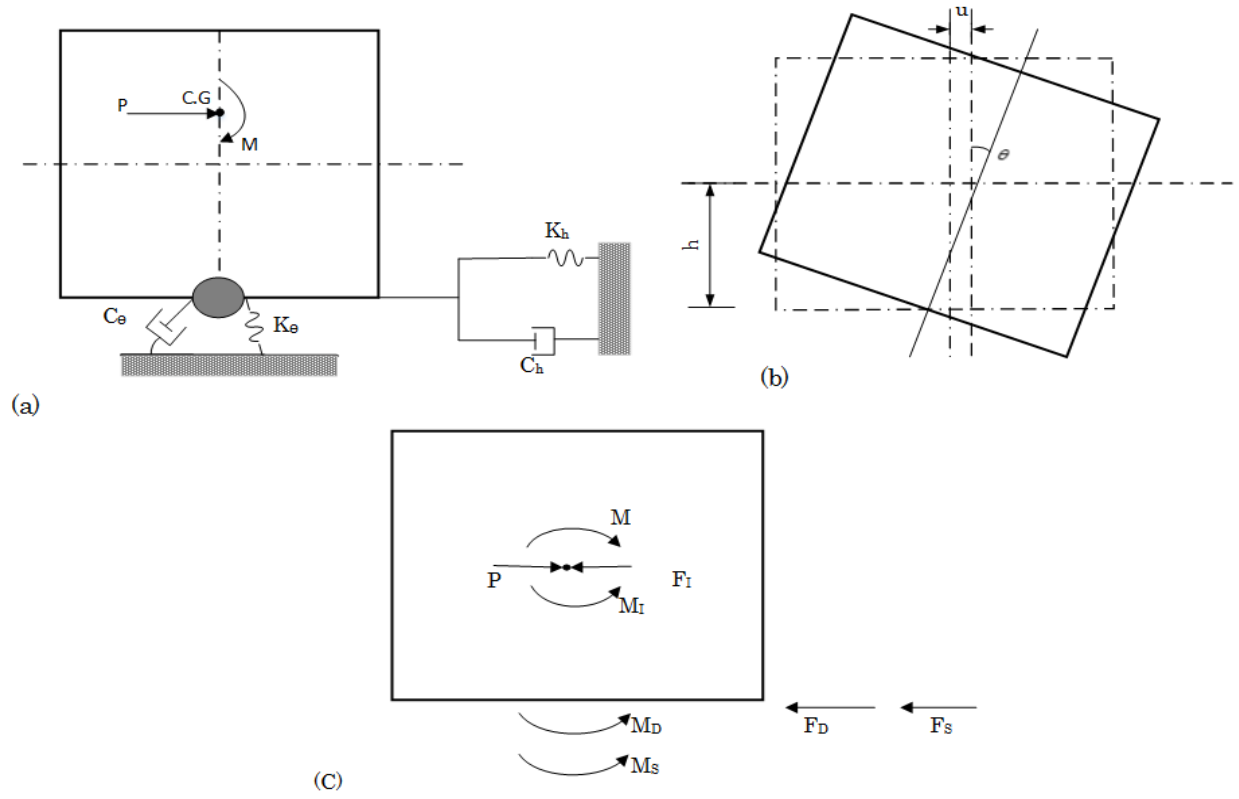

Figure 3.1 coupled horizontal and rocking motions of a block machine foundation (a) model; and (b) displaced position; (c) free-body diagram

The height h, is the vertical offset of the centroid of the machine foundation system from the bottom of the foundation, and the soil resistance is represented by the two

pairs of spring and dashpots for the two coupled modes of vibration. The indices h and r stand for the horizontal and rocking degrees of freedom, respectively.

Response to Harmonic loading

The equilibrium equation can be easily formulated on the basis of Alembert's principle in the matrix equation of motion that has the usual general form of

$$[m]\{\ddot{u}\}+[C]\{\dot{u}\}+[K]\{u\}=\{F(t)\} \tag{3.5}$$

Where $U(t)=\begin{bmatrix}u_o\\ \theta_o\end{bmatrix}e^{i\varpi t}$ and $F(t)=\begin{bmatrix}P_o\\ M_o\end{bmatrix}e^{i\varpi t}$

A simpler approach for harmonic loading is to directly solve the coupled equation of (3.5) using the harmonic substitution

$$\{u(t)\}=\{u_o\}e^{i\varpi t}, \text{ in which}$$
$$u=u_o e^{i\omega t} \qquad \theta=\theta_o e^{i\omega t} \tag{3.6}$$

Inserting Equation (3.6) and its derivative in Equation (3.5), one obtains the following simple system of algebraic equations:

$$\begin{bmatrix}(K_{11}-\bar{\omega}^2 m)+i\bar{\omega}C_{11} & K_{12}+i\bar{\omega}C_{12}\\ K_{21}+i\bar{\omega}C_{21} & (K_{22}-\bar{\omega}^2 I)+i\bar{\omega}C_{22}\end{bmatrix}\begin{Bmatrix}u_o\\ \theta_o\end{Bmatrix}=\begin{Bmatrix}P_o\\ M_o\end{Bmatrix} \tag{3.7}$$

Equation (3.7) can be solved by Cramer's rule, according to which the complex displacement and rotation amplitudes are obtained from

$$u_o=\frac{D_1}{D}; \qquad \theta_o=\frac{D_2}{D} \tag{3.8}$$

It is to be noted that the displacement and rotation are complex numbers due to the phase difference between the loading and the response.

In Equation (3.8), D_1 and D_2 are determinants of the respective matrices obtained by replacing the first and the second columns of the coefficient matrix in equation (3.7) by the loading column as follows:

$$
\begin{aligned}
D_1 &= \begin{vmatrix} P_o & K_{12} + i\bar{\omega}C_{12} \\ M_o & (K_{22} - \bar{\omega}^2 I) + i\bar{\omega}C_{22} \end{vmatrix} = D_{1r} + iD_{1i} \\
D_1 &= P_o\left[(K_{22} - \bar{\omega}^2 I) + i\bar{\omega}C_{22}\right] - M_o\left[K_{12} + i\bar{\omega}C_{12}\right] \\
D_2 &= \begin{vmatrix} (K_{11} - \bar{\omega}^2 m) + i\bar{\omega}C_{11} & P_o \\ K_{21} + i\bar{\omega}C_{21} & M_o \end{vmatrix} = D_{2r} + iD_{2i} \\
D_2 &= M_o\left[(K_{11} - \bar{\omega}^2 m) + i\bar{\omega}C_{11}\right] - P_o\left[K_{21} + i\bar{\omega}C_{21}\right]
\end{aligned}
\tag{3.9}
$$

The denominator in equation (3.8) is the determinant of the coefficient matrix in equation (3.7) given by

$$
D = \begin{vmatrix} (K_{11} - \bar{\omega}^2 m) + i\bar{\omega}C_{11} & K_{12} + i\bar{\omega}C_{12} \\ K_{21} + i\bar{\omega}C_{21} & (K_{22} - \bar{\omega}^2 I) + i\bar{\omega}C_{22} \end{vmatrix} = D_r + iD_i \tag{3.10}
$$

The real and imaginary parts of these determinants, identified by the indices r (real) and I (imaginary), are obtained after expansion and rearranging as follows:

$$
\begin{aligned}
D_{1r} &= P_o(K_{22} - \bar{\omega}^2 I) - M_o K_{12} \\
D_{1i} &= \bar{\omega}(P_o C_{22} - M_o C_{12}) \\
D_{2r} &= M_o(K_{11} - \bar{\omega}^2 m) - P_o K_{21} \\
D_{2i} &= \bar{\omega}(M_o C_{11} - P_o C_{21}) \\
D_r &= (K_{11} - \bar{\omega}^2 m)(K_{22} - \bar{\omega}^2 I) - K_{12}K_{21} - \bar{\omega}^2(C_{11}C_{22} - C_{12}C_{21}) \\
D_i &= \bar{\omega}\left[C_{22}(K_{11} - \bar{\omega}^2 m) + C_{11}(K_{22} - \bar{\omega}^2 I) - 2K_{12}C_{12}\right]
\end{aligned}
\tag{3.11}
$$

The real valued displacement and rotation amplitudes are obtained as the moduli of the complex amplitudes of equation (3.8).Thus

$$
\begin{aligned}
|u_o| &= \left|\frac{D_1}{D}\right| = \frac{|D_1|}{|D|} = \sqrt{\frac{N_u}{D_r^{\,2} + D_i^{\,2}}} \\
|\theta_o| &= \left|\frac{D_2}{D}\right| = \frac{|D_2|}{|D|} = \sqrt{\frac{N_\theta}{D_r^{\,2} + D_i^{\,2}}}
\end{aligned}
\tag{3.12}
$$

Where

$$
N_u = P_o^2\left[(K_{22} - \bar{\omega}^2 I)^2 + \bar{\omega}^2 C_{22}^{\,2}\right] + M_o^{\,2}(K_{12}^{\,2} + \bar{\omega}^2 C_{12}^{\,2}) - 2P_o M_o\left[K_{12}(K_{22} - \bar{\omega}^2 I) + \bar{\omega}^2 C_{22}C_{12}\right]
$$

$$
N_\theta = P_o^2(K_{12}^{\,2} - \bar{\omega}^2 C_{12}^{\,2})^2 + M_o^{\,2}\left[(K_{11} + \bar{\omega}^2 m)^2 + \bar{\omega}^2 C_{11}\right] - 2P_o M_o\left[K_{12}(K_{11} - \bar{\omega}^2 m) + \bar{\omega}^2 C_{11}C_{12}\right]
$$

It must be noted that in equation 3.12 the combined effect of force and the rocking moment is included.

For embedded footings the impedance function method incorporates the side reaction of damping and stiffness coefficients in the base stiffness and damping coefficients therefore direct approach is appropriate for both surface and embedded footings.

3.2 SUPERPOSITION METHOD

The motion of the block may be expressed in terms of translation Y of the center of gravity and the rotation angle θ. The equation of motion may be obtained by considering the equilibrium of the exciting and resisting forces and moments in terms of Newton's second law.

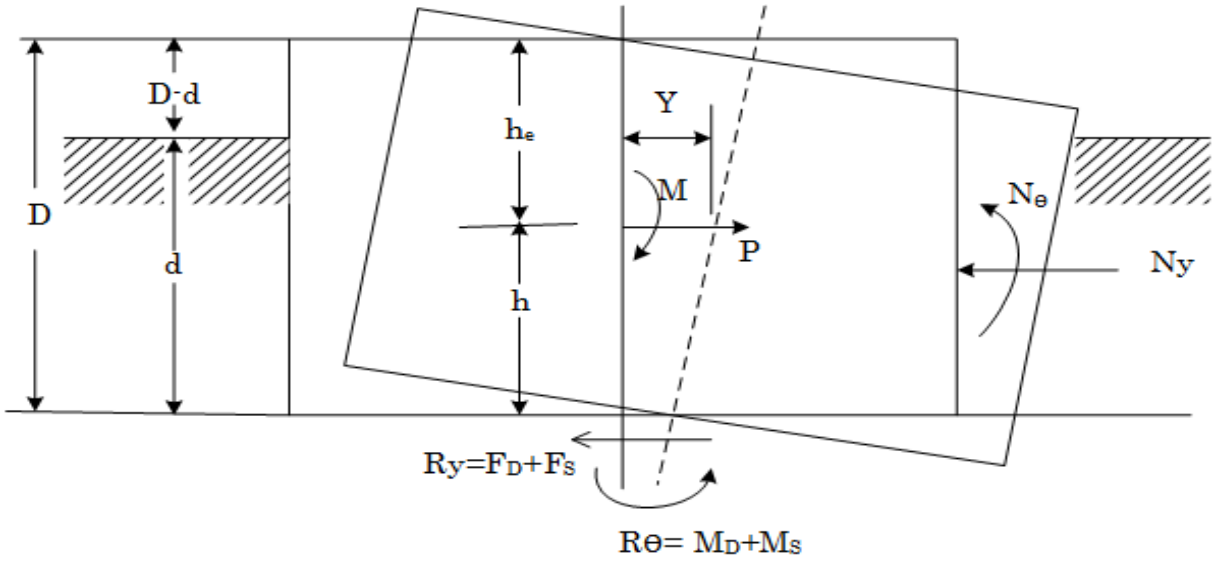

Figure 3.2 Mathematical model of rigid block embedded in elastic half-space with soil side layer in coupled motion

From equilibrium of the system in Figure 3.2 the equation of motion in sliding for embedded foundation is

$$m\ddot{u} + R_y + N_y = P_o e^{i\omega t} \tag{3.13}$$

where $R_y = F_D + F_S$ and , $F_D = C_{hb}(\dot{u} - h\dot{\theta})$, $F_S = K_{hb}(u - h\theta)$

$$N_y = C_{hs}(\dot{u} - (h - \frac{d}{2})\dot{\theta}) + K_{hs}(u - (h - \frac{d}{2})\theta)$$

Substitution of R_y and N_y in equation (3.13) the equation of motion in sliding becomes:

$$m\ddot{u}+(C_{hb}+C_{hs})\dot{u}+(K_{hb}+K_{hs})u-\left[(h-\frac{d}{2})C_{hs}+hC_{hb}\right]\dot{\theta}-\left[(h-\frac{d}{2})K_{hs}+hK_{hb}\right]\theta=P_o e^{i\omega t} \quad (3.14)$$

The equation of motion in rocking is

$$I\ddot{\theta}+R_\theta+N_\theta=M_0 e^{i\omega t}+N_y(h-\frac{d}{2})+hR_y \quad (3.15)$$

where $R_\theta=M_D+M_s$, $M_D=c_{\theta b}\dot{\theta}$, $M_S=K_{\theta b}\theta$ $R_\theta=K_{\theta b}\theta+C_{\theta b}\dot{\theta}$; $N_\theta=K_{\theta s}\theta+C_{\theta s}\dot{\theta}$

Substitution of R_θ *and* N_θ in equation (3.15) the equation of motion in rocking becomes

$$I\ddot{\theta}+\left[(C_{\theta b}+C_{\theta s})+h^2C_{hb}+C_{hs}(h-\frac{d}{2})^2\right]\dot{\theta}+\left[(K_{\theta b}+K_{\theta s})+h^2K_{hb}+C_{hs}(h-\frac{d}{2})^2\right]\theta$$
$$-\left[hC_{hb}+(h-\frac{d}{2})C_{hs}\right]\dot{u}-\left[hK_{hb}+(h-\frac{d}{2})K_{hs}\right]u=M_o e^{i\omega t} \quad (3.16)$$

Writing equation (3.14) and (3.16) in matrix form

$$\begin{bmatrix} m & 0 \\ 0 & I \end{bmatrix}\begin{Bmatrix}\ddot{u}\\ \ddot{\theta}\end{Bmatrix}+\begin{bmatrix} C_{hb}+C_{hs} & -\left[hC_{hb}+(h-\frac{d}{2})C_{hs}\right] \\ -\left[hC_{hb}+(h-\frac{d}{2})C_{hs}\right] & \left[(C_{\theta b}+C_{\theta s})+h^2C_{hb}+(h-\frac{d}{2})^2C_{hs}\right]\end{bmatrix}\begin{Bmatrix}\dot{u}\\ \dot{\theta}\end{Bmatrix} \quad (3.17)$$
$$+\begin{bmatrix} K_{hb}+K_{hs} & -\left[hK_{hb}+(h-\frac{d}{2})K_{hs}\right] \\ -\left[hK_{hb}+(h-\frac{d}{2})K_{hs}\right] & \left[(K_{\theta b}+K_{\theta s})+h^2K_{hb}+(h-\frac{d}{2})^2K_{hs}\right]\end{bmatrix}\begin{Bmatrix}u\\ \theta\end{Bmatrix}=\begin{Bmatrix}P_o\\ M_o\end{Bmatrix}e^{i\omega t}$$

The above equation is derived for embedded footings it can also be used for surface footings by making $K_{hs}=C_{hs}=d=o$

$$\begin{bmatrix} m & 0 \\ 0 & I \end{bmatrix}\begin{Bmatrix}\ddot{u}\\ \ddot{\theta}\end{Bmatrix}+\begin{bmatrix} C_{hb} & -\left[hC_{hb}\right] \\ -\left[hC_{hb}\right] & \left[(C_{\theta b})+h^2C_{hb}\right]\end{bmatrix}\begin{Bmatrix}\dot{u}\\ \dot{\theta}\end{Bmatrix}+\begin{bmatrix} K_{hb} & -\left[hK_{hb}\right] \\ -\left[hK_{hb}\right] & \left[(K_{\theta b})+h^2K_{hb}\right]\end{bmatrix}\begin{Bmatrix}u\\ \theta\end{Bmatrix}=\begin{Bmatrix}P_o\\ M_o\end{Bmatrix}e^{i\omega t} \quad (3.18)$$

In general we can write for both embedded and surface footings

$$\begin{bmatrix} m & 0 \\ 0 & I \end{bmatrix}\begin{Bmatrix}\ddot{u}\\ \ddot{\theta}\end{Bmatrix}+\begin{bmatrix} C_{11} & C_{12} \\ C_{21} & C_{22}\end{bmatrix}\begin{Bmatrix}\dot{u}\\ \dot{\theta}\end{Bmatrix}+\begin{bmatrix} K_{11} & K_{12} \\ K_{21} & K_{22}\end{bmatrix}\begin{Bmatrix}u\\ \theta\end{Bmatrix}=\begin{Bmatrix}P(t)\\ M(t)\end{Bmatrix} \quad (3.19)$$

Inserting Equation (3.6) and its derivative in Equation (3.19), one obtains the following simple system of algebraic equations:

$$\begin{bmatrix} (K_{11}-\bar{\omega}^2 m)+i\bar{\omega}C_{11} & K_{12}+i\bar{\omega}C_{12} \\ K_{21}+i\bar{\omega}C_{21} & (K_{22}-\bar{\omega}^2 I)+i\bar{\omega}C_{22} \end{bmatrix} \begin{Bmatrix} u_o \\ \theta_o \end{Bmatrix} e^{i\omega t} = \begin{Bmatrix} P(t) \\ M(t) \end{Bmatrix} \quad (3.20)$$

Damped amplitudes of rocking and sliding can be found by solving equation (3.20) for either an exciting force $P(t)=P_o e^{i\varpi t}$ or moment $M(t)=M_o e^{i\varpi t}$

When excited by horizontal force only:

Solving equation 3.20 for only horizontal exciting force gives the amplitudes as follows

$$U_{op}=\frac{P_o\sqrt{\left[(K_{11}-m\bar{\omega}^2)^2-\bar{\omega}^2 {c_{11}}^2\right]}}{mI\Delta} \quad (3.21a)$$

$$\theta_{op}=\frac{P_o\sqrt{\left[(K_{12}-\bar{\omega}^2 {C_{12}}^2)^2\right]}}{mI\Delta} \quad (3.21b)$$

When excited by rocking moment only:

Solving equation 3.20 for moment only acting, gives the amplitudes as follows:

$$U_{om}=\frac{M_o\sqrt{\left[({K_{12}}^2-\bar{\omega}^2 {C_{12}}^2)^2\right]}}{mI\Delta} \quad (3.22a)$$

$$\theta_{om}=\frac{M_o\sqrt{\left[(K_{22}-I\bar{\omega}^2)^2-\bar{\omega}^2 C_{22}\right]}}{mI\Delta} \quad (3.22b)$$

Where, $\Delta=\sqrt{\left[\begin{array}{l}\left\{\bar{\omega}^4-\left(\frac{K_{11}}{m}+\frac{K_{22}}{I}+\frac{C_{11}C_{22}}{mI}-\frac{{C_{12}}^2}{mI}\right)\bar{\omega}^2+\left(\frac{K_{11}K_{22}}{mI}-\frac{{K_{12}}^2}{mI}\right)\right\}^2+ \\ \left\{\left(\frac{K_{11}C_{22}}{mI}+\frac{K_{22}C_{11}}{mI}-\frac{2K_{12}C_{12}}{mI}\right)\bar{\omega}-\left(\frac{C_{22}}{I}+\frac{C_{11}}{m}\right)\bar{\omega}^3\right\}^2\end{array}\right]}$ (3.23)

When the footing is subjected to the action of both moment and horizontal force, the resulting amplitudes of sliding and rocking are obtained by adding the corresponding

solutions from Equations of (3.21) and (3.22) and we obtain Equation (3.24). (Prakash and Puri, 1995)

$$|U_o| = \frac{\sqrt{P_o^2\left[(K_{11}-m\bar{\omega}^2)^2-\bar{\omega}^2 c_{11}^{\,2}\right]}}{mI\Delta} + \frac{\sqrt{M_o^{\,2}\left[(K_{12}^{\,2}-\bar{\omega}^2 C_{12}^{\,2})^2\right]}}{mI\Delta}$$
$$|\theta_o| = \frac{\sqrt{P_o^2\left[(K_{12}-\bar{\omega}^2 C_{12}^{\,2})^2\right]}}{mI\Delta} + \frac{\sqrt{M_o^{\,2}\left[(K_{22}-I\bar{\omega}^2)^2-\bar{\omega}^2 C_{22}\right]}}{mI\Delta} \qquad (3.24)$$

To make clear comparison between superposition and direct method we can write Equation (3.12) for the direct method.

$$|u_o| = \left|\frac{D_1}{D}\right| = \frac{|D_1|}{|D|} = \sqrt{\frac{N_u}{D_r^{\,2}+D_i^{\,2}}}$$

$$|u_o| = \sqrt{\frac{P_o^2\left[(K_{22}-\bar{\omega}^2 I)^2+\bar{\omega}^2 C_{22}^{\,2}\right]+M_o^{\,2}(K_{12}^{\,2}+\bar{\omega}^2 C_{12}^{\,2})-2P_oM_o\left[K_{12}(K_{22}-\bar{\omega}^2 I)+\bar{\omega}^2 C_{22}C_{12}\right]}{\left[(K_{11}-\bar{\omega}^2 m)(K_{22}-\bar{\omega}^2 I)-K_{12}K_{21}-\bar{\omega}^2(C_{11}C_{22}-C_{12}C_{21})\right]^2+\left[\bar{\omega}\left[C_{22}(K_{11}-\bar{\omega}^2 m)+C_{11}(K_{22}-\bar{\omega}^2 I)-2K_{12}C_{12}\right]\right]^2}}$$

$$|\theta_o| = \left|\frac{D_2}{D}\right| = \frac{|D_2|}{|D|} = \sqrt{\frac{N_\theta}{D_r^{\,2}+D_i^{\,2}}} \qquad (3.25)$$

$$|\theta_o| = \sqrt{\frac{P_o^2(K_{12}^{\,2}-\bar{\omega}^2 C_{12}^{\,2})^2+M_o^{\,2}\left[(K_{11}+\bar{\omega}^2 m)^2+\bar{\omega}^2 C_{11}\right]-2P_oM_o\left[K_{12}(K_{11}-\bar{\omega}^2 m)+\bar{\omega}^2 C_{11}C_{12}\right]}{\left[(K_{11}-\bar{\omega}^2 m)(K_{22}-\bar{\omega}^2 I)-K_{12}K_{21}-\bar{\omega}^2(C_{11}C_{22}-C_{12}C_{21})\right]^2+\left[\bar{\omega}\left[C_{22}(K_{11}-\bar{\omega}^2 m)+C_{11}(K_{22}-\bar{\omega}^2 I)-2K_{12}C_{12}\right]\right]^2}}$$

As we observe from Equation (3.24) and (3.25) direct method considers combined effect of force and moment while superposition method evaluates the responses in isolation and use simple superposition to determine the total response.

3.3 DAMPED AND UNDAMPED NATURAL FREQUENCIES

Impedance function method is used to obtain stiffness and damping coefficients. The aim of this subsection is to derive damped and undamped equations to determine natural frequencies. Damped and undamped natural frequencies, can be derived from Equation (3.5) or (3.19) by setting P(t) and M(t)=0

$$\begin{bmatrix} m & 0 \\ 0 & I \end{bmatrix}\begin{Bmatrix} \ddot{u} \\ \ddot{\theta} \end{Bmatrix}+\begin{bmatrix} C_{11} & C_{12} \\ C_{21} & C_{22} \end{bmatrix}\begin{Bmatrix} \dot{u} \\ \dot{\theta} \end{Bmatrix}+\begin{bmatrix} K_{11} & K_{12} \\ K_{21} & K_{22} \end{bmatrix}\begin{Bmatrix} u \\ \theta \end{Bmatrix}=\begin{Bmatrix} 0 \\ 0 \end{Bmatrix} \qquad (3.26)$$

Solution of the equation obtained by substituting

$\mathrm{u} = u_o e^{i\omega t}$ $\theta = \theta_o e^{i\omega t}$

Let $\lambda = \mathrm{i}\omega$

$\mathrm{u} = \mathrm{u}_o e^{\lambda t}$ $\theta = \theta_o e^{\lambda t}$

$$\begin{bmatrix} \lambda^2 m + K_{11} + \lambda C_{11} & K_{12} + \lambda C_{12} \\ K_{21} + \lambda C_{21} & \lambda^2 I + K_{22} + \lambda C_{22} \end{bmatrix} \begin{Bmatrix} u_o \\ \theta_o \end{Bmatrix} e^{\lambda t} = \begin{Bmatrix} 0 \\ 0 \end{Bmatrix} \quad (3.27)$$

Solving for the determinant of equation 3.27

$$\mathrm{mI}\lambda^4 + (mC_{22} + IC_{11})\lambda^3 + (mK_{22} + IK_{11} + C_{11}C_{22} - C_{21}C_{12})\lambda^2 + (K_{11}C_{22} + C_{11}K_{22} - K_{22}C_{12} - C_{21}K_{12})\lambda + K_{11}K_{22} - K_{21}K_{12} = 0 \quad (3.28)$$

Equation 3.28 is a quartic equation which gives complex roots

For undamped natural frequency *with* $C_{11} = C_{12} = C_{22} = C_{21} = 0$ Equation 3.28 simplifies to

$$\mathrm{mI}\omega^4 - (mK_{22} + IK_{11})\omega^2 + K_{11}K_{22} - K_{21}K_{12} = 0 \quad (3.29a)$$

$$\text{Let } \omega^2 = \delta; \quad \mathrm{mI}\delta^2 - (mK_{22} + IK_{11})\delta + K_{11}K_{22} - K_{21}K_{12} = 0 \quad (3.29b)$$

Solving equation (3.29b) by using quadratic formula we get

$$\delta = \frac{(mK_{22} + IK_{11}) \pm \sqrt{(mK_{22} + IK_{11})^2 - (4 \times \mathrm{mI} \times (K_{11}K_{22} - K_{21}K_{12}))}}{2 \times mI} \quad (3.30)$$

The natural frequencies obtained from equation 3.28 and 3.30 are for damped and undamped frequencies respectively.

Stiffness and damping are generally frequency dependent parameters so that an iterative procedure is implemented to obtain frequency and damping ratios.

3.4 EXISTING EXPERIMENTAL DATA

To check the validity of the two approaches the model footing tests reported by Beredugo on his PhD thesis is used in this paper. The tests are performed at the University of Western Ontario, London (Beredugo, 1971). Two concrete blocks with base area of 0.46 m^2 have been used in the field tests. The shape of the block is square and rectangular with (L/B) aspect ratio of 1 and 2 respectively. Both footings are 1.22m high.

A hand auger investigation of the test site was carried out to supplement the information available from previous seismic investigation. The investigation shows that

the subsoil condition under the test site consisted of 0.10-0.28 meter of dark grey top soil underlain by 1.524 meter of brown silty clay. Below the silty clay was a glacial till of considerable thickness. The water table was not encountered at the maximum investigation depth of 4.572 meter below ground level. Insitu density determination were carried out in test pits at several depths using both sand replacement and balloon methods. Disturbed and undisturbed samples were recovered from the test pits for laboratory testing.

The excitation equipment consisted of:

i. A Lazan mechanical oscillator producing a frequency dependent exciting force with a maximum eccentric moment, ew_e, of 2.034 N-m in horizontal direction.
ii. A 220 volts, three phase motor fitted with kopp variator to provide step less speed variation from 300 to 3600 revolutions per minute (5Hz-60Hz). The motor was connected to the oscillator with a flexible cable.
iii. A dual beam storage oscilloscope.
iv. A brush two channel recorder.
v. A "strobotac" stroboscope for accurate measurement of speed.

Different embedment depths were obtained by carefully excavating a trench 0.4572 meter wide around the footing to the desired depth. Embedment depth of 0.9144 meter, 0.4572 meter, 0.2286 meter and zero were used in the test program. In the case of zero embedment, the footing was completely surrounded by an "air gap".

Dynamic soil properties

In order to determine the dynamic soil properties required for dynamic calculations, steady state vibration is used and measurements of Rayleigh wave velocity and primary wave velocity were made.

From field and laboratory testing, the following soil properties required for the dynamic calculations were obtained for the site:

Mean bulk density of undisturbed soil=1649kg/m^3

Mean moisture content of soil=16%

Specific gravity of soil particles=2.7

Void ratio of undisturbed soil=0.9

Shear modulus of undisturbed soil=31601kN/m^2

Poisson's ratio of undisturbed soil=0.38

These experimental data are used to conduct analysis using the two approaches presented above.

Illustration example; Natural frequencies and vibration amplitudes of a rigid block under horizontal harmonic load.

Foundation on the surface

The square plan block machine foundation has base width of 0.68m and a height of 1.22m. It is excited by a horizontal force and a rocking moment. From the field and laboratory testing, the following soil properties required for dynamic calculations were obtained for the test site;

Mean bulk density of undisturbed soil=1649 kg/m^3

Mean moisture content of soil=16%

Specific gravity of soil particles=2.7

Void ratio of undisturbed soil=0.9

Shear wave velocity=138.41m/s

Shear modulus of undisturbed soil=31600kN/m^2

Poisson's ratio of undisturbed soil=0.38

The additional soil data are given in Table 3.1

Table 3.1 Properties of test footings (Beredugo, 1971)

Mass of footing +oscillator base+oscilator	1449.612kg
Mass moment of inertia of I_θ,of footing, oscillator about horizontal axis passing through the C.G	272.3842 kgm^2
Zc,center of gravity above base of footing	0.65806m
Ze,point of application of horizontal force above C.G	0.7309m
Equivalent radius for translational mode	0.3845m
Equivalent radius for rocking	0.3886m

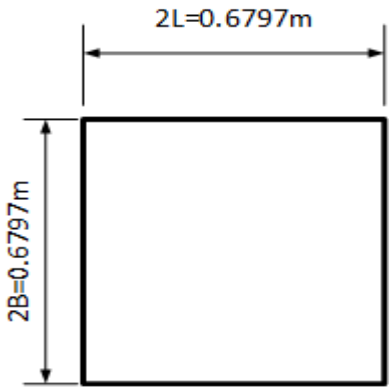

Plan view of square footing

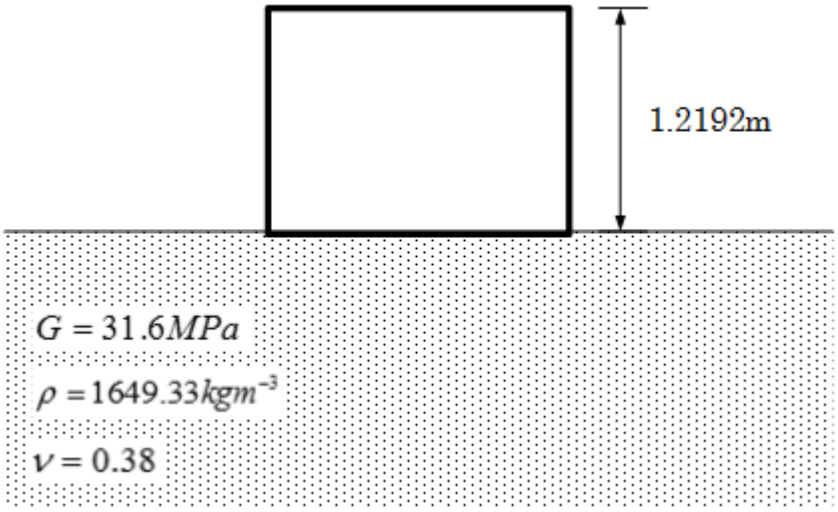

Section view of square footing

The damped natural frequency of the system and the amplitude of vibration under the 50 Hz operating frequency are to be determined. Vibration tests are carried out using a Lazan-type mechanical oscillator under different eccentric moments. For the illustration example we use eccentric moment (eWe)=0.09605Nm

Solution

The soil stiffness and damping are obtained using frequency dependent impedance function method

Assumed material damping = β =2.5%

$$\chi = \frac{A_b}{4L^2} = 1$$

$$V_{La} = \frac{3.4V_s}{\pi(1-\nu)} = 241.6\, m/s$$

$$I_{bx} = \frac{1}{12} * 2L * (2B)^3 = 0.0178 m^4$$

From table A1 the static stiffness is

$$K_y = K_h = \left[2GL/(2-\nu)\right](2 + 2.5\chi^{0.85})$$

$$= 59.664 * 10^6 N/m$$

$$Krx = [\frac{G}{(1-\nu)}] I_{bx}{}^{0.75} (L/B)^{0.25} [2.4 + 0.5(B/L)]$$

$$= 7.2 * 10^6 Nm$$

$C_h = (\rho V_s A_b)\bar{c}_h$ where $\bar{c}_h = \bar{c}_h(\frac{L}{B}; a_o)$ is plotted in Appendx Figure A1(d)

$\bar{c}_h$=0.462

$$C_h = 105,465.18 Ns/m$$

$$C_{rx} = C_\theta = (\rho V_{La} I_{bx}) = 7.093 * 10^3$$

$\omega = \sqrt{\frac{K_h}{M_t}} = 202.8$, $a_o = \frac{\omega B}{V_s} = 0.498$

Where K_h is the horizontal stiffness,

M_t=Total mass of footing, oscilator base and oscillator

ω this frequency is used as a first estimate to evaluate the impedance functions.

Dynamic stiffness and damping coefficients $K_h(\frac{L}{B}, a_o)$ and $\bar{c}_h = \bar{c}_h(\frac{L}{B}; a_o)$ are obtained from Figure A1 in Appendix or using the best fit equations developed from Gazetas 1991 chart.

$$\alpha K_h = 0.0323(a_o)^6 - 0.2017(a_o)^5 + 0.464(a_o)^4 - 0.4339(a_o)^3 - 0.0763(a_o)^2 - 0.0174(a_o) + 1.0459$$
$$= 1.025$$

$$\alpha C_h = -0.0462(a_o)^6 + 0.2949(a_o)^5 - 0.71(a_o)^4 + 0.7851(a_o)^3 - 0.3259(a_o)^2 - 0.1047(a_o) + 0.8865 = 0.815$$

$$\alpha C_{rx} = -0.083(a_o)^6 + 0.4861(a_o)^5 - 0.9933(a_o)^4 + 0.729(a_o)^3 - 0.0093(a_o)^2 - 0.1466(a_o) + 0.8865 = 0.1183$$

$$\alpha K_{rx} = 1 - 0.2a_o = 1 - 0.2 \times 0.498 = 0.9004$$

$$\bar{K}_h = \alpha K_h \times K_h = 1.025 \times 59.664 * 10^6 = 61.18 * 10^6 \; N/m$$

$$\bar{C}_h = \alpha C_h \times C_h = 0.815 \times 105,465.18 = 85,954.1217 \; Ns/m$$

$$\bar{K}_{rx} = \alpha K_{rx} \times K_{rx} = 0.9004 \times 7.2 \times 10^6 = 6.483 \times 10^6 \; Nm$$

$$\bar{C}_{rx} = \alpha C_{rx} \times C_{rx} = 0.1183 \times 7.093 \times 10^3 = 838.63 Nsm$$

$$Total\ C_h = radiation\ C + \frac{2K_h\beta}{\omega} = 85,954.1217 + 2 \times 61.18 \times 10^6 \times \frac{0.025}{202.8} = 1.01 \times 10^5$$

$$Total\ C_{rx} = radiation\ C + \frac{2K_{rx}\beta}{\omega} = 838.63 + 2 \times 6.483 \times 10^6 \times \frac{0.025}{202.8} = 2.437 \times 10^3$$

From Equation (3.4b) or (3.18) the damping and stiffness coefficients are given by the following formula using impedance function method

$$[C] = \begin{bmatrix} C_h & -hC_h \\ -hC_h & h^2C_h + C_r \end{bmatrix}; \; [K] = \begin{bmatrix} k_h & -hK_h \\ -hK_h & h^2K_h + K_r \end{bmatrix}$$ where, h=Z_c

$$[K] = \begin{bmatrix} K_{11} & K_{12} \\ K_{21} & K_{22} \end{bmatrix}; \qquad [C] = \begin{bmatrix} C_{11} & C_{12} \\ C_{21} & C_{22} \end{bmatrix}$$

$$[K] = \begin{bmatrix} 61.18 \times 10^6 & -0.65806 \times 61.18 \times 10^6 \\ -0.65806 \times 61.18 \times 10^6 & 0.65806^2 \times 61.18 \times 10^6 + 6.483 \times 10^6 \end{bmatrix}$$

$$= \begin{bmatrix} 61.18 \times 10^6 \, Nm^{-1} & -40.26 \times 10^6 \, N \\ -40.26 \times 10^6 \, N & 32.976 \times 10^6 \, Nm \end{bmatrix}$$

By applying the same procedure as the stiffness we get the damping matrix as

$$[C] = \begin{bmatrix} 1.01 \times 10^5 \, N.s.m^{-1} & -6.65 \times 10^4 \, N.s \\ -6.65 \times 10^4 \, N.s & 4.6 \times 10^4 \, N.s.m \end{bmatrix}$$

Damped natural frequency

As explained previously in equation 3.27

$$\begin{bmatrix} \lambda^2 m + K_{11} + \lambda C_{11} & K_{12} + \lambda C_{12} \\ K_{21} + \lambda C_{21} & \lambda^2 I + K_{22} + \lambda C_{22} \end{bmatrix} \begin{Bmatrix} u_o \\ \theta_o \end{Bmatrix} e^{i\omega t} = \begin{Bmatrix} 0 \\ 0 \end{Bmatrix}$$

Since, $e^{i\omega t} \neq 0$, for Equation (3.19) to be true, the determinant of the coefficient matrix should be zero. This results in (see also Equation (3.28))

$$\mathrm{mI}\lambda^4 + (mC_{22} + IC_{11})\lambda^3 + (mK_{22} + IK_{11} + C_{11}C_{22} - C_{21}C_{12})\lambda^2 + (K_{11}C_{22} + C_{11}K_{22} - K_{22}C_{12} - C_{21}K_{12})\lambda + K_{11}K_{22} - K_{21}K_{12} = 0$$

$$394851.4\lambda^4 + 94492675.68\lambda^3 + 6.471270 * 10^{10}\lambda^2 + 8.0405529 * 10^{11}\lambda + 3.9656222 * 10^{14} = 0$$

Solving for the above quartic equation we get a complex solution

$$\lambda_1^{(1)} = -1.671719 + 80.0423185i$$

$$\lambda_1^{(2)} = -1.671719 - 80.0423185i$$

$$\lambda_2^{(1)} = -117.984277 + 377.852450i$$

$$\lambda_2^{(2)} = -117.984277 - 377.852450i$$

Since the system has two degrees of freedom, the characteristic equation will thus yield two values of λ.

$$\omega = |\lambda|; \qquad \xi = \left|\frac{\mathrm{Re}\,\lambda}{\lambda}\right|$$

$$\omega_{n1} = \left|1.671719^2 + 80.0423185^2\right|^{0.5} = 80.0597$$

$$\omega_{n2} = \left|117.984277^2 + 377.852450^2\right|^{0.5} = 395.844$$

$$\xi_1 = \frac{1.671719}{80.0597} = 2.09\% \;\; ; \quad \xi_2 = \frac{117.984277}{395.8440} = 29.8\%$$

Iteration is better conducted with respect to the fundamental natural frequency

$$a_o = \frac{\omega B}{V_s} = \frac{80.0597 \times 0.3399}{138.41} = 0.1966$$

Repeating the same procedure as shown above until we get the same natural frequency we arrived at

$$\lambda_1^{(1)} = -2.755542 + 82.388247i$$

$$\lambda_1^{(2)} = -2.755542 - 82.388247i$$

$\lambda_2^{(1)} = -151.472154 - 370.409141i$

$\lambda_2^{(2)} = -151.472154 + 370.409141i$

$\omega_{n1} = \left|2.755542^2 + 82.388247^2\right|^{0.5} = 82.434315$

$\omega_{n2} = \left|151.472154^2 + 370.409141^2\right|^{0.5} = 400.183390$

$\xi_1 = \frac{2.755542}{82.434315} = 3.34\%$; $\xi_2 = \frac{151.472154}{400.183390}$

The iteration now may be stopped as the frequencies barely changed

The first mode natural frequency is $f = \omega_{n1}/2\pi = 82.434315/2\pi = 13.12Hz$

The second mode natural frequency $f = \omega_{n2}/2\pi == 400.183390/2\pi = 63.69Hz$

$a_o = \frac{\omega B}{V_s} = \frac{82.434315 \times 0.3399}{138.41} = 0.2024$

$K_{11} = 62207212.63Nm^{-1}$; $K_{21} = K_{12} = -40936078.34N$; $K_{22} = 338,45994.91Nm$

$C_{11} = 128160.6096Nsm^{-1}$; $C_{21} = C_{12} = -84337.3708Ns$; $C_{22} = 59936.8122Nm$

For the case of frequency dependent excitations caused by unbalance rotating mass horizontal exciting force and excitation moment is given by

$P = m_e e\omega^2$ $M = m_e e\omega^2 Z_e$

Where m_e= rotating mass ; ω=excitation frequency ;

e= eccentricity of rotating mass

Z_e=height of horizontal exciting force above center of gravity

$eW_e = 0.09605Nm$ $em_e = \frac{0.09605}{9.81} = 9.791 * 10^{-3} kgm$

$P = 9.791 \times 10^{-3} \times (314.159)^2 = 966.331N$

$M = 966.331 \times 0.7309 = 706.291Nm$

To solve for horizontal and rotational amplitude we use both direct and superposition approach method.

Using direct approach method

Substitution of the above values in the Equation (3.11) and (3.12) solving for D_r,D_i,N_u and N_θ to get horizontal and angular amplitude.

$$D_r = (K_{11} - \varpi^2 m)(K_{22} - \varpi^2 I) - K_{12}K_{21} - \varpi^2(C_{11}C_{22} - C_{12}C_{21})$$

$$D_r = -2.2949 \times 10^{15} N^2$$

$$D_i = \varpi\left[C_{22}(K_{11} - \varpi^2 m) + C_{11}(K_{22} - \varpi^2 I) - 2K_{12}C_{12}\right]$$

$$D_i = -3.4115 \times 10^{15} N^2$$

$$N_u = P_o^2\left[(K_{22} - \varpi^2 I)^2 + \varpi^2 {C_{22}}^2\right] + {M_o}^2(K_{12} + \varpi^2 {C_{12}}^2) - 2P_oM_o\left[K_{12}(K_{22} - \varpi^2 I) + \varpi^2 C_{22}C_{12}\right]$$

$$N_u = 2.63 * 10^{21} N^4 m^2$$

$$N_\theta = P_o^2({K_{12}}^2 - \varpi^2 {C_{12}}^2)^2 + {M_o}^2\left[(K_{11} + \varpi^2 m)^2 + \varpi^2 C_{11}\right] - 2P_oM_o\left[K_{12}(K_{11} - \varpi^2 m) + \varpi^2 C_{11}C_{12}\right]$$

$$N_\theta = 3.23 * 10^{21} N^4 rad^2$$

$$|u_o| = \left|\frac{D_1}{D}\right| = \frac{|D_1|}{|D|} = \sqrt{\frac{N_u}{{D_r}^2 + {D_i}^2}} \qquad |\theta_o| = \left|\frac{D_2}{D}\right| = \frac{|D_2|}{|D|} = \sqrt{\frac{N_\theta}{{D_r}^2 + {D_i}^2}}$$

$$|U_o| = \sqrt{\frac{2.63 \times 10^{21}}{(-2.29 \times 10^{15})^2 + (-3.4115 \times 10^{15})^2}} = 1.25 \times 10^{-5} m$$

$$|\theta_o| = \sqrt{\frac{3.23 \times 10^{21}}{(-2.29 \times 10^{15})^2 + (-3.4115 \times 10^{15})^2}} = 1.38 \times 10^{-5} rad$$

The total horizontal and rotational amplitude for excitation of force and moment by applying direct approach method is $1.25 \times 10^{-5} m$ and $1.38 \times 10^{-5} rad$ respectively.

Using the superposition / simplified method

In applying superposition approach we use equation (3.21) for force only acting and equation (3.22) for moment only acting.

When excited by horizontal force only

$$U_{op} = \frac{P_o\sqrt{\left[(K_{11} - m\varpi^2)^2 - \varpi^2 {c_{11}}^2\right]}}{mI\Delta}$$

$$u_{op} = 1.65 \times 10^{-5} m$$

Where, $\Delta = \sqrt{\left[\begin{array}{l}\left\{\varpi^4 - \left(\frac{K_{11}}{m} + \frac{K_{22}}{I} + \frac{C_{11}C_{22}}{mI} - \frac{{C_{12}}^2}{mI}\right)\varpi^2 + \left(\frac{K_{11}K_{22}}{mI} - \frac{{K_{12}}^2}{mI}\right)\right\}^2 + \\ \left\{\left(\frac{K_{11}C_{22}}{mI} + \frac{K_{22}C_{11}}{mI} - \frac{2K_{12}C_{12}}{mI}\right)\varpi - \left(\frac{C_{22}}{I} + \frac{C_{11}}{m}\right)\varpi^3\right\}^2\end{array}\right]} = 1.04\times10^{10}$

$$\theta_{op} = \frac{P_o\sqrt{\left[(K_{12} - \varpi^2{C_{12}}^2)^2\right]}}{mI\Delta}$$

$$\theta_{op} = 7.33\times10^{-6}\,rad$$

When excited by vertical moment only

$$U_{om} = \frac{M_o\sqrt{\left[({K_{12}}^2 - \varpi^2{C_{12}}^2)^2\right]}}{mI\Delta}$$

$$u_{om} = 5.36\times10^{-6}\,m$$

$$\theta_{om} = \frac{M_o\sqrt{\left[(K_{22} - I\varpi^2)^2 - \varpi^2C_{22}\right]}}{mI\Delta}$$

$$\theta_{om} = 1.2\times10^{-6}\,rad$$

When the footing is subjected to the action of both moment and horizontal force, the resulting amplitudes of sliding and rocking are obtained by adding the above solutions.

$$u_o = u_{op} + u_{om} = 1.65\times10^{-5} + 5.56\times10^{-6} = 2.18\times10^{-5}\,m$$

$$\theta_o = \theta_{op} + \theta_{om} = 7.33\times10^{-6} + 1.2\times10^{-6} = 8.53\times10^{-6}\,rad$$

The total horizontal and rotational amplitude for excitation of force and moment by applying superposition approach is $2.18\times10^{-5}\,m$ and $8.53\times10^{-6}\,rad$ respectively.

As we see from the above example the horizontal amplitude obtained by superposition method is larger than the direct approach method the reverse holds true for angular amplitude.

For the sensitivity and further comparative studies we use procedures that are explained in illustration example.

4 RESULTS AND DISCUSSION

In this chapter, a sensitivity and comparative studies are conducted using different solution methods. This is mainly to evaluate the accuracy, reliability and range of practical applicability of the proposed theoretical solutions. Thus for the sensitivity study the effect of aspect ratio, type of the soil, and embedment depth has been investigated. Furthermore, a comparative study has been conducted between the theoretical and experimental solutions. The experimental data are taken from Beredugo (1971). The two different theoretical formulations described in chapter 3 have been used. These are direct method which directly considers the combined effect of the force and the moment without simplification, and superposition method uses simple superposition of the separate action of force and moment. Both the horizontal translation and rocking amplitude are compared in surface and embedded footings. For embedded footing it is necessary to remember the impedance function method incorporates the side reaction of damping and stiffness coefficients in the base stiffness and damping coefficients therefore direct approach is appropriate to employ. For rectangular foundation for the two analytical approaches the force is applied in the short (lateral) direction on the other hand moment (rocking) is applied to the longer axis for the sensitivity study, we can refer to Figure (2.1).

The characteristics of machine foundation response is dependent on the following factors; the shape of the foundation-soil interface, the amount of embedment, the nature of the soil profile and the mode of vibration and frequencies of excitation.

For the sensitivity study the parameters varied include type of soil, aspect ratio and embedment ratio.

4.1 SENSITIVITY STUDY

The sensitivity study is carried out for three block foundations of size 6.36m X 6.36m X 2m, 4.5m X 9m X 2m and 3.18m X 12.72m X 2m, subjected to coupled horizontal and rocking vibrations. Three types of soil are considered (sand, clay and gravel). The embedment is also varied and different embedment ratios d/D (0, 0.25, 0.5, 0.75 and 1) are considered. The recommended and taken soil properties are given in table 4.1.

Table 4.1 Dynamic soil properties ((Briaud, 2013) and (Arya et al., 1984))

	Recommended values		Values taken	
Soil type	G_{max} (MPa)	ν	G_{max} (MPa)	ν
Medium dense sand and gravel	34-172	0.30-0.40	96.5	0.35
Firm Clay	7-36	0.20-0.40	30	0.40
Dense sand and Gravel	72-360	0.40-0.50	216	0.45

4.1.1 Machine data

To check how the theoretical methods work in real life reciprocating compressor having the following data is analyzed for the sensitivity study.

Weight of compressor=12755kg

Weight of gas coolers=1970kg

Weight of snubbers=3180kg

Weight of motor=8165kg

Total weight of machine=26070kg

Mass moment of inertia of machine=129643.5kgm^2

Combined center of gravity of machinery and equipment from top of foundation=0.7m

Point of application of horizontal force from top of foundation=0.9m

Compressor operating speed=585rpm

Maximum horizontal primary force=3.22kN

Maximum Rocking primary moment=15.32kN

An approach involving normalized quantities is employed whereby the ordinates for frequency includes both the excitation and natural frequency and the abscissa for the aspect ratio and embedment ratio are in normalized fashion as normalization covers wide range of frequencies and to make generalization without considering the unit of measurement.

4.1.1.1 Soil type medium dense sand

Undamped natural frequency

In the sensitivity study constant force excitation is used. The procedures implemented in this subsection are the same as in illustration example. To evaluate the natural frequency Equation (3.28) is used.

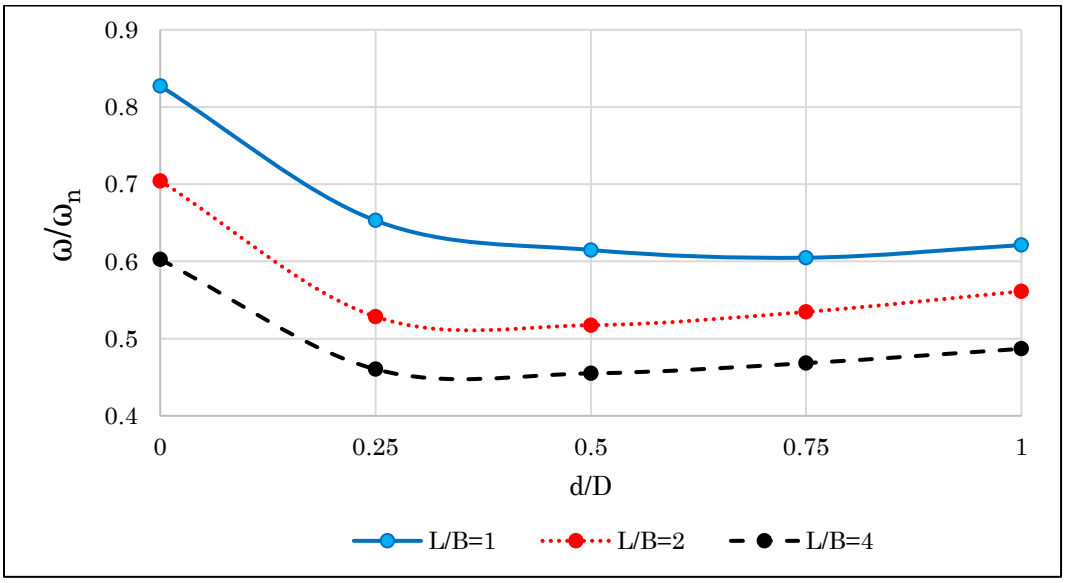

Figure 4.1 effect of aspect ratio and embedment ratio on frequency ratio utilizing undamped natural frequency for sand

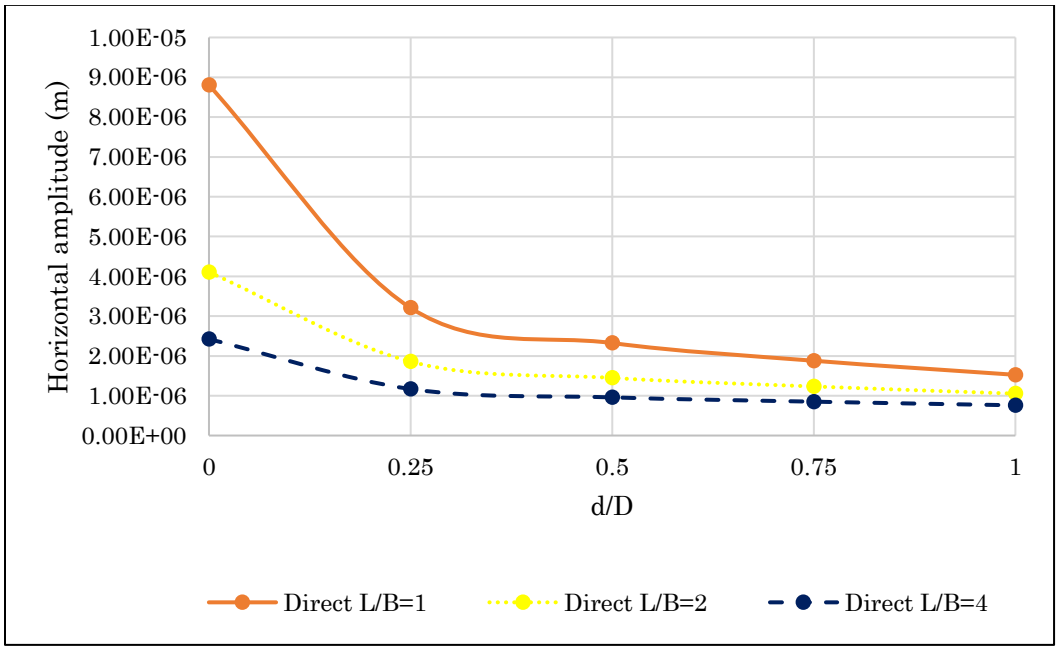

(a)

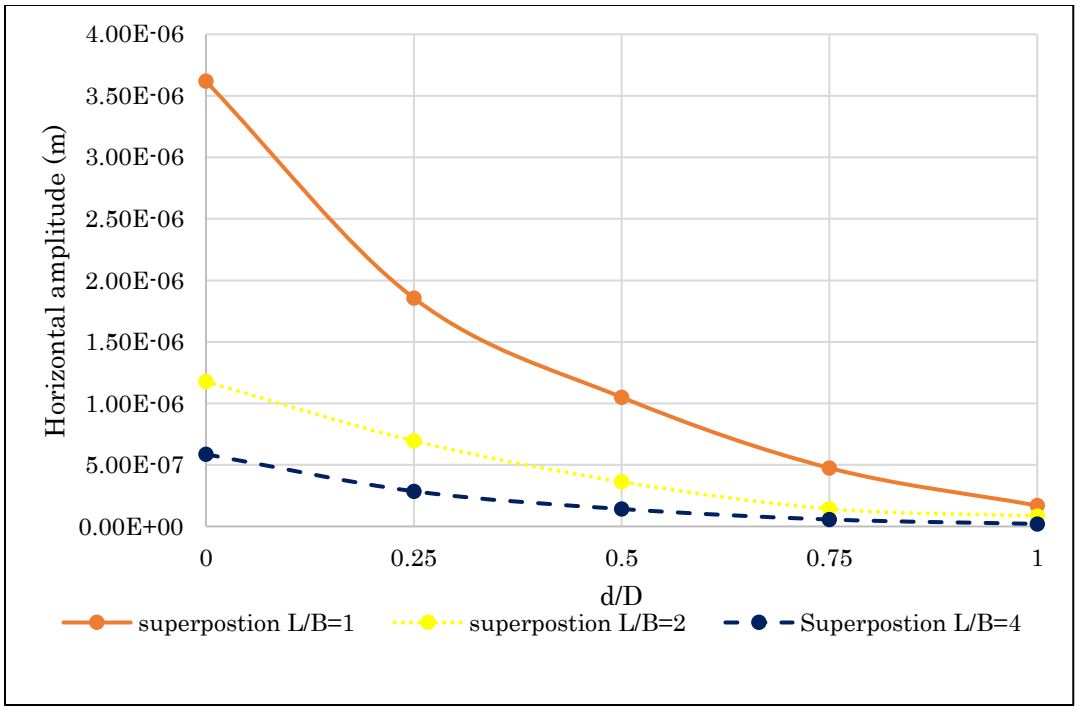

(b)

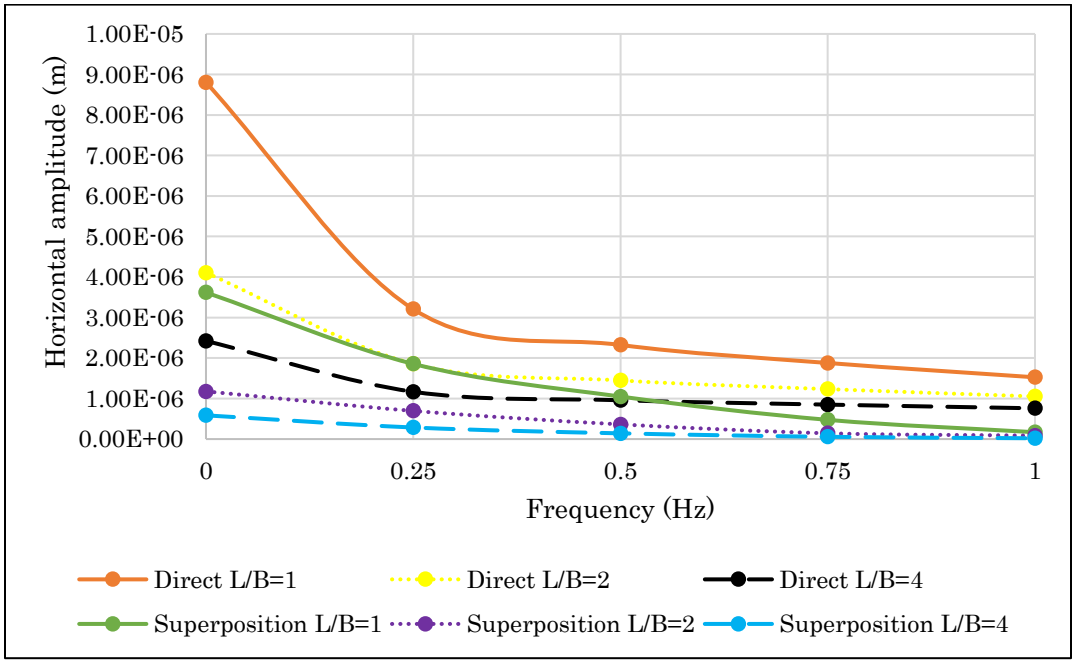

(c)

Figure 4.2 effect of aspect ratio and embedment ratio on horizontal amplitude utilizing undamped natural frequency and (a) direct (b) superposition approach (c) comparison between direct and superposition method for sand

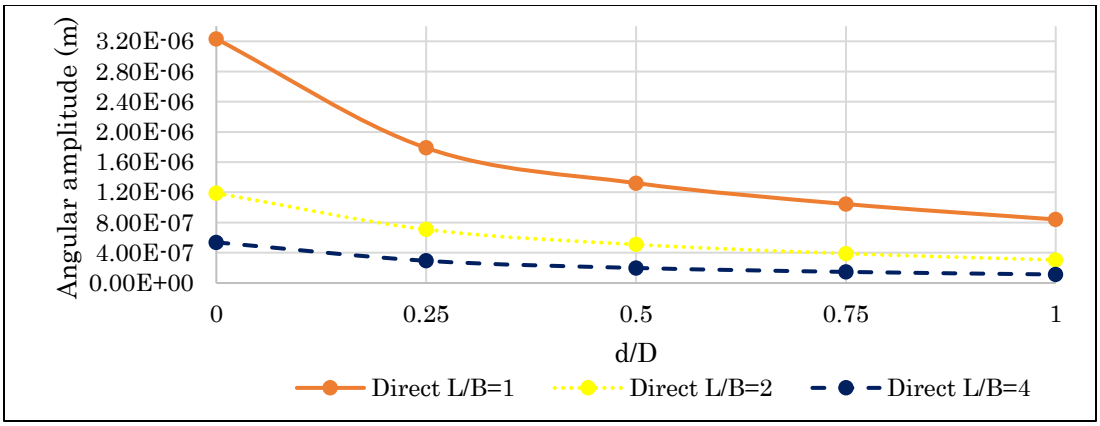

(a)

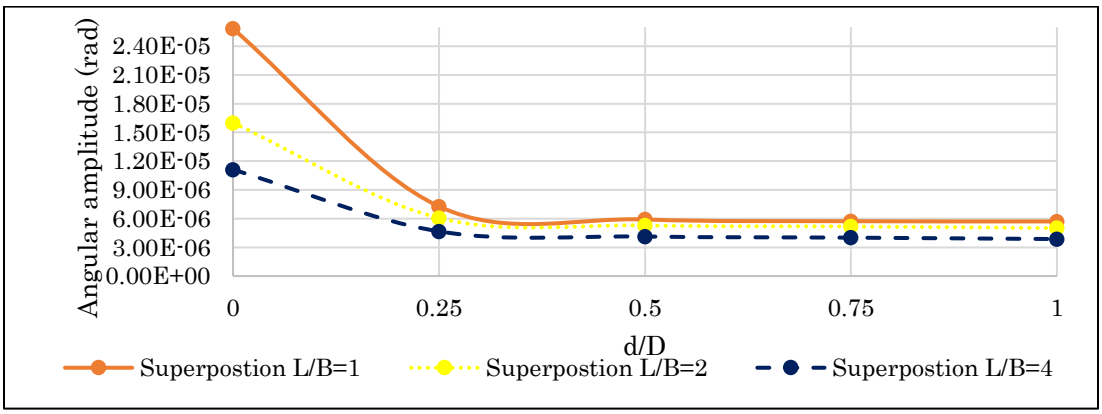

(b)

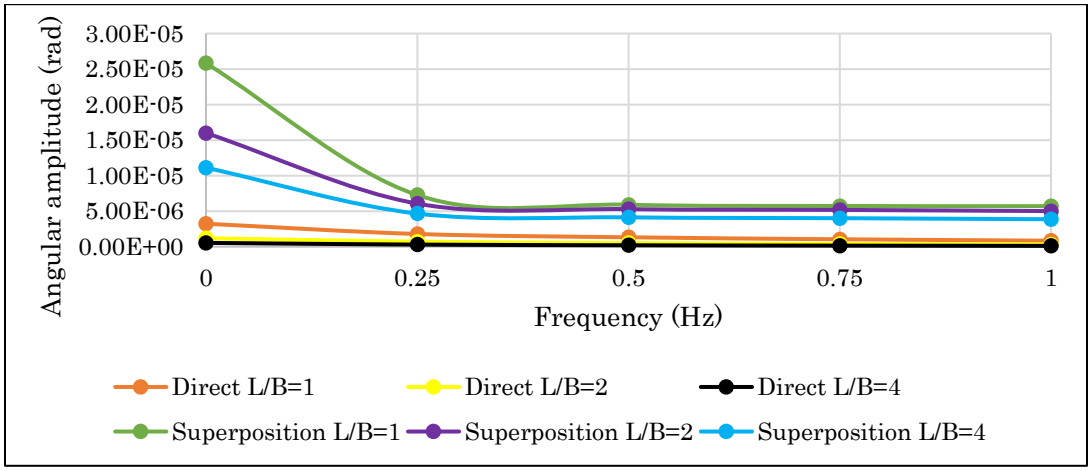

(c)

Figure 4.3 effect of aspect ratio and embedment ratio on Angular amplitude utilizing undamped natural frequency and (a) direct (b) superposition approach (c) comparison between direct and superposition method for sand

In order to make an easy comparison between the direct and superposition approach the plot of horizontal and angular amplitude are presented in Figure 4.2(c) and 4.3 (c) respectively for undamped natural frequency.

In the case of undamped natural frequency as shown in Figures 4.1-4.3, in general we can observe that

- Regardless of the embedment of the foundation the natural frequency is smaller for square foundations these increases with increasing aspect ratio. Note that ω_n is the denominator of the normalized ordinates.
- Regardless of the aspect ratio the natural frequency increases with increasing embedment.
- Direct approach regard less of the emedemet and the aspect ratio consistently larger estimates of horizontal vibration amplitude in contrast with superposition approach this trend is reversed in the case of angular amplitude.
- Horizontal and angular amplitude decreases when the aspect ratio increases regardless of embedment depth for both direct and superposition approach.

Damped natural frequency

In the following subsection the damped natural frequency is evaluated by Equation (3.26).

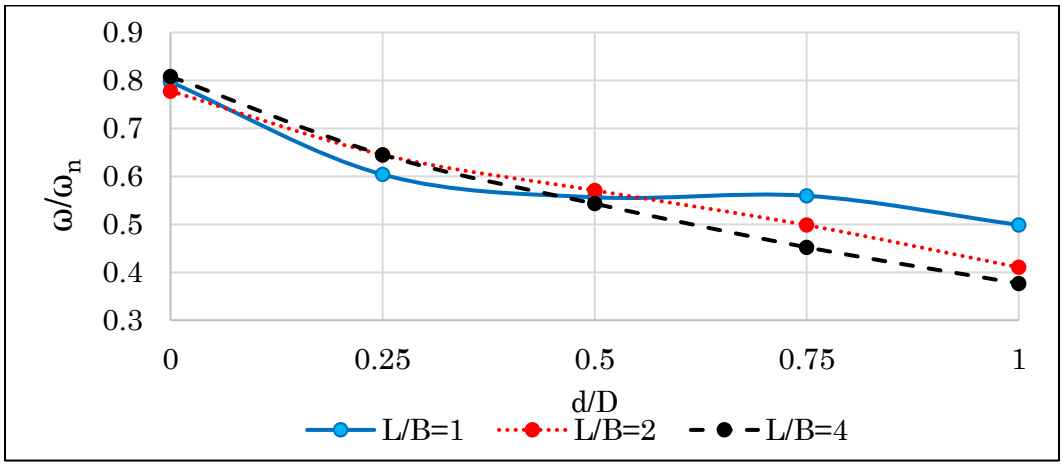

Figure 4.4 effect of aspect ratio and embedment ratio on frequency ratio utilizing damped natural frequency for sand

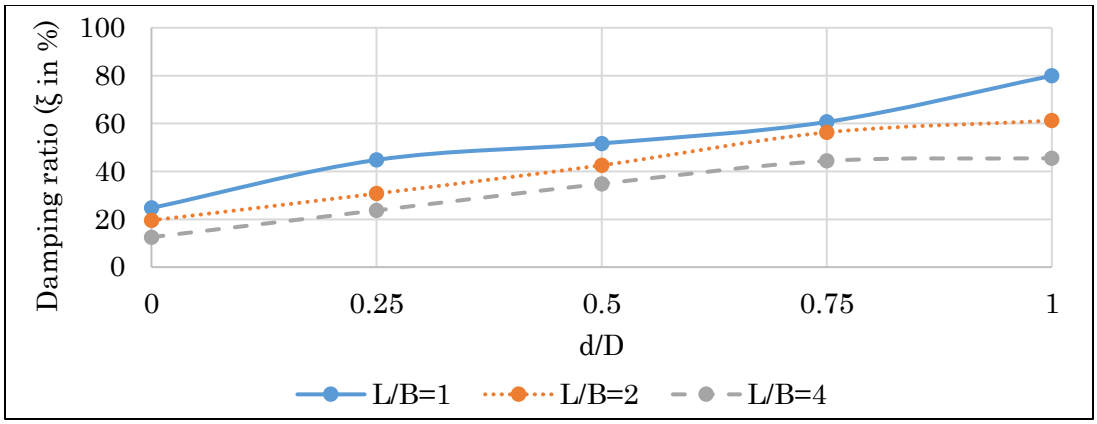

Figure 4.5 effect of aspect ratio and embedment ratio on damping ratio utilizing damped natural frequency for sand

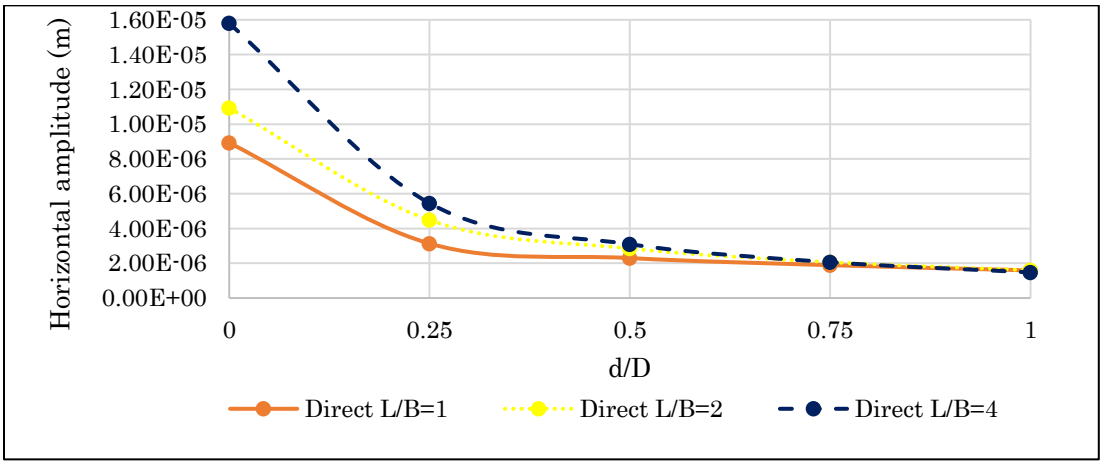

(a)

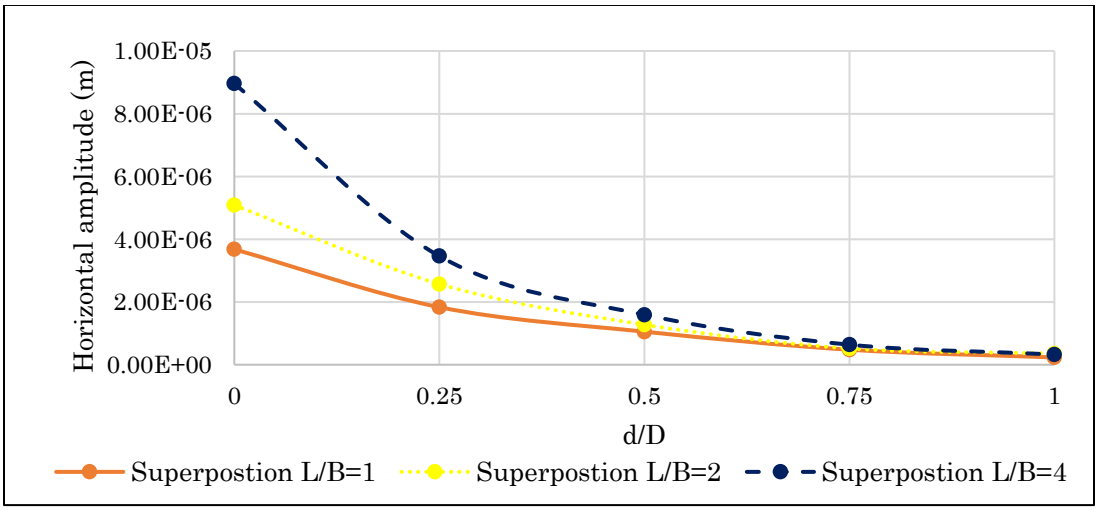

(b)

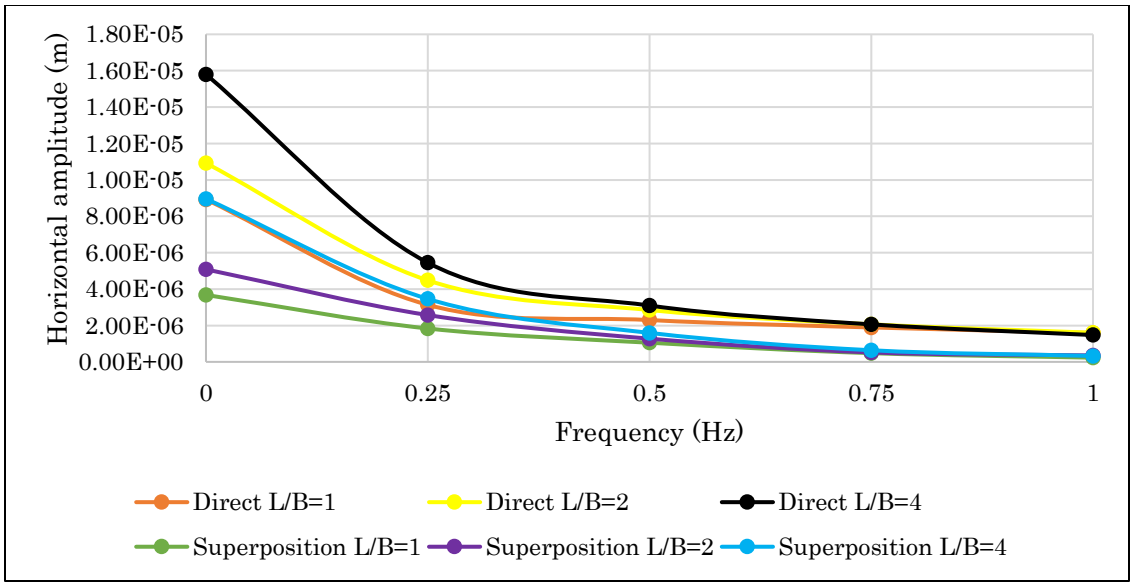

(c)

Figure 4.6 effect of aspect ratio and embedment ratio on horizontal amplitude utilizing damped natural frequency and (a) Direct (b) Superposition approach (c) comparison between direct and superposition method for sand

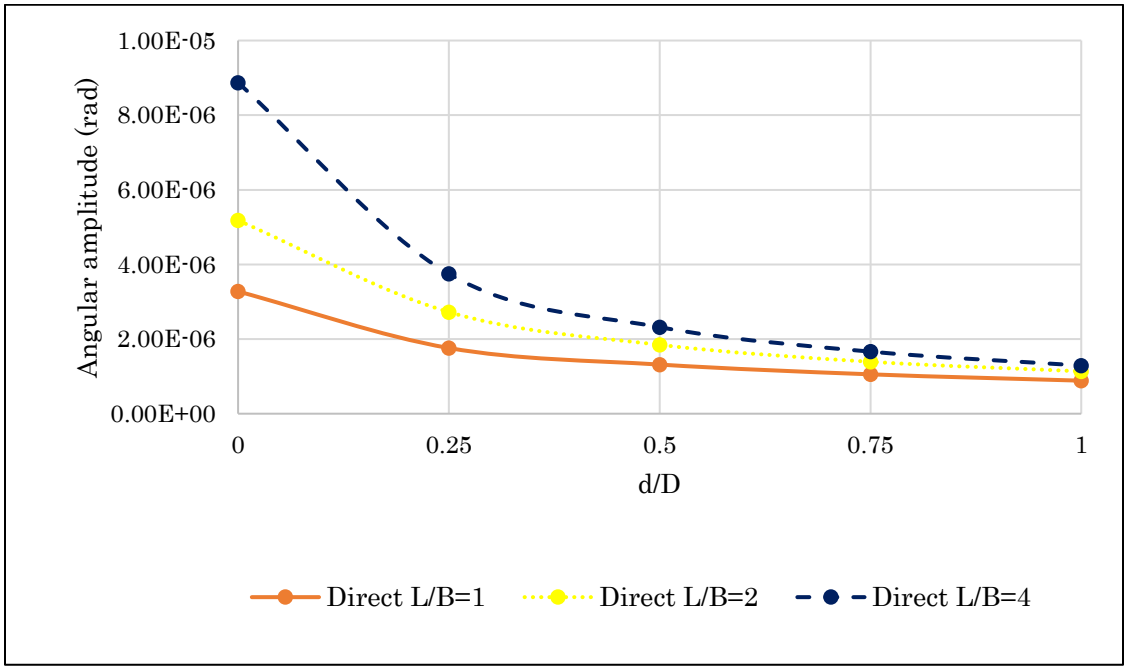

(a)

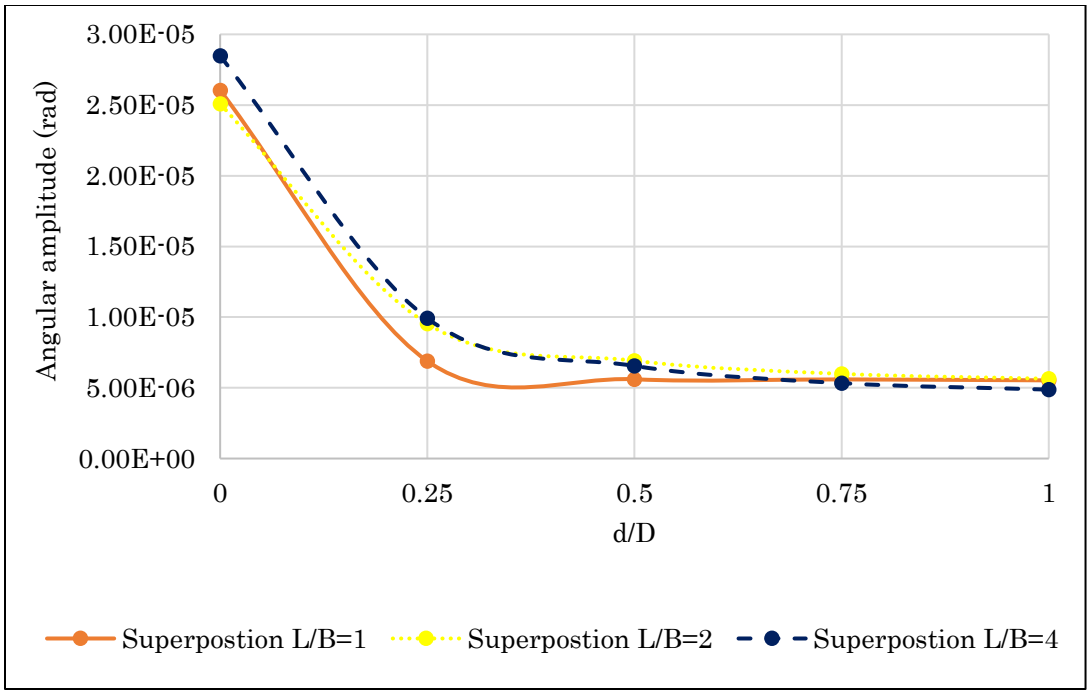

(b)

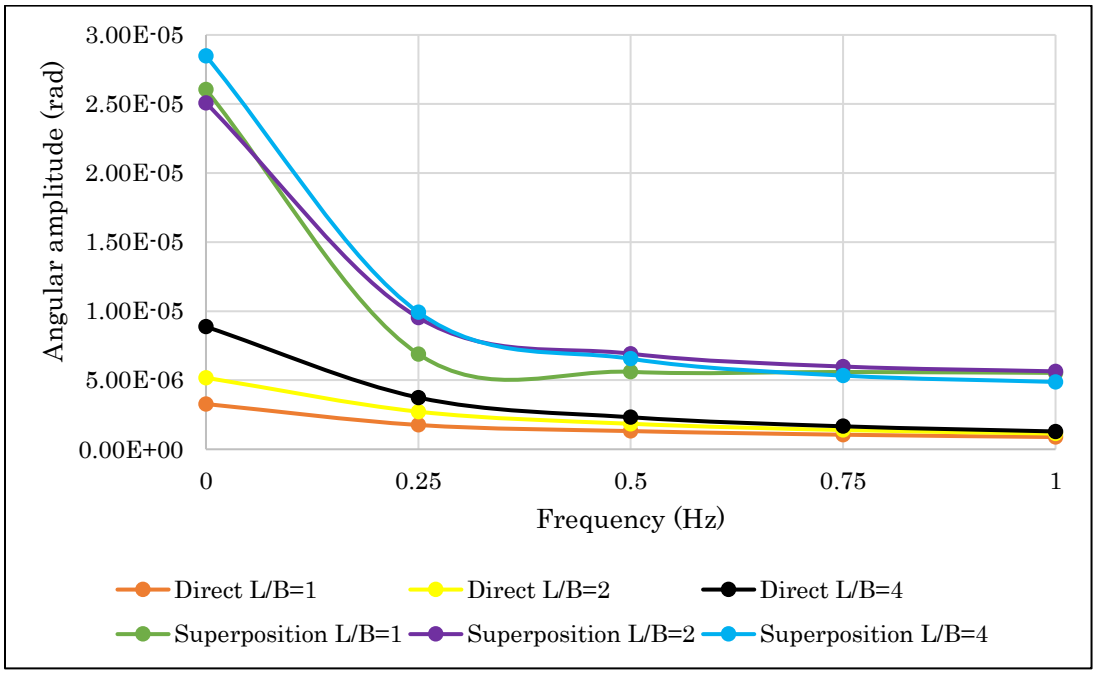

(c)

Figure 4.7 effect of aspect ratio and embedment ratio on Angular amplitude utilizing damped natural frequency and (a) Direct (b) Superposition approach (c) comparison between direct and superposition method for sand

In order to make an easy comparison between the direct and superposition approach the plot of horizontal and angular amplitude are presented in Figure 4.6(c) and 4.7 (c) respectively for damped natural frequency.

In the case of damped natural frequency as shown in (Figures 4.4-4.7), we can conclude the following

- The influence of aspect ratio is not as clear as in the case of undamped system in this case the influence of aspect ratio is less on the frequency of the damped system compared to that of the undamped system.
- As embedment increases the natural frequency also increases as before
- As embedment increases the damping ratio also increases this is because the embedment of the material on the side of the foundation is an additional medium for waves to propagate sideways therefore there is an additional damping.
- When the aspect ratio increases damping decreases note that the area of the footing is constant.
- When the aspect ratio increases the horizontal and angular amplitude increases regardless of embedment depth this is because of the effect of damping is high when the aspect ratio decreases.
- Superposition approach regard less of the emedemet and the aspect ratio consistently larger estimates of angular vibration amplitude in contrast with direct approach this trend is reversed in the case of horizontal amplitude.

The sensitivity study shown above is for sand using undamped and damped natural frequency. The same results are found for other type of soils (clay and gravel) as shown in Appendix B.

In general we can conclude that for the three types of soil gravel has relatively smaller horizontal and angular amplitude than sand whereas sand relatively has smaller translational and rocking amplitude than clay regardless of aspect ratio and embedment for both direct and superposition method.

4.2 COMPARISON WITH EXISITING EXPERIMENTAL DATA

A comparative study is conducted between theoretical formulas by applying direct approach and superposition approach method to compare with experimental field data reported by (Beredugo, 1971) for determining horizontal and angular amplitude in surface and embedded footings.

The properties of test footings, soil and machine are given in section 3.2. The stiffness and damping are determined using formula and charts developed by (Gazetas G. , 1991).

Similar to the illustration example the damping and stiffness are determined iteratively and listed in summarized form Table 4.2 and 4.3.

4.2.1.1.1.1Table 4.2 damping values for different embedment depth

d (m)	crx,emb	crx,tot	cy,emb	cy,tot
0	248.002	4437.76	90429.22747	128160
0.2286	67353.0646	73614.7882	282835.0895	357227.554
0.4572	146392.3575	155075.8593	475515.961	534667.857
0.9144	305637.035	319587.6677	862746.563	900036.297

Table 4.3 stiffness and damping ratio values for different embedment depth

d (m)	K_{rx},sta (Nm)	K_{rx},dyn(Nm)	K_y,sta (N/m)	K_y,dyn (N/m)	ξ1	ξ2
0	7199007.205	6907599.2	59664388.5	62207212.63	0.033427	0.378507
0.2286	19036597.84	17714353.84	201781563	210455544.8	0.283776	0.67583
0.4572	39376328.86	35431560.99	234714335	241359311.9	0.426648	0.950053
0.9144	101159822.9	85871673.38	264444779	229533092.1	0.559356	1

4.2.2 Surface Foundation for Undamped and Damped natural frequency

Horizontal amplitude for surface

The analysis based on the theoretical formulas is generally conducted using impedance function method. From the analysis Figure 4.8 to 4.10 represents the value of horizontal amplitudes using different eccentric moments (0.04859Nm, 0.09605Nm and 0.19323Nm) for excitation frequency range of 10-60Hz

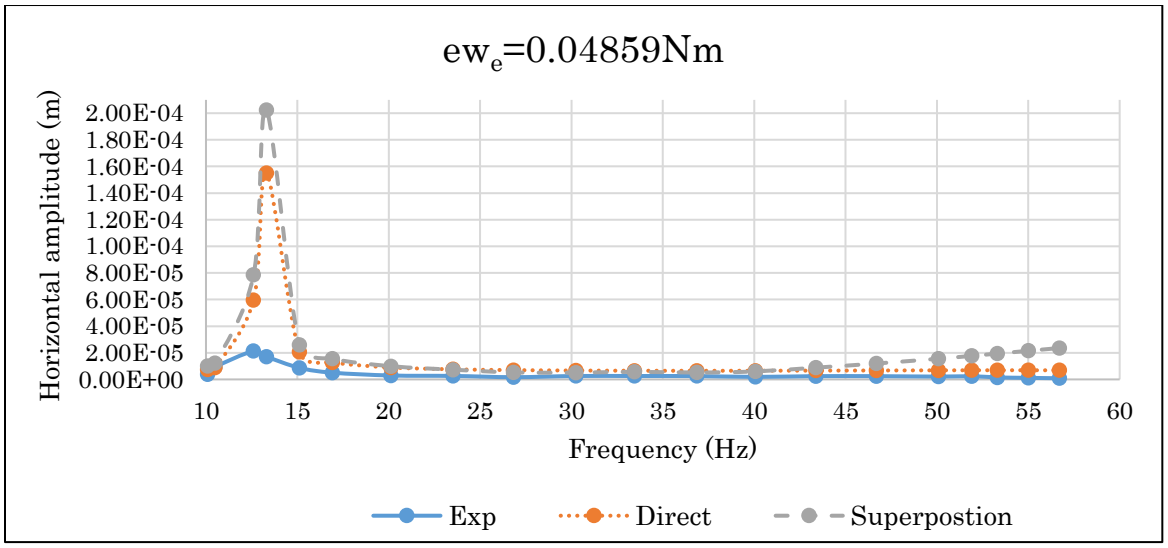

(a)

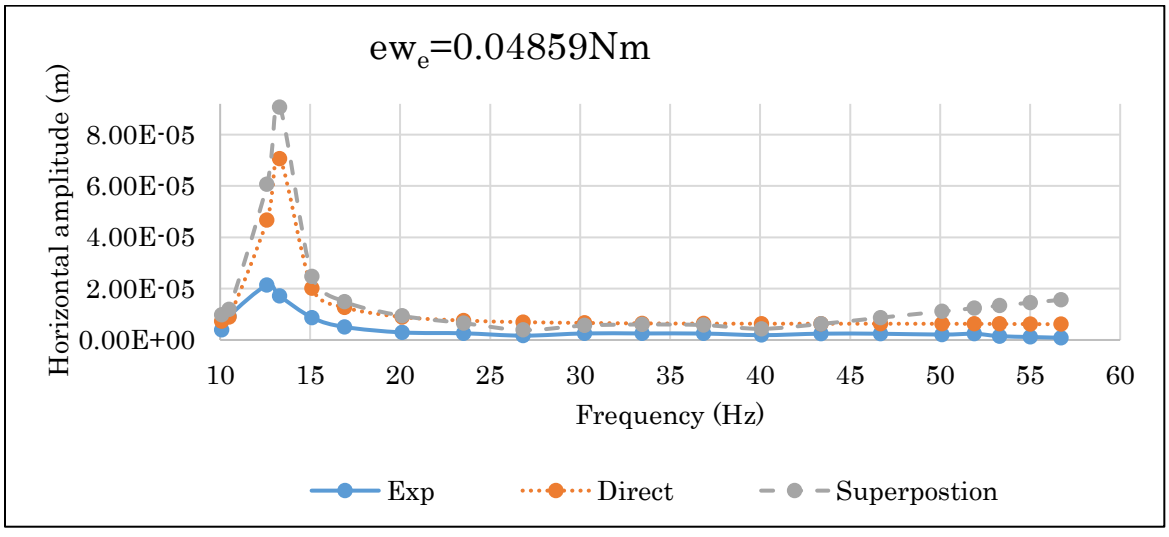

(b)

Figure 4.8 Surface horizontal amplitude (a) undamped natural frequency (b) damped natural frequency, ew$_e$=0.04859Nm

Observations from Figure 4.8

- ✓ The experimental natural frequency occur at 12.6Hz with resonant horizontal amplitude of $2.135*10^{-5}$m.The undamped and damped natural frequency using impedance function method occur at 13Hz for both direct approach and superposition approach method. The resonant horizontal amplitude for direct approach method is $1.55*10^{-4}$m and $7.07*10^{-5}$ and for superposition approach method is $2.02*10^{-4}$m and $9.07*10^{-5}$ undamped and damped respectively.

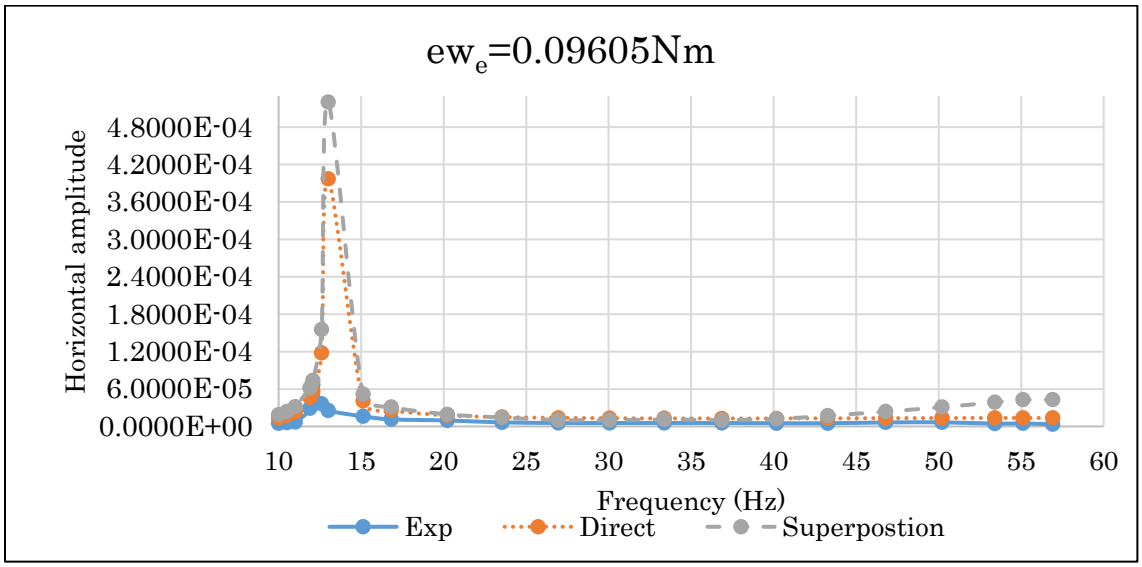

(a)

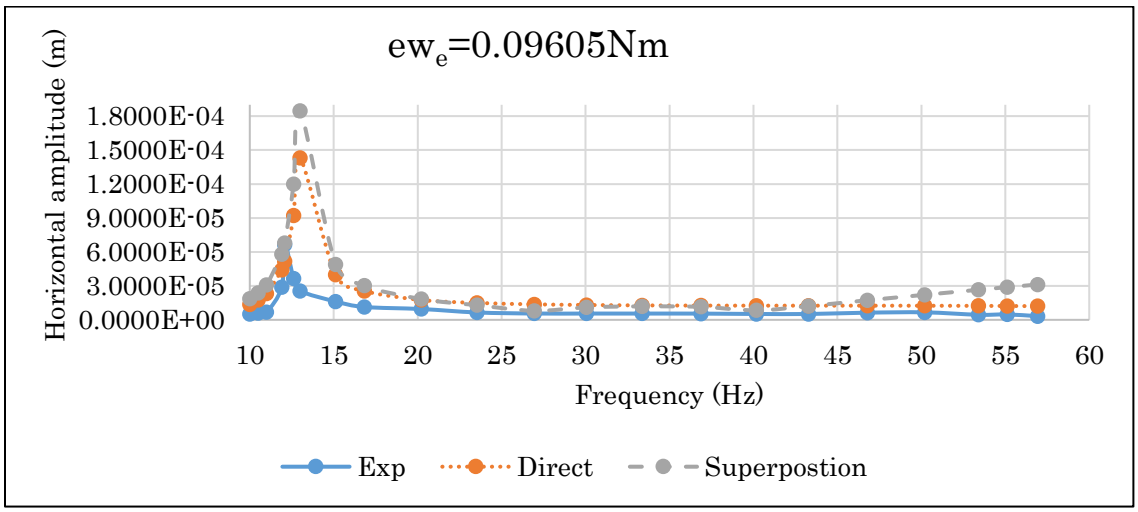

(b)

Figure 4.9 Surface horizontal amplitude (a) undamped natural frequency (b) damped natural frequency, ew_e=0.09605Nm

Observations from figure 4.9

- ✓ The experimental natural frequency occur at 12.08Hz with resonant horizontal amplitude of $6.6548*10^{-5}$m, the undamped and damped natural frequency for direct approach and superposition approach method using impedance function method occur at 13Hz. The resonant horizontal amplitude for direct approach method is $3.97*10^{-4}$m and $1.43*10^{-4}$ and for superposition approach method is $5.2*10^{-4}$m and $1.85*10^{-4}$ damped and undamped respectively.

.

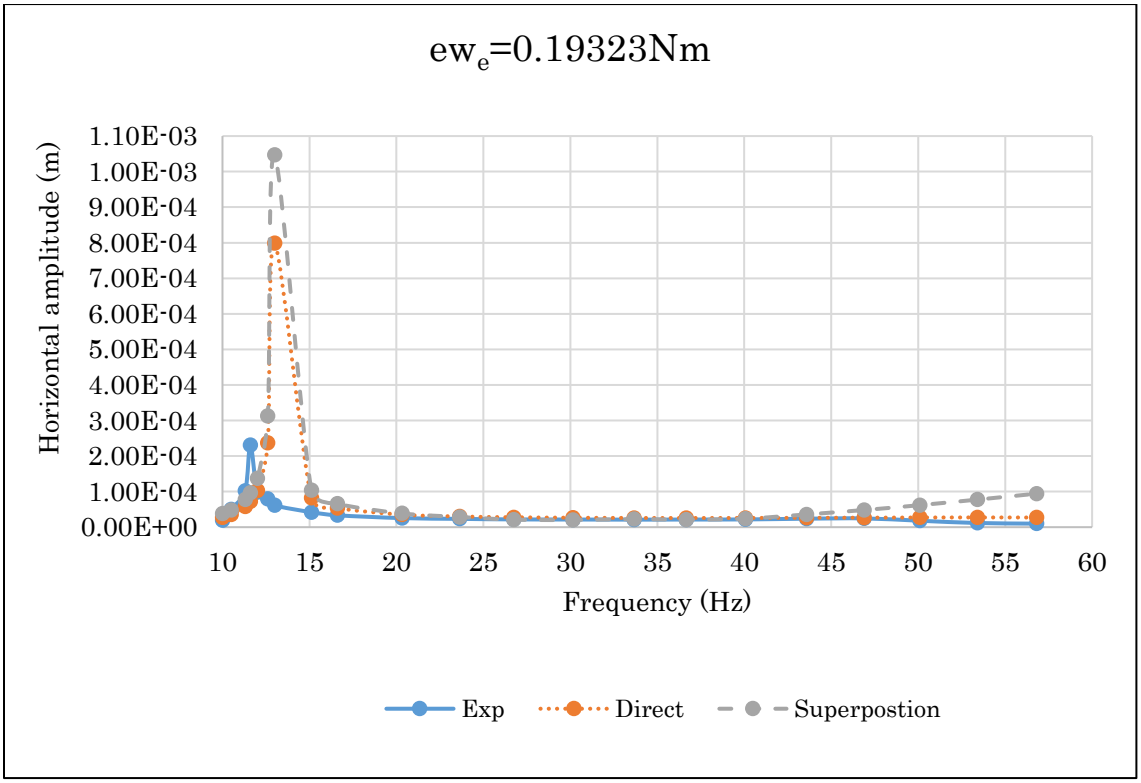

(a)

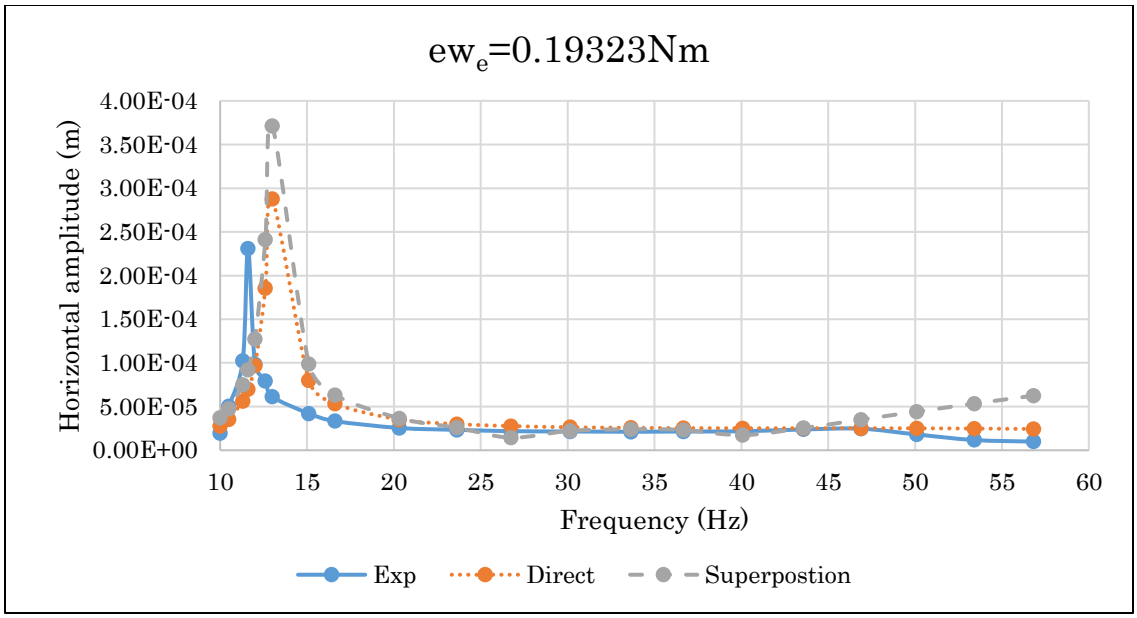

(b)

Figure 4.10 Surface horizontal amplitude (a) undamped natural frequency (b) damped natural frequency, ew$_e$=0.19323Nm

Observations from Figure 4.10 for horizontal amplitude

- ✓ The experimental natural frequency occur at 11.5Hz with resonant horizontal amplitude of $2.3114*10^{-4}$m.The undamped and damped natural frequency using impedance function method occur at 13Hz for both direct and superposition approach method. The resonant horizontal amplitude for direct approach method is $7.98*10^{-4}$m and $2.88*10^{-4}$ and for superposition approach method is $1.05*10^{-3}$ and $3.71*10^{-4}$ undamped and damped respectively.

Over all observation for Figure 4.8-4.10

The resonant frequency has shifted a little bit to the right in the case of the two analytical methods with respect to the experimental value while these difference is insignificant. However the difference of horizontal amplitude is quite high. Comparison between the two analytical methods shows that the difference in terms of frequency is nonexistence but there is some noticeable difference in terms of amplitude particularly at resonance. Stiffness is over estimated and the actual damping is much

larger than estimated by the impedance function method it is not the shortcoming of the two approaches. When we go slightly beyond the resonant to either side there is no significance difference.

When the eccentric moment increases the percentage error decreases for the direct and superposition methods in predicting the experimental results.

Direct approach is better than superposition approach method in predicting experimental horizontal amplitude.

Rocking (Angular) amplitude for surface

From the analysis Figure 4.11 and 4.12 represents the value of angular amplitude for eccentric moment (0.09605Nm and 0.19323Nm) for excitation frequency range of 10-60Hz.

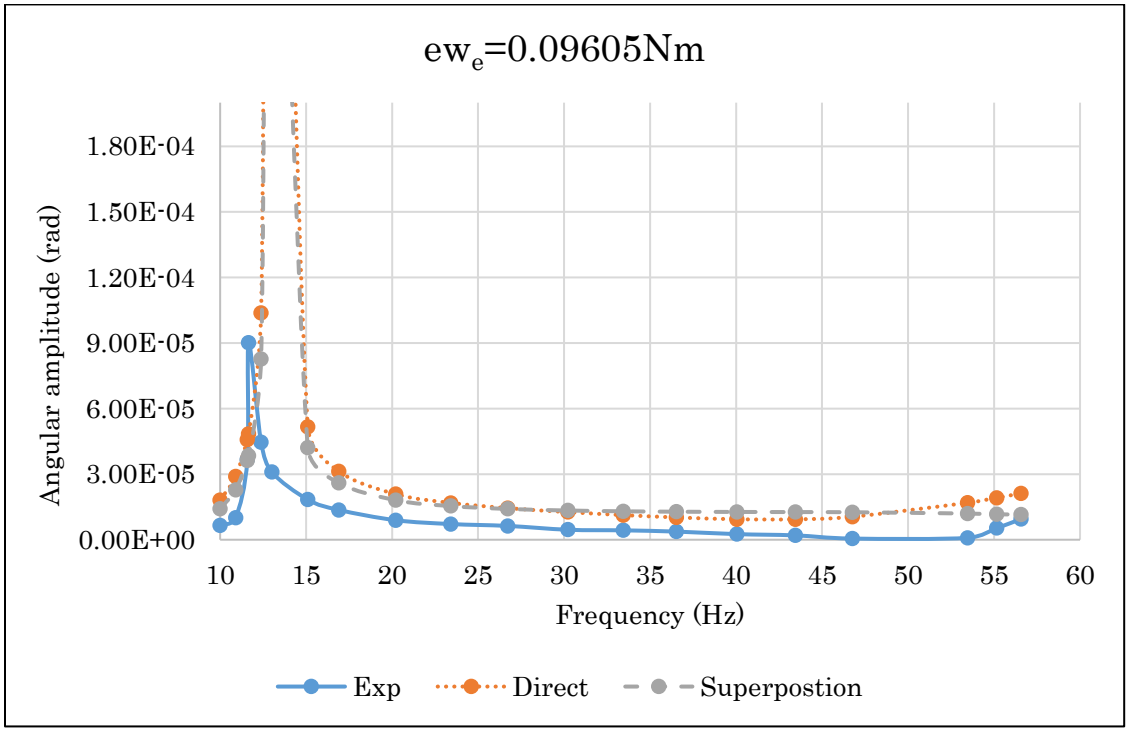

(a)

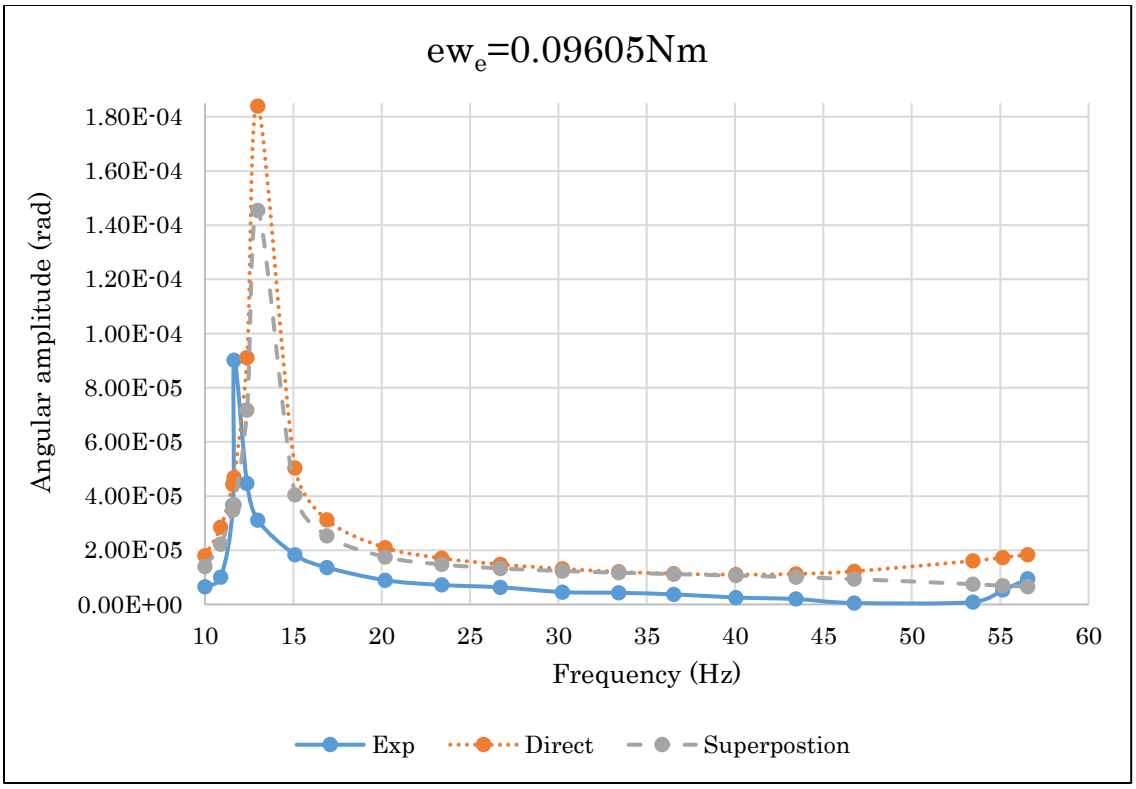

(b)

Figure 4.11 Surface angular amplitude (a) undamped natural frequency (b) damped natural frequency, ew$_e$=0.09605Nm

Observations from Figure 4.11 for angular amplitude

- ✓ The experimental natural frequency occur at 11.5Hz with resonant angular amplitude of 9.2*10-5rad.The undamped and damped natural frequency using impedance function method occur at 13Hz for both direct and superposition approach method. The resonant angular amplitude for direct approach method is 5.09*10-4rad and 1.84*10-4rad and for superposition method is 4.08 *10-4 and 1.45*10-4rad undamped and damped respectively.

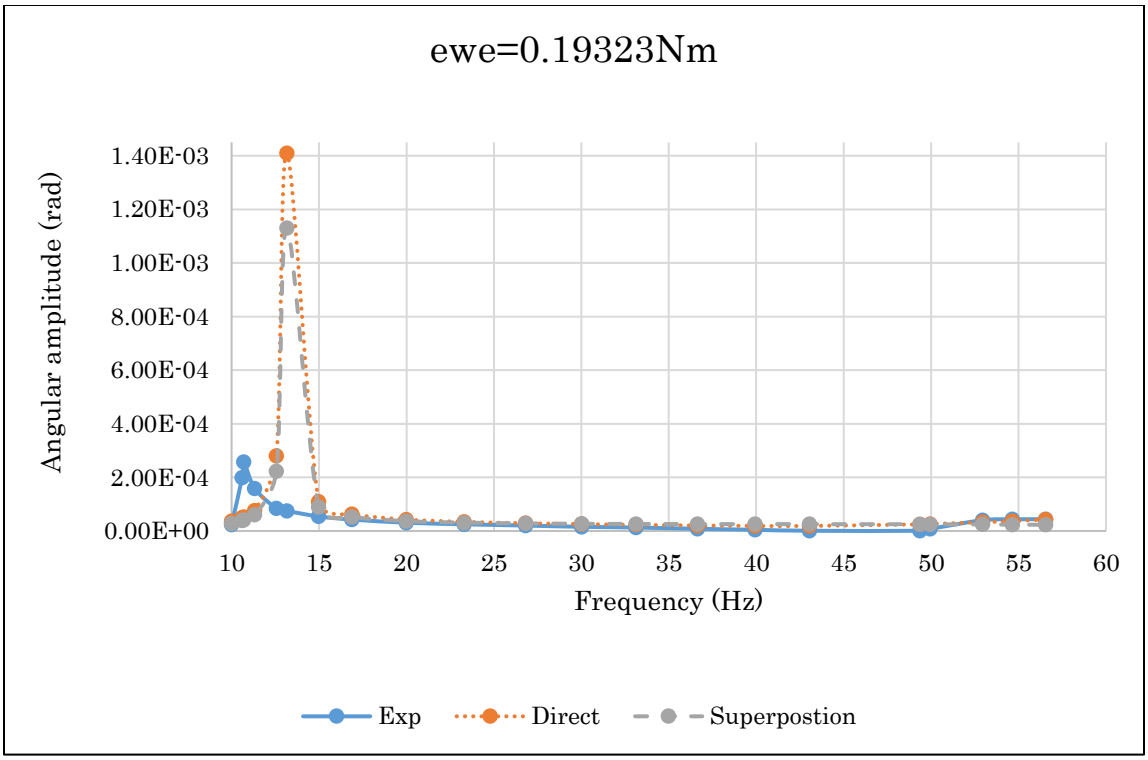

(a)

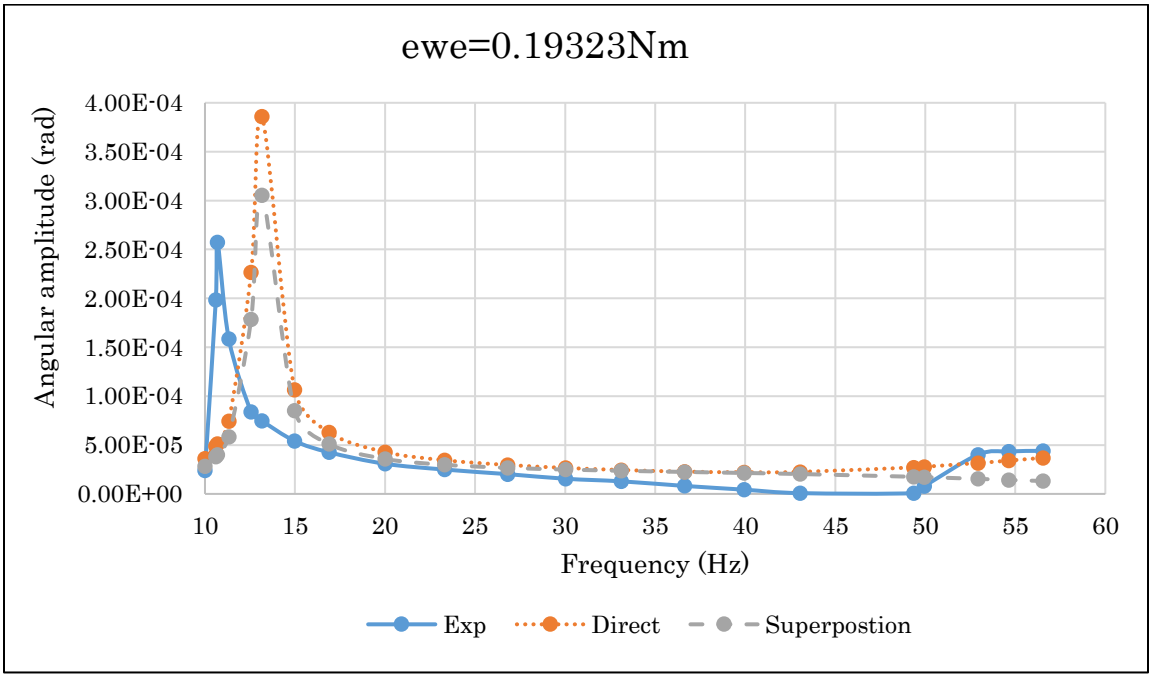

(b)

Figure 4.12 Surface angular amplitude (a) undamped natural frequency (b) damped natural frequency, ew_e=0.19323Nm

Observations from figure 4.12 for angular amplitude

- ✓ The experimental natural frequency occur at 10.75Hz with resonant angular amplitude of $2.57*10^{-4}$rad.The undamped and damped natural frequency using impedance function method occur at 13Hz for both direct and superposition approach method. The resonant angular amplitude for direct approach method is $1.41*10^{-3}$rad and $3.86*10^{-4}$rad and for superposition approach method is $1.13*10^{-3}$ and $3.05*10^{-4}$rad undamped and damped respectively.

Over all observation for Figure 4.11-4.12

The resonant frequency has shifted a little bit to the right in the case of the two analytical methods with respect to the experimental value while these difference is insignificant. However the difference of angular amplitude is quite high. Comparison between the two analytical methods shows that the difference in terms of frequency is nonexistence but there is some noticeable difference in terms of amplitude particularly at resonance. When we go slightly beyond the resonant to either side there is no significance difference. When the eccentric moment increases the percentage error decreases for the direct and superposition methods in predicting the experimental results. Superposition approach better than direct approach method in predicting experimental angular amplitude.

When the eccentric moment increases the discrepancy between the two analytical approaches is nearly constant for resonant horizontal and angular amplitudes. Stiffness is over estimated and the actual damping is much larger than estimated by the impedance function method it is not the shortcoming of the two approaches.

4.2.3 Embedded Foundations for Undamped and Damped natural frequency

Horizontal amplitude for effective contact height d=0.2286m (d/D=0.1875)

From the analysis of Figure 4.13 to 4.15 represents the of value of the horizontal amplitude for effective embedment depth (d) of 0.2286m for different eccentric moments (0.09605Nm,0.19323Nm and 0.28928Nm) and for excitation frequency range of 10-60Hz.

Observations from figure 4.13 for horizontal amplitude

- ✓ The experimental natural frequency occur at 22.4Hz with resonant horizontal amplitude of $4.4196*10^{-5}$m, whereas applying impedance function method for direct approach method occur at 24.6Hz with $1.884*10^{-5}$m and $1.86*10^{-5}$m and for superposition approach method 23.8Hz with $2.667*10^{-5}$ and $2.62*10^{-5}$ for undamped and damped natural frequency respectively.

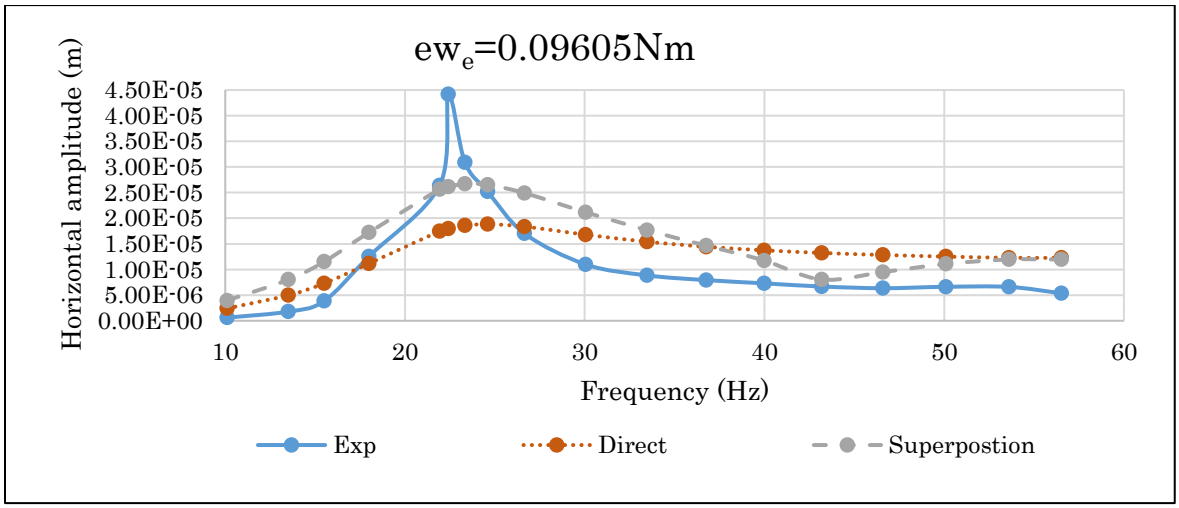

(a)

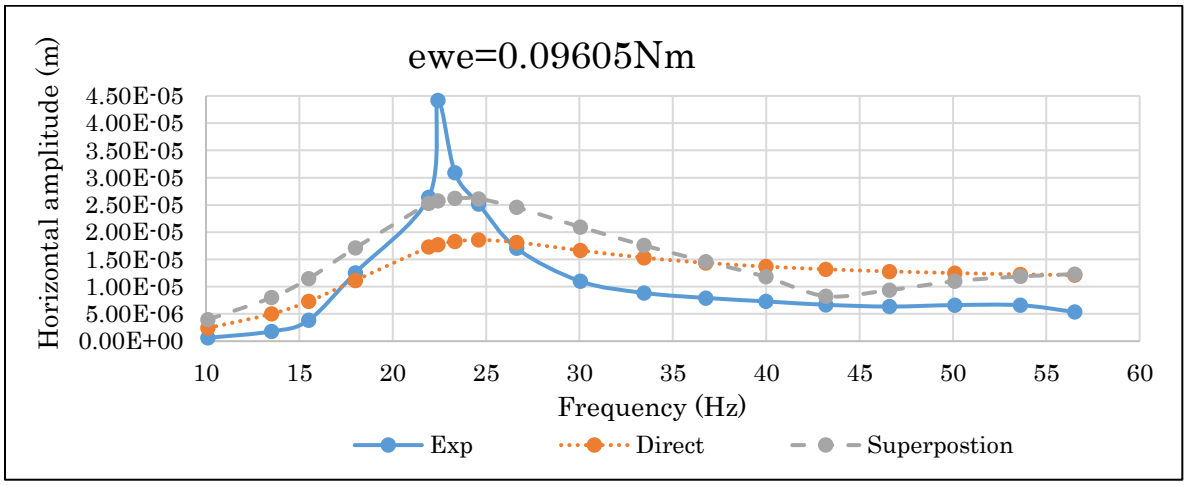

(b)

Figure 4.13 Embedded horizontal amplitude (a) undamped natural frequency (b) damped natural frequency, ew$_e$=0.09605Nm and d=0.2286m

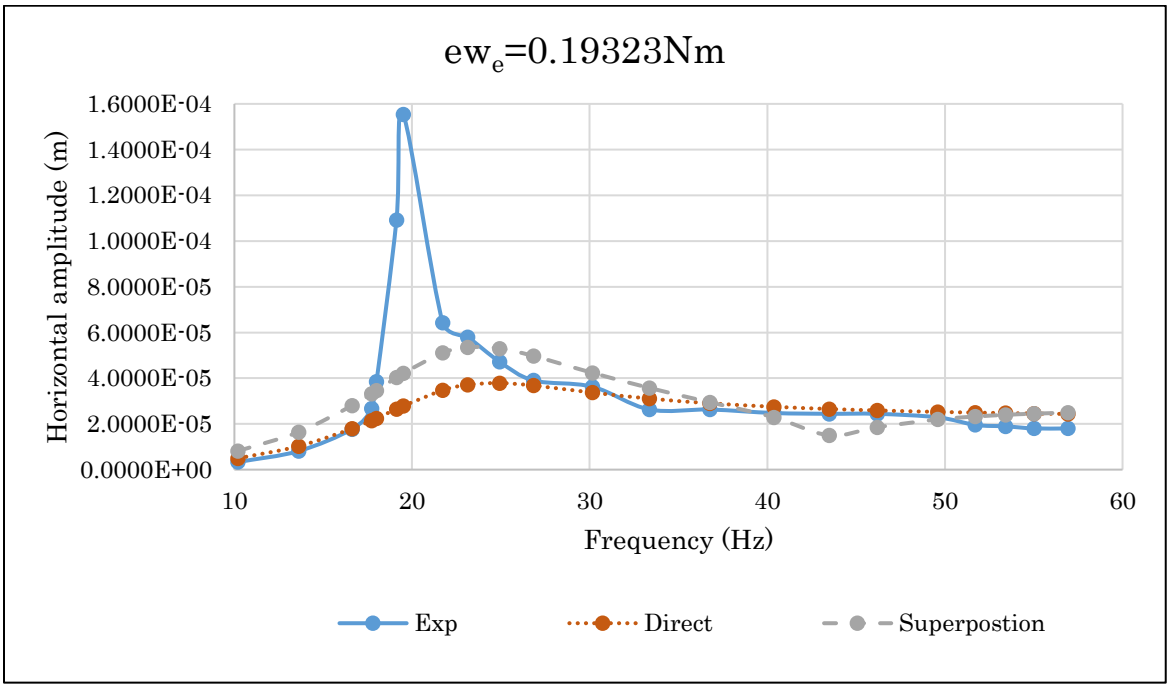

(a)

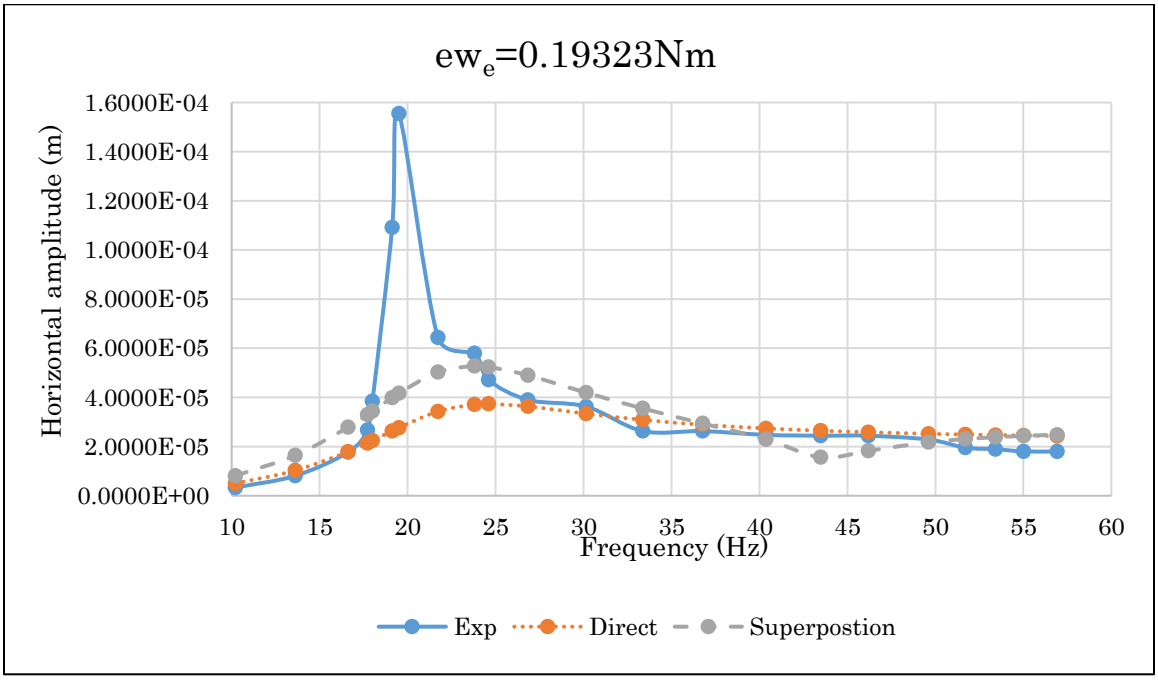

(b)

Figure 4.14 Embedded horizontal amplitude (a) undamped natural frequency (b) damped natural frequency, ew$_e$=0.19323Nm and d=0.2286m

Observations from figure 4.14 for horizontal amplitude

- ✓ The experimental natural frequency occur at 19.5Hz with resonant horizontal amplitude of $1.5545*10^{-4}$m, whereas applying impedance function method for direct approach method occur at 24.6Hz with $3.79*10^{-5}$m and $3.74*10^{-5}$m and for superposition approach method 23.8Hz with $5.37*10^{-5}$ and $5.28*10^{-5}$ for undamped and damped natural frequency respectively.

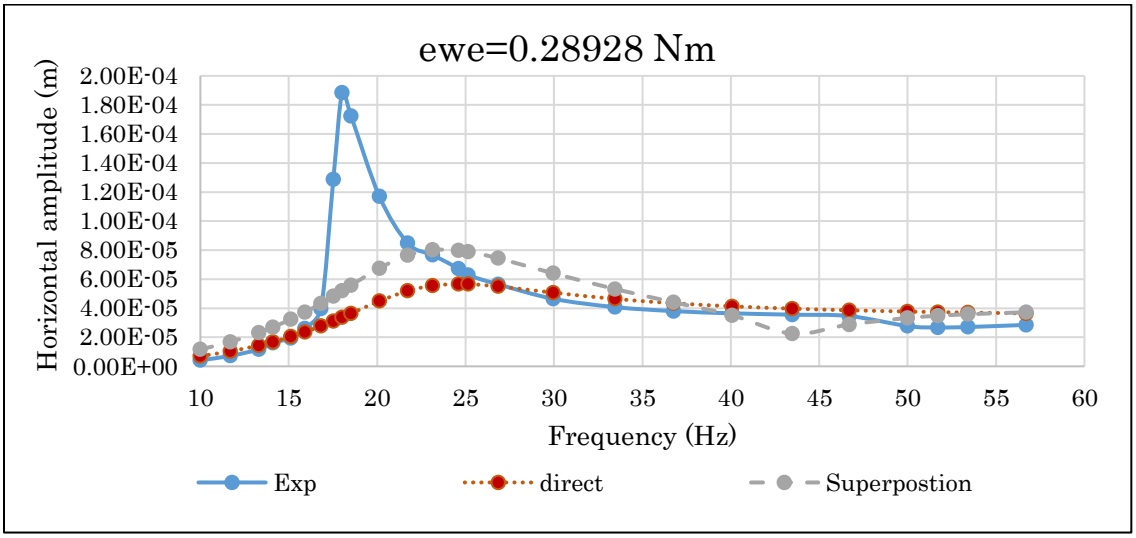

(a)

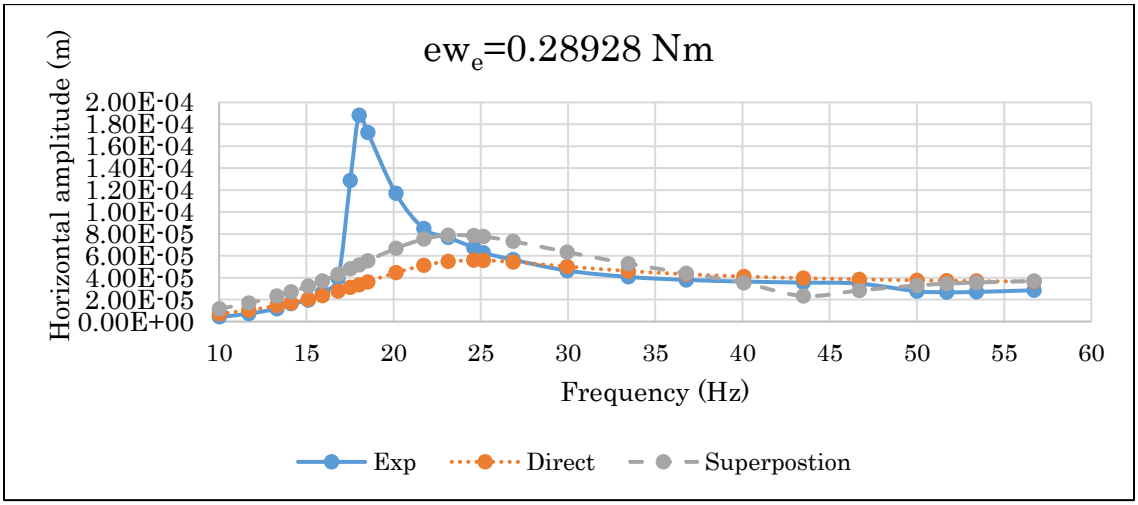

(b)

Figure 4.15 Embedded horizontal amplitude (a) undamped natural frequency (b) damped natural frequency, ew_e=0.28928Nm and d=0.2286m

Observations from figure 4.15 for horizontal amplitude

- ✓ The experimental natural frequency occur at 18Hz with resonant horizontal amplitude of $1.88*10^{-4}$m, whereas using impedance function method for direct approach method occur at 24.6Hz with $5.67*10^{-5}$m and $5.59*10^{-5}$m and superposition approach method 23.8Hz with $8.01*10^{-5}$ and $7.88*10^{-5}$ for undamped and damped natural frequency respectively.

Rocking (angular) amplitude for effective contact height d=0.2286m (d/D=0.1875)

From the analysis of Figure 4.16 to 4.18 represents the of value of the angular amplitude for effective embedment depth (d) of 0.2286m for different eccentric moments (0.09605Nm,0.19323Nm and 0.28928Nm) and for excitation frequency range of 10-60Hz.

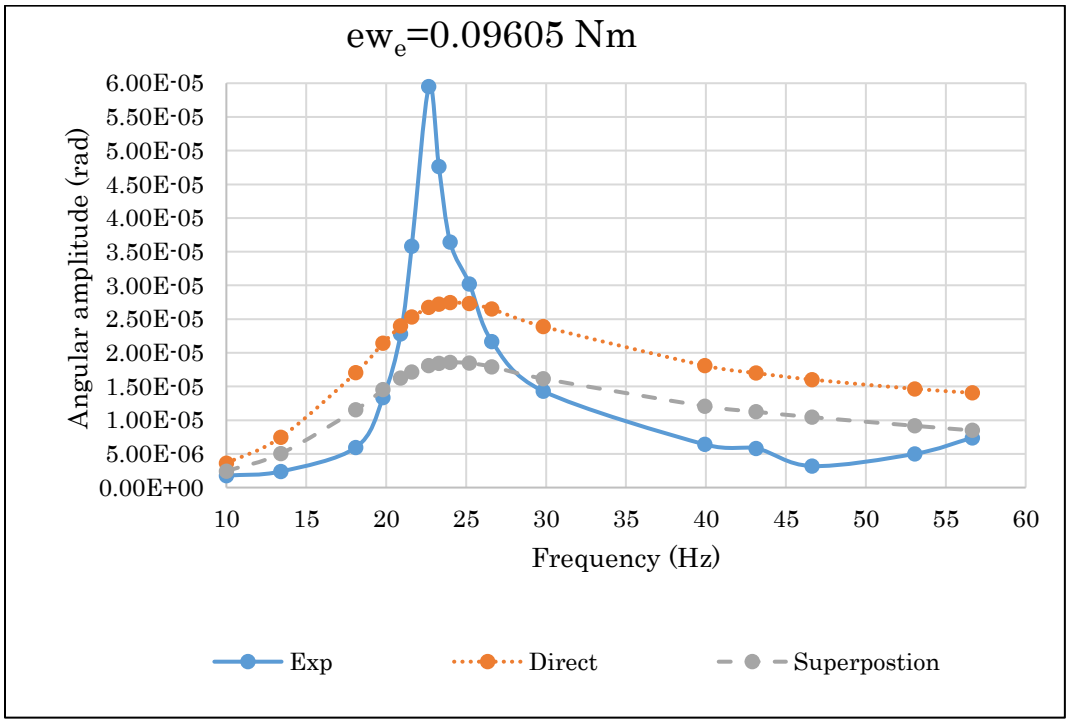

(a)

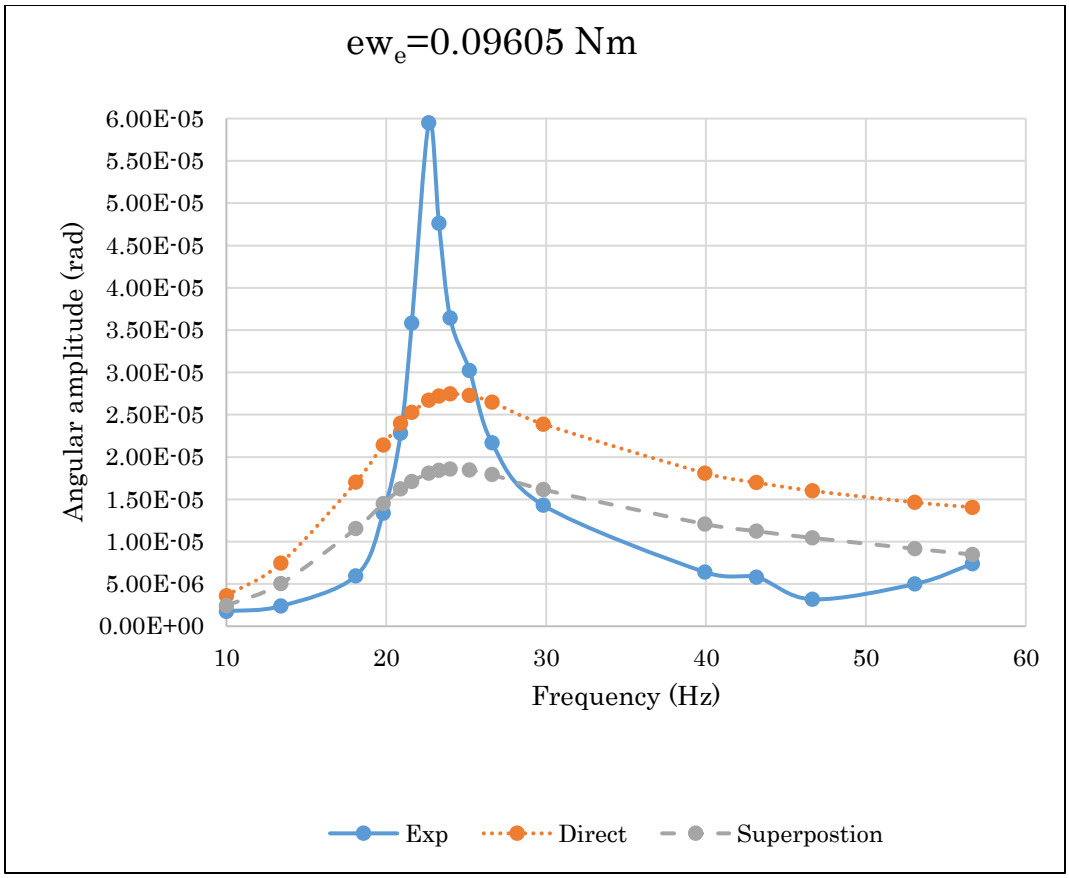

(b)

Figure 4.16 Embedded angular amplitude (a) undamped natural frequency (b) damped natural frequency, ew$_e$=0.09605Nm and d=0.2286m

Observations from figure 4.16 for angular amplitude

- ✓ The experimental natural frequency occur at 22.67Hz with resonant angular amplitude of 5.95*10^{-5}rad, whereas both direct and superposition approach using impedance function method occur at 24Hz. The resonant angular amplitude for Worku occur at 2.75*10^{-5}rad and 2.7*10^{-5}rad and for Prakash 1.859*10^{-5} and 1.84*10^{-5} rad for undamped and damped natural frequency respectively.

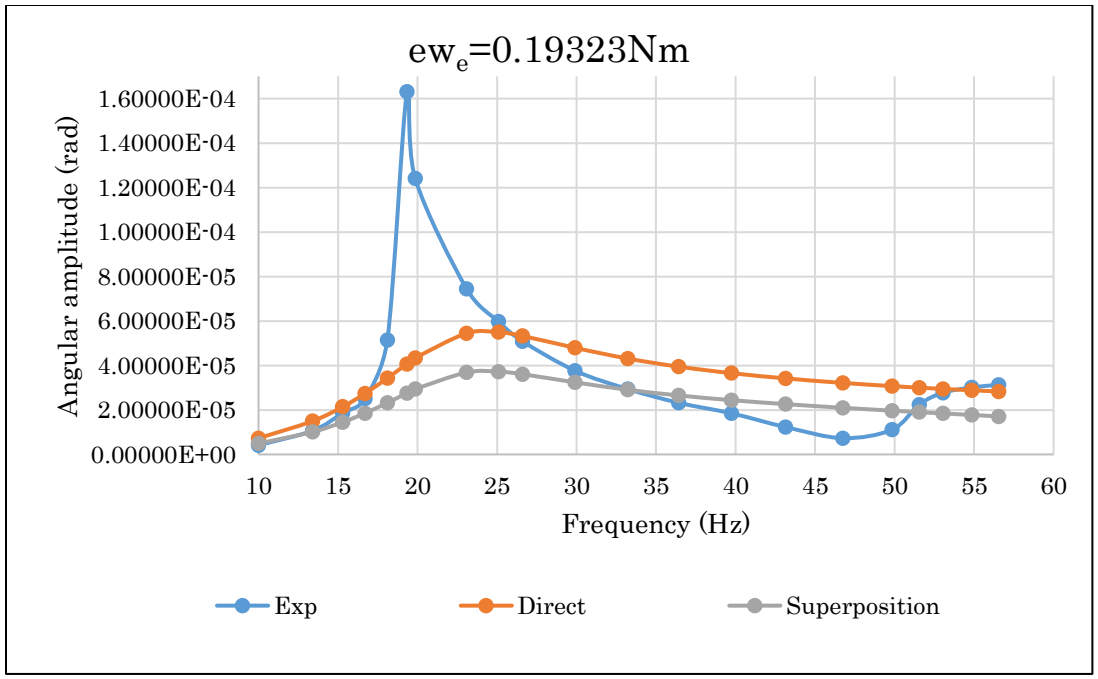

(a)

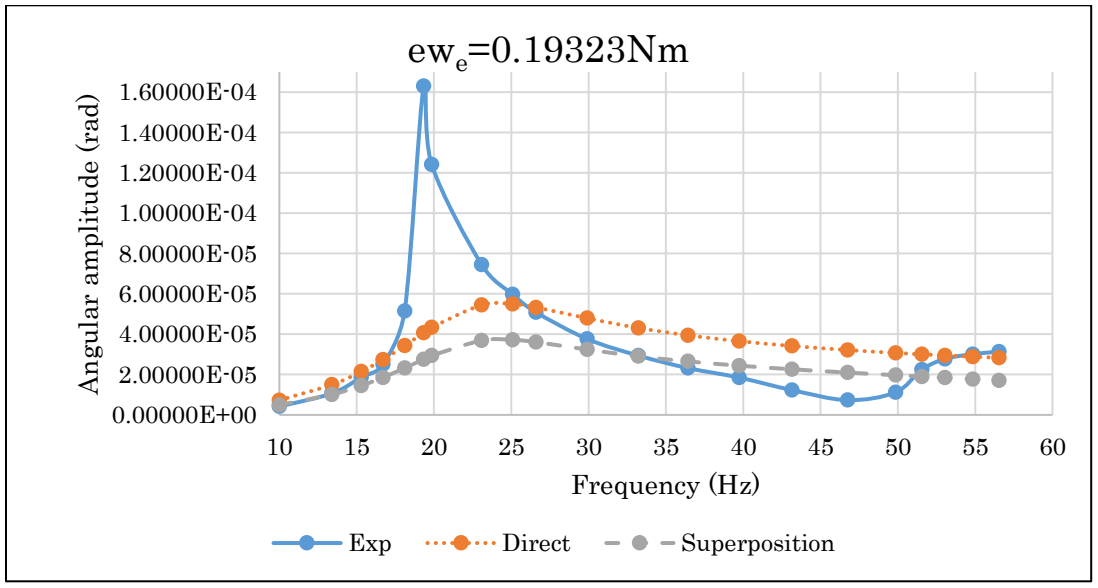

(b)

Figure 4.17 Embedded angular amplitude (a) undamped natural frequency (b) damped natural frequency, ew_e=0.19323Nm and d=0.2286m

Observations from figure 4.17 for angular amplitude

- ✓ The experimental natural frequency occur at 19.33Hz with resonant angular amplitude of $1.63*10^{-4}$rad, whereas both direct and superposition approach using impedance function method occur at 24Hz. The resonant angular amplitude for direct approach method is $5.52*10^{-5}$rad and $5.42*10^{-5}$rad and for superposition approach method is $3.74*10^{-5}$ and $3.69*10^{-5}$ rad for undamped and damped natural frequency respectively.

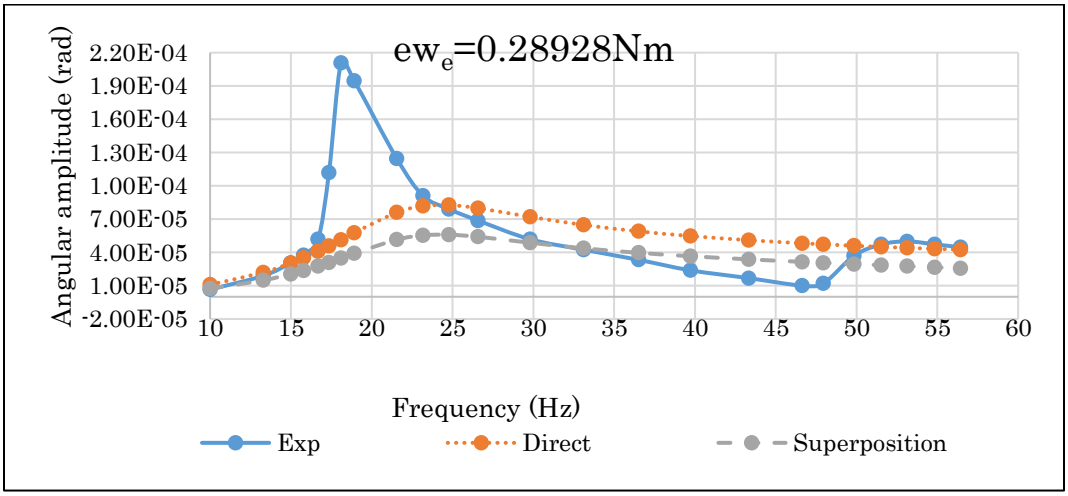

(a)

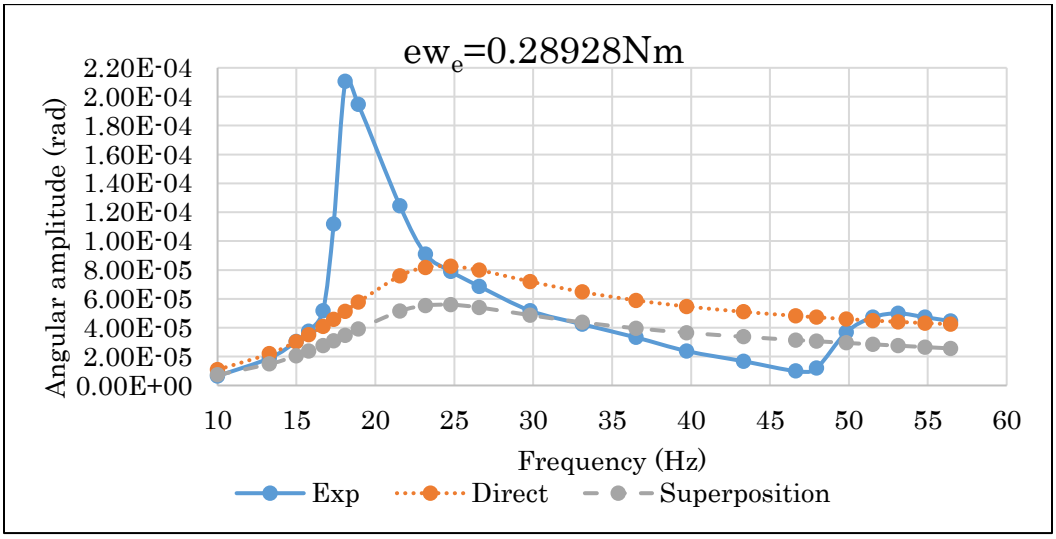

(b)

Figure 4.18 Embedded angular amplitude (a) undamped natural frequency (b) damped natural frequency, ew$_e$=0.28928Nm d=0.2286m

Observations from figure 4.18 for angular amplitude

- ✓ The experimental natural frequency occur at 18.5Hz with resonant angular amplitude of $2.11*10^{-4}$rad, whereas both direct approach and superposition approach using impedance function method occur at 24Hz. The resonant angular amplitude for direct approach method is $8.26*10^{-5}$rad and $8.11*10^{-5}$rad and for superposition approach method is $5.592*10^{-5}$ and $5.526*10^{-5}$rad for undamped and damped natural frequency respectively.

Over all observation for Figure 4.13-4.18

The resonant frequency has shifted a little bit to the right in the case of the two analytical methods with respect to the experimental value while these difference is insignificant for (0.09605Nm and 0.19323Nm) eccentric moment in contrary for the larger eccentric moment (0.28928Nm) the difference is significant but as a general truth the natural frequency is independent of excitation force and moment it shows the shortcoming of the experimental results. However the difference of horizontal and angular amplitude is quite high. Comparison between the two analytical methods shows that the difference in terms of frequency is nonexistence but there is some noticeable difference in terms of amplitude particularly at resonance. When we go slightly beyond the resonant to either side there is significance difference for eccentric moment (0.09605Nm) and for the other eccentric moment it insignificant. When the eccentric moment increases the percentage error decreases for the direct and superposition methods in estimating the experimental results. Superposition approach is better than direct approach method in predicting experimental resonant horizontal amplitude the trend is reversed in the case of angular amplitude.

It must be noted that stiffness and damping evaluated by the impedance function are higher than the actual response.

Horizontal amplitude for effective contact height (d)=0.4572m (d/D=0.375)

From the analysis of Figure 4.19 to 4.21 represents the of value of the horizontal amplitude for effective embedment depth (d) of 0.4572m for different eccentric moments (0.09605Nm,0.19323Nm and 0.28928Nm) and between excitation frequency range of 10-60Hz.

Observations from figure 4.19 for horizontal amplitude

- ✓ The experimental natural frequency occur at 29.33Hz with resonant horizontal resonant amplitude of $3.048*10^{-5}$m, whereas using impedance function method for direct approach occur at 40Hz with $1.39*10^{-5}$m and $1.35*10^{-5}$m and superposition approach 31.7Hz with $1.39*10^{-5}$ and $1.372*10^{-5}$ for undamped and damped natural frequency respectively.

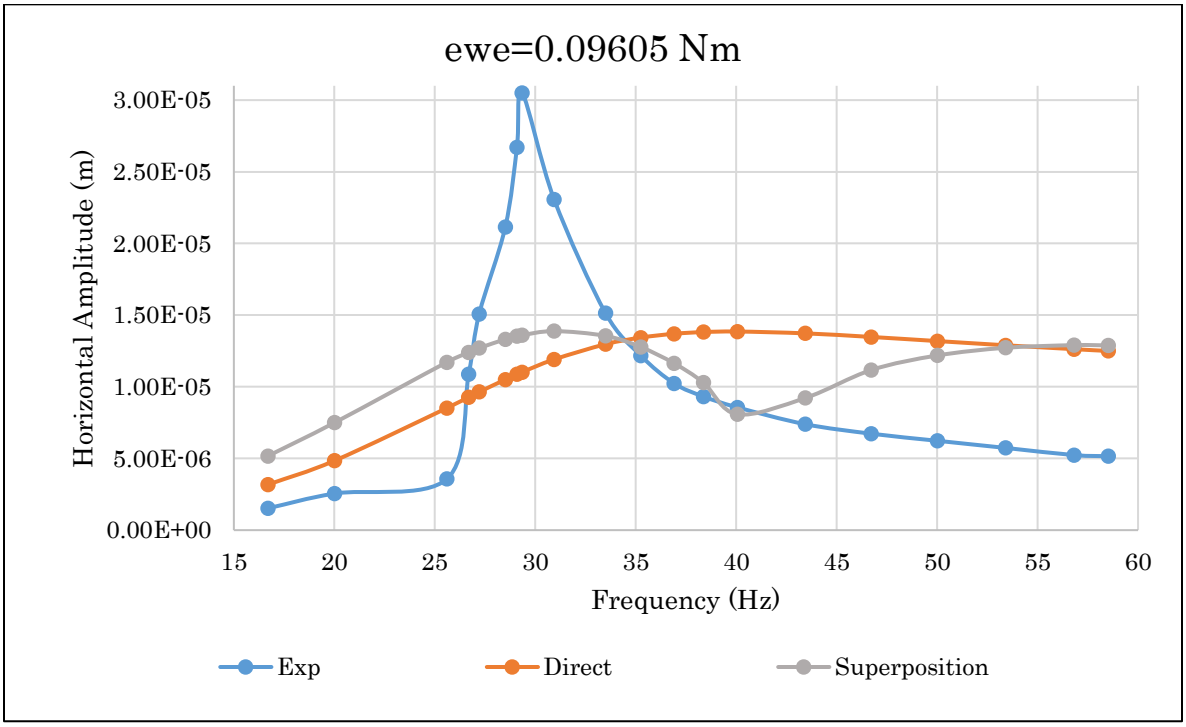

(a)

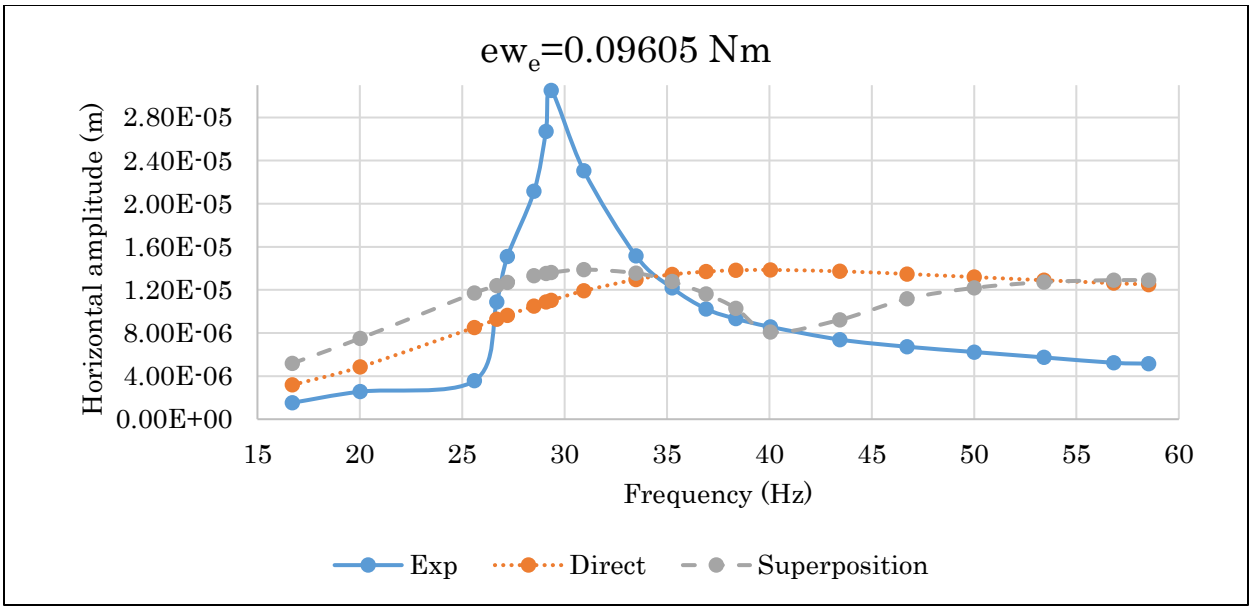

(b)

Figure 4.19 Embedded horizontal amplitude (a) undamped natural frequency (b) damped natural frequency, ew$_e$=0.09605Nm and d=0.4572m

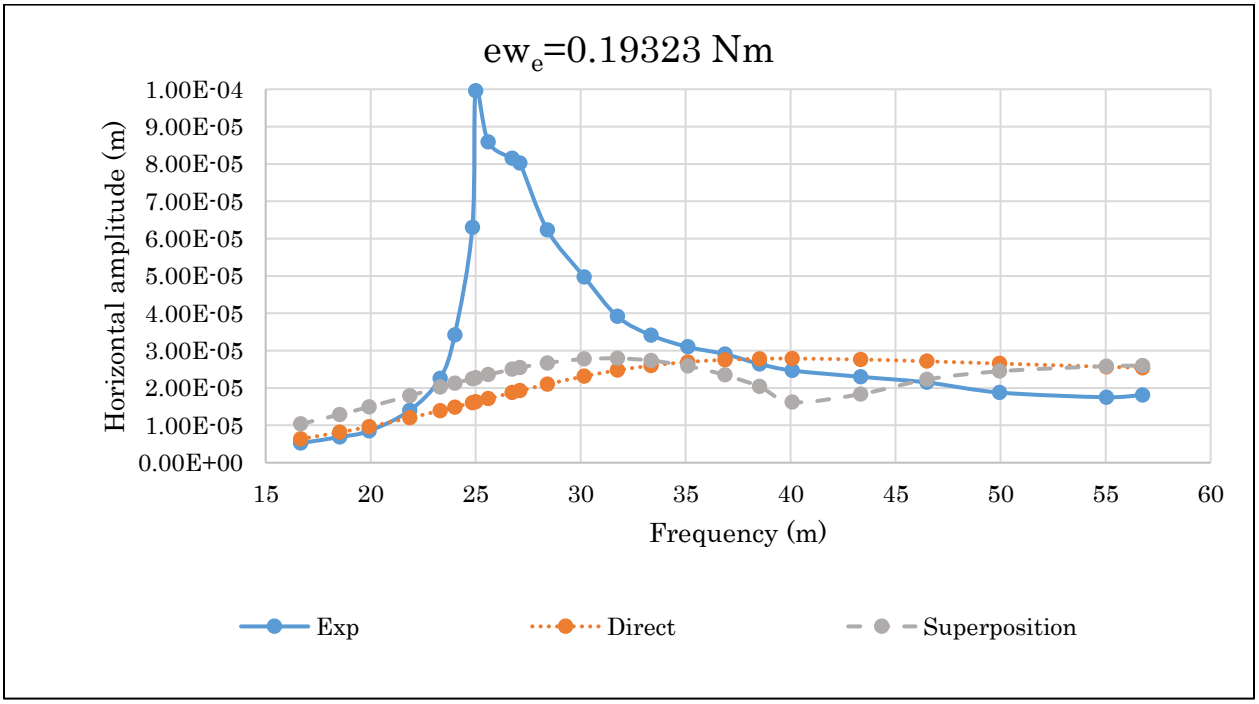

(a)

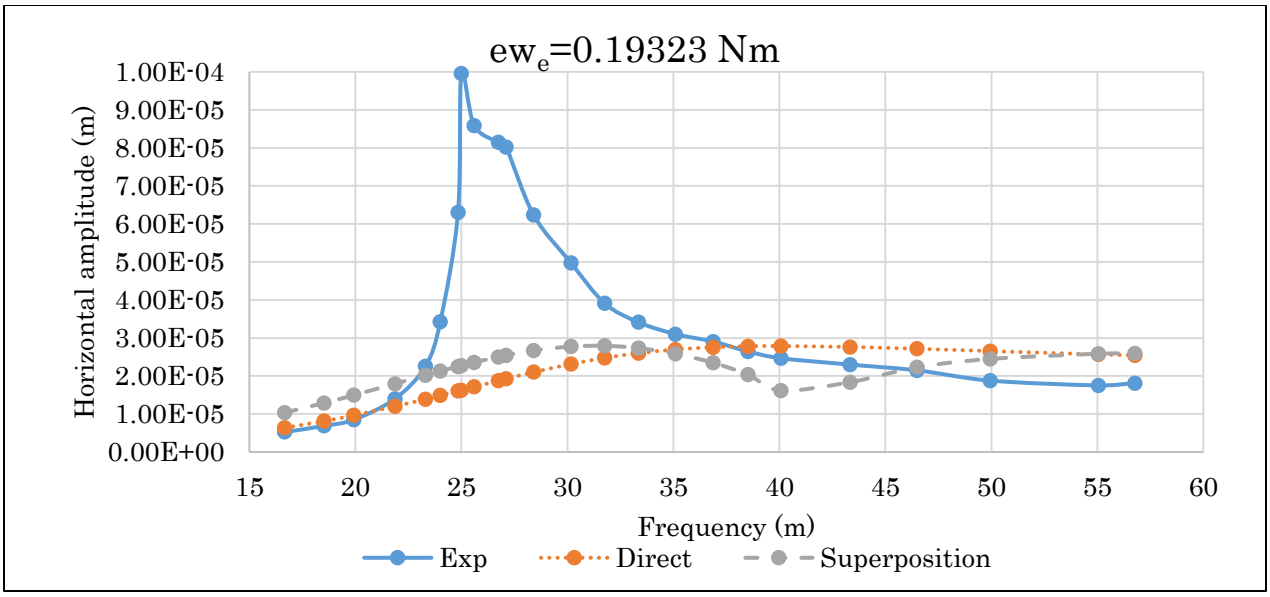

(b)

Figure 4.20 Embedded horizontal amplitude (a) undamped natural frequency (b) damped natural frequency, ew$_e$=0.19323Nm and d=0.4572m

Observations from figure 4.20 for horizontal amplitude

- ✓ The experimental natural frequency occur at 25Hz with resonant horizontal amplitude of 1.006*10^{-4}m, whereas using impedance function method for direct approach method occur at 40Hz with 2.788*10^{-5}m and 2.706*10^{-5}m and for superposition approach 31.7Hz with 2.793*10^{-5} and 2.76*10^{-5} for undamped and damped natural frequency respectively.

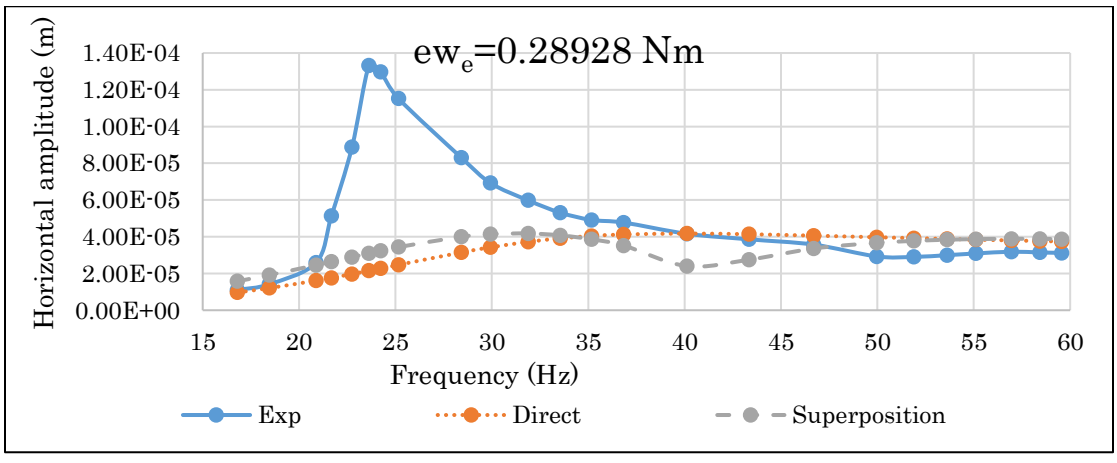

(a)

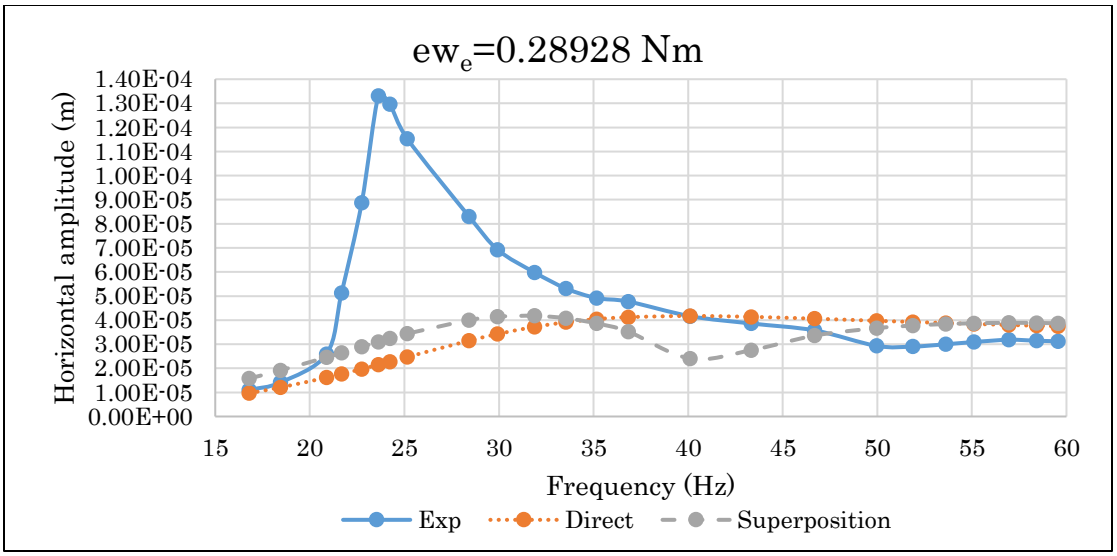

(b)

Figure 4.21 Embedded horizontal amplitude (a) undamped natural frequency (b) damped natural frequency, ew$_e$=0.28928Nm and d=0.4572m

Observations from figure 4.21 for horizontal amplitude

- ✓ The experimental natural frequency occur at 23.6Hz with resonant horizontal amplitude of 1.33*10^{-4}m, whereas using impedance function method for direct approach method occur at 40Hz with 4.17*10^{-5}m and 4.05*10^{-5}m and superposition approach method 31.7Hz with 4.18*10^{-5} and 4.13*10^{-5} for undamped and damped natural frequency respectively.

Rocking (Angular) amplitude *effective contact height (d) =0.4572m (d/D=0.375)*

From the analysis of Figure 4.22 to 4.24 represents the of value of the angular amplitude for effective embedment depth (d) of 0.4572m for different eccentric moments (0.09605Nm,0.19323Nm and 0.28928Nm) and for excitation frequency range of 10-60Hz.

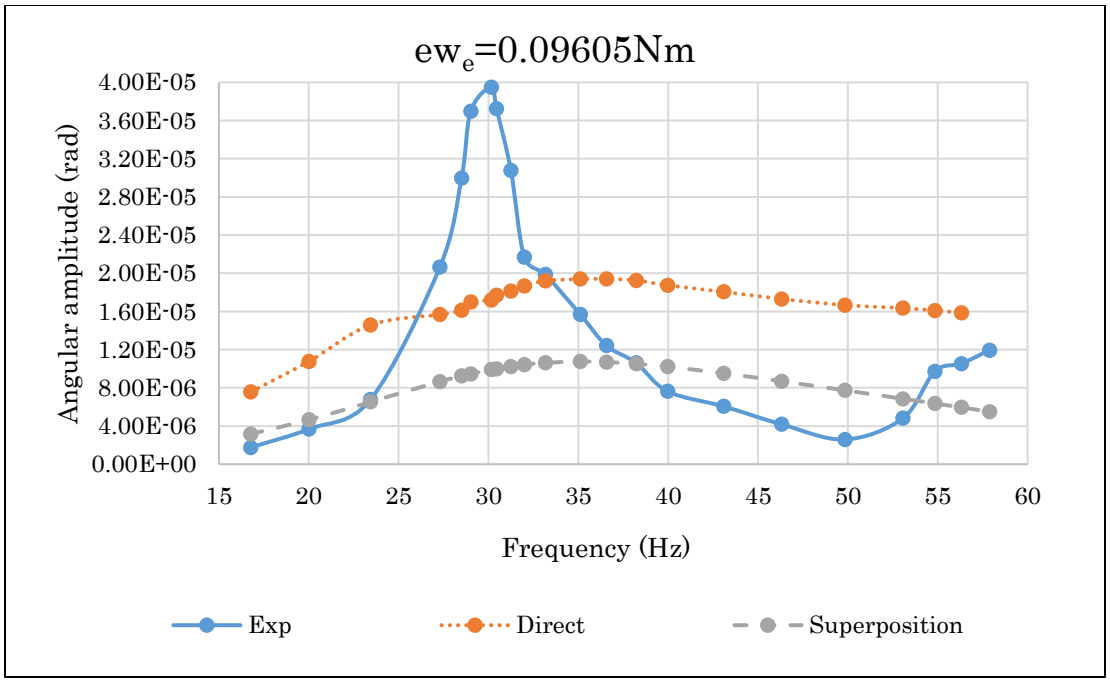

(a)

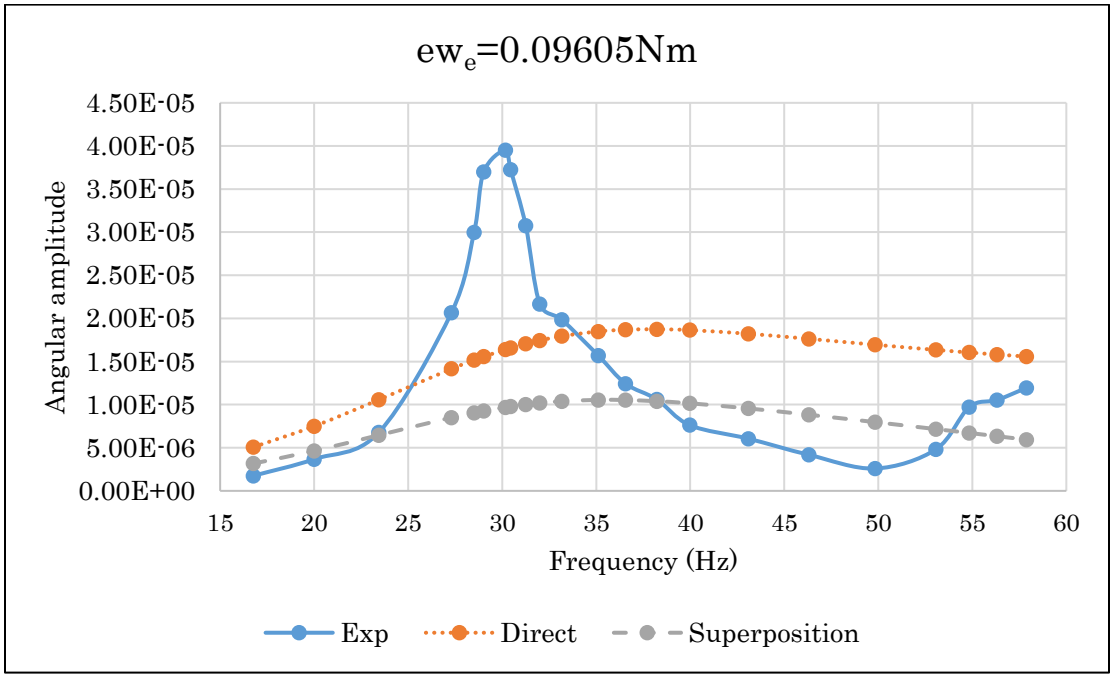

(b)

Figure 4.22 Embedded angular amplitude (a) undamped natural frequency (b) damped natural frequency, ew$_e$=0.09605Nm and d=0.4572m

Observations from figure 4.22 for angular amplitude

- ✓ The experimental natural frequency occur at 30.17Hz with resonant angular amplitude of $3.95*10^{-5}$rad, whereas using impedance function method direct approach method at 38Hz with $1.94*10^{-5}$rad and $1.874*10^{-5}$rad and superposition approach method occur at 35Hz with $1.07*10^{-5}$ and $1.055*10^{-5}$rad for undamped and damped natural frequency respectively.

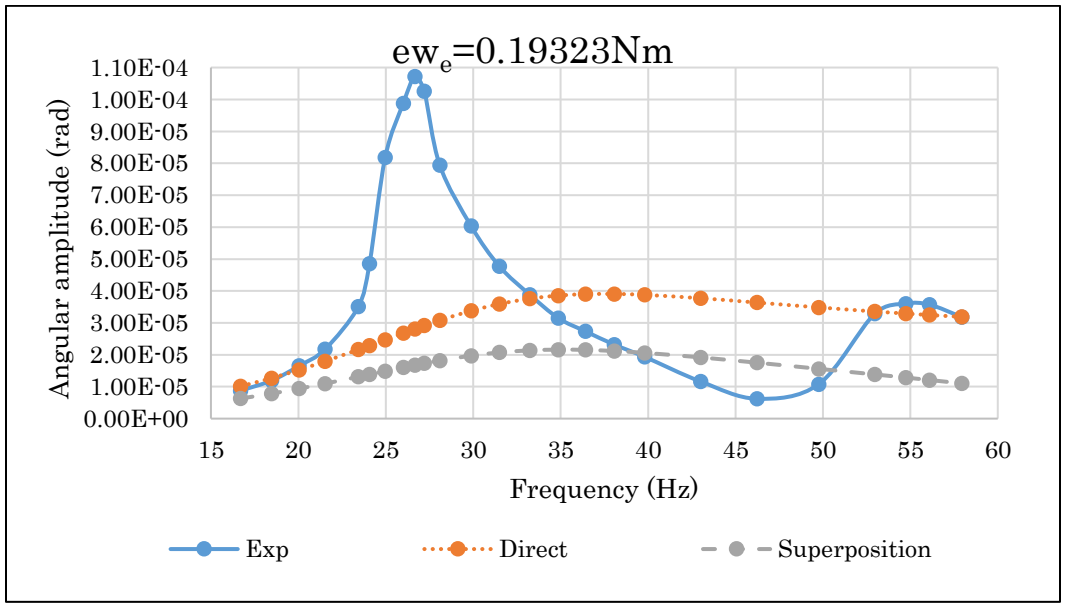

(a)

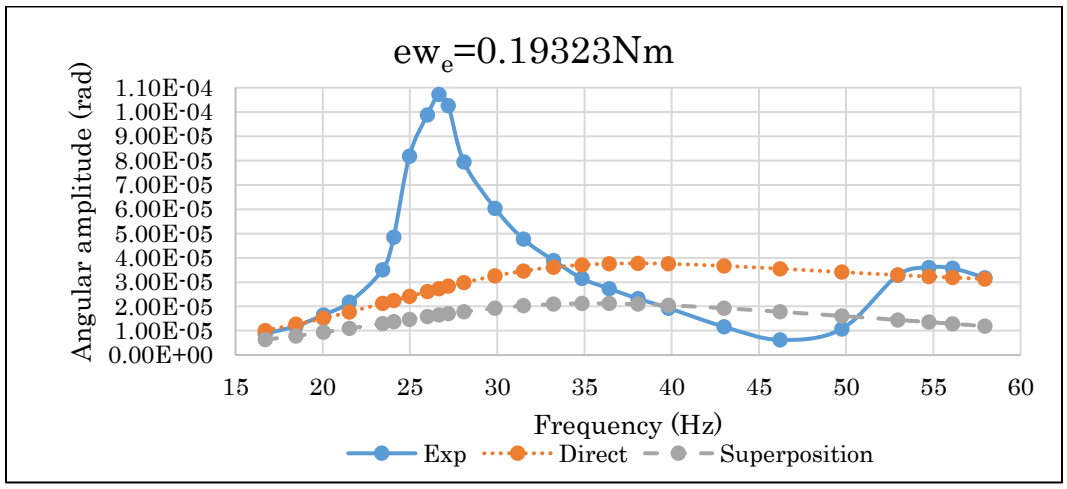

(b)

Figure 4.23 Embedded angular amplitude (a) undamped natural frequency (b) damped natural frequency, ew_e=0.19323Nm and d=0.4572m

Observations from Figure 4.23 for angular amplitude

✓ The experimental natural frequency occur at 26.67Hz with resonant angular amplitude of $1.07*10^{-4}$rad, whereas using impedance function method for direct approach occur at 38Hz with $3.905*10^{-5}$rad and $3.77*10^{-5}$rad and superposition approach occur at 35Hz with $2.16*10^{-5}$ and $2.12*10^{-5}$rad for undamped and damped natural frequency respectively.

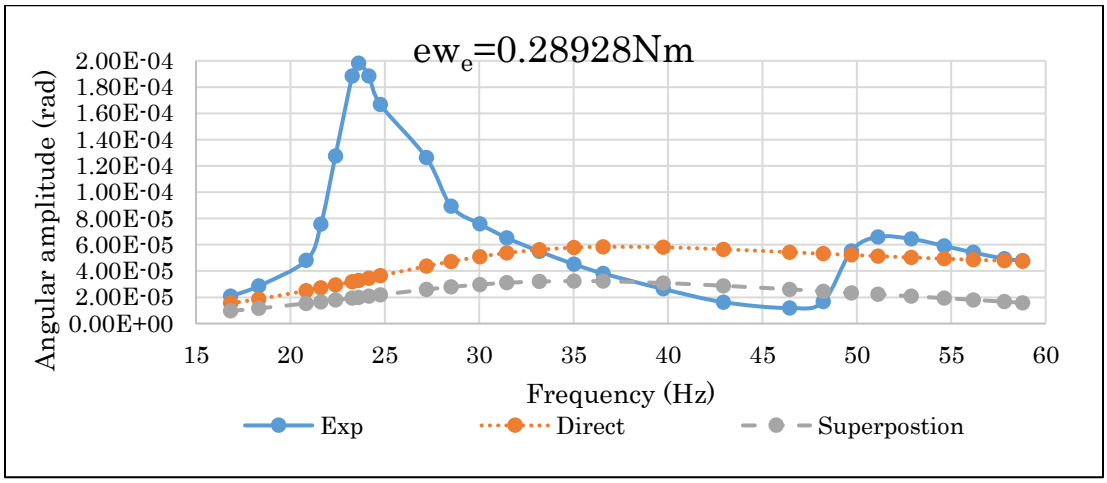

(a)

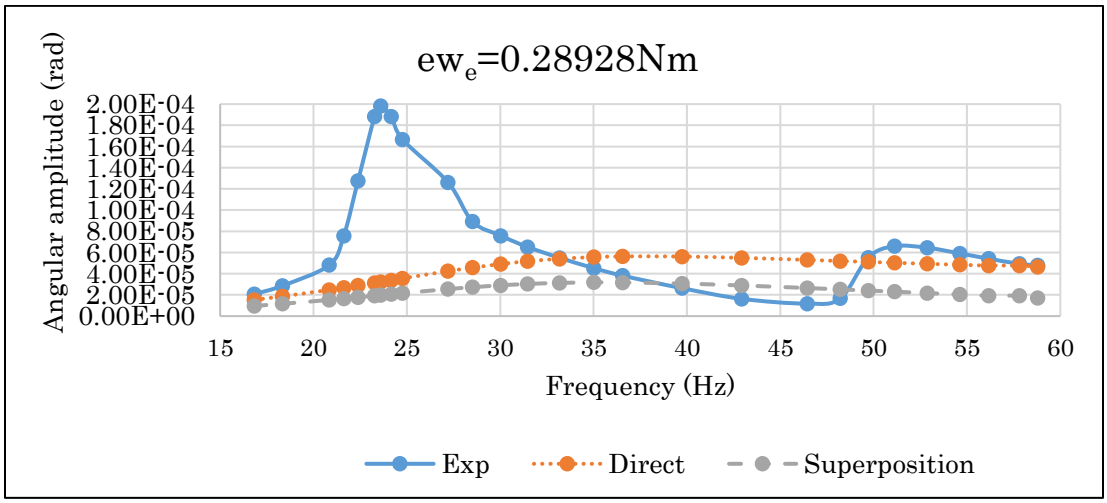

(b)

Figure 4.24 Embedded angular amplitude (a) undamped natural frequency (b) damped natural frequency, ew$_e$=0.28928Nm and d=0.4572m

Observations from figure 4.24 for angular amplitude

- ✓ The experimental natural frequency occur at 24Hz with resonant angular amplitude of $1.88*10^{-4}$rad, whereas using impedance function method for direct approach occur at 36.5Hz with $5.84*10^{-5}$rad and $5.63*10^{-5}$rad and superposition occur at 35Hz with $3.23*10^{-5}$ and $3.176*10^{-5}$rad for undamped and damped natural frequency respectively.

Overall observation from Figure 4.19-4.24

The resonant frequency has shifted to the right in the case of the two analytical methods with respect to the experimental value while these difference is significant. However the difference of resonant horizontal and angular amplitude is quite high. Comparison between the two analytical methods shows noticeable difference in terms of amplitude particularly at resonance. When we go slightly beyond the resonant to either side there is significance difference. When the eccentric moment increases the percentage error decreases for the direct and superposition methods in estimating the experimental results. Superposition approach is relatively better than direct approach method in estimating experimental resonant horizontal amplitude the trend is reversed in the case of angular amplitude.

It must be noted that stiffness and damping evaluated by the impedance function are higher than the actual response.

Horizontal amplitude for *effective contact height (d) =0.9144m (d/D=0.75)*

From the analysis of Figure 4.25 to 4.27 represents the of value of the horizontal amplitude for effective embedment depth (d) of 0.9144m for different eccentric moments (0.09605Nm,0.19323Nm and 0.28928Nm) and for excitation frequency range of 10-60Hz.

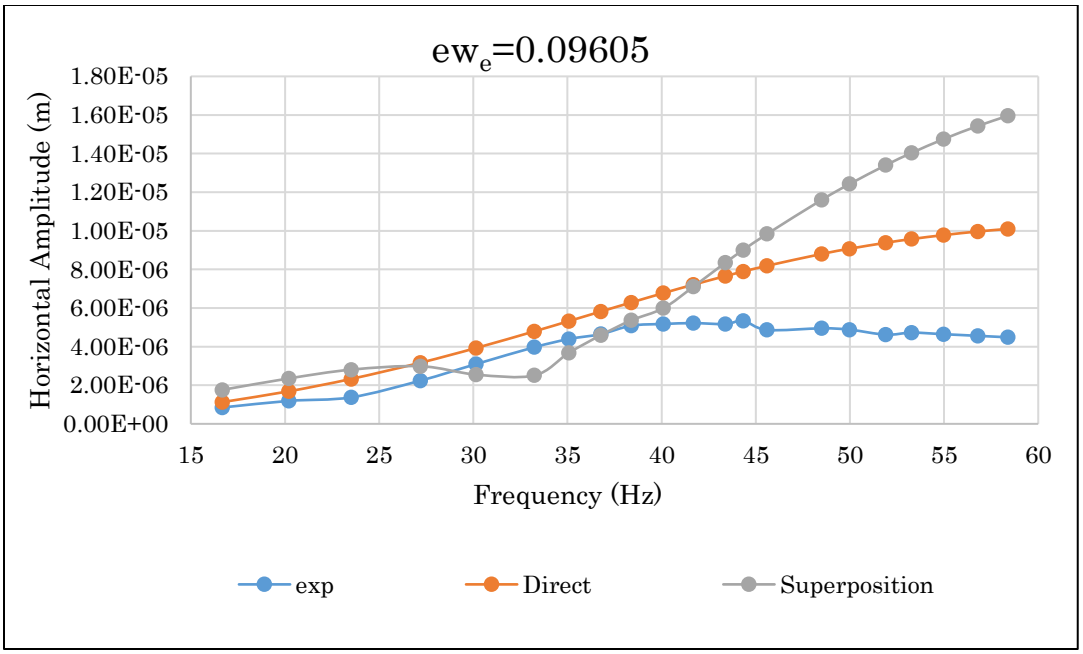

(a)

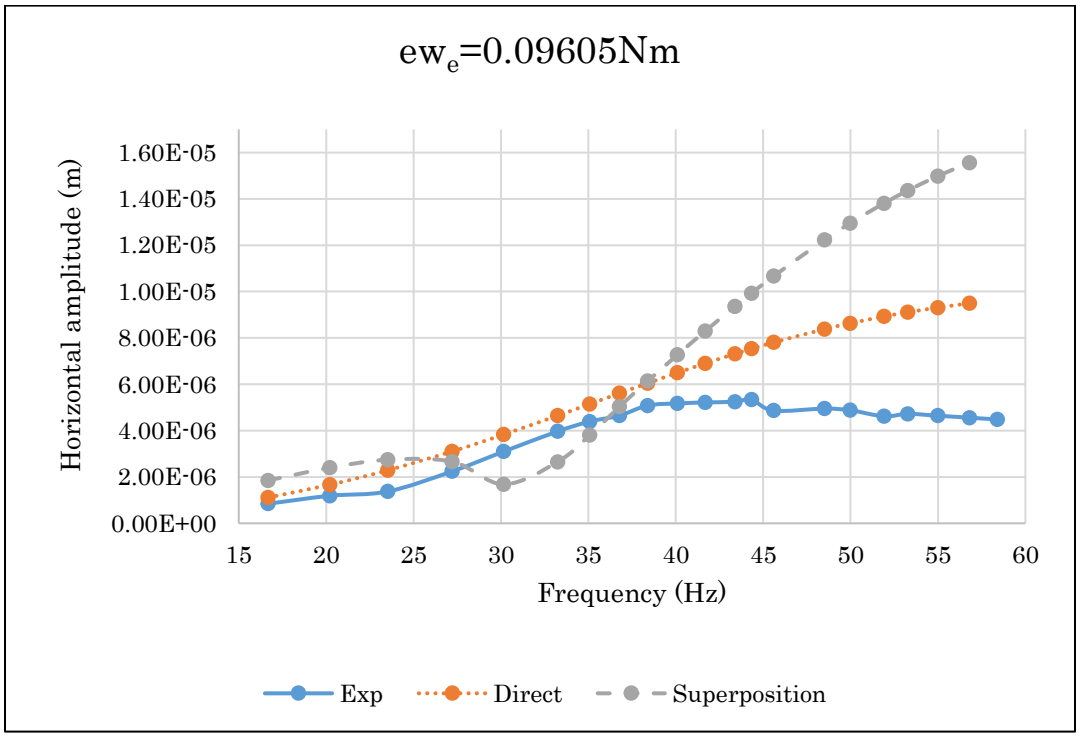

(b)

Figure 4.25 Embedded Horizontal amplitude (a) undamped natural frequency (b) damped natural frequency, ew$_e$=0.09605Nm and d=0.9144m

Observations from the Figure 4.25 for Horizontal amplitude

- ✓ The experimental natural frequency occur at 44.33Hz with resonant horizontal amplitude of $5.33*10^{-6}$m, whereas using impedance function method superposition approach occur at 27.2Hz with $2.98*10^{-6}$ and $2.66*10^{-5}$m for undamped and damped natural frequency respectively.

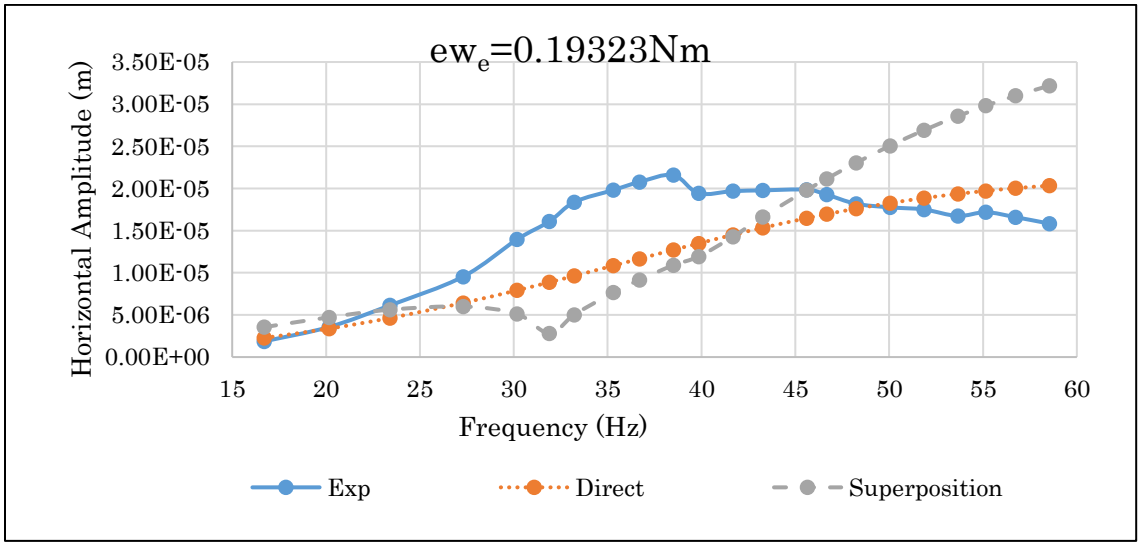

(a)

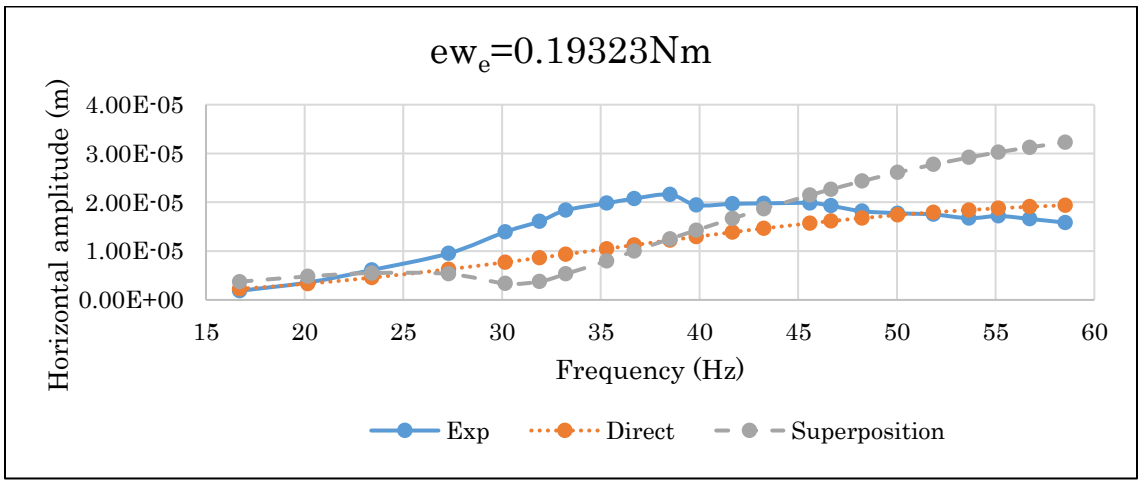

(b)

Figure 4.26 Embedded Horizontal amplitude (a) undamped natural frequency (b) damped natural frequency, ew_e=0.19323Nm and d=0.9144m

Observations from Figure 4.26 for Horizontal amplitude

- ✓ The experimental natural frequency occur at 38.5Hz with resonant horizontal amplitude of $2.159*10^{-5}$m, whereas using impedance function method superposition approach occur at 27.2Hz with $5.998*10^{-6}$m and $5.33*10^{-6}$m for undamped and damped natural frequency respectively.

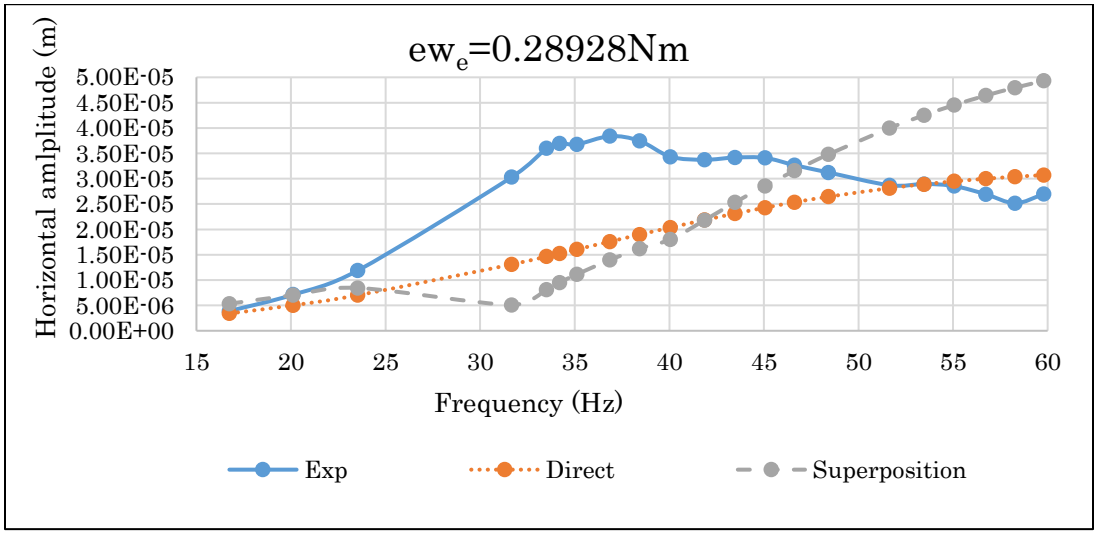

(a)

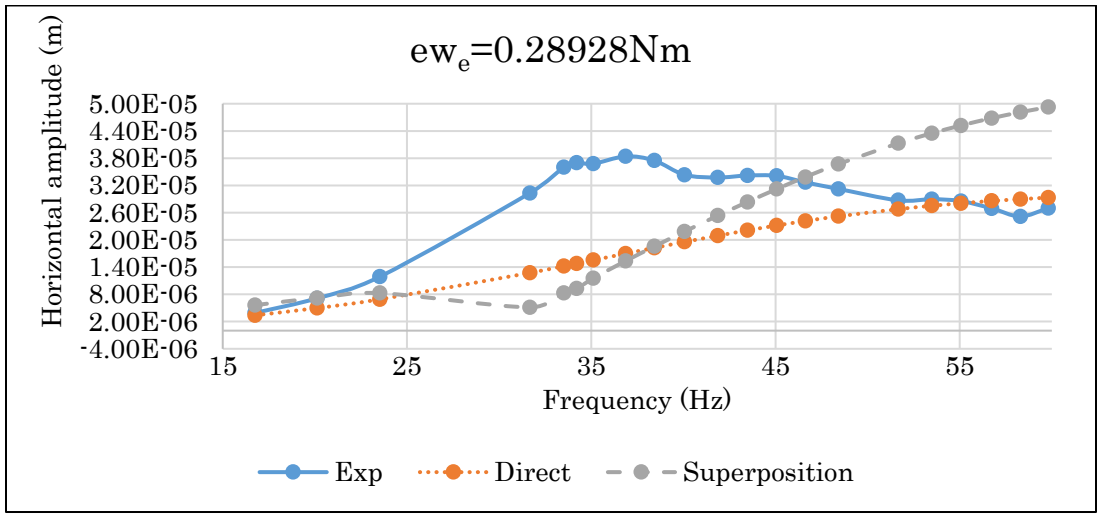

(b)

Figure 4.27 Embedded Horizontal amplitude (a) undamped natural frequency (b) damped natural frequency, ew$_e$=0.28928Nm and d=0.9144m

Observations from Figure 4.27 for Horizontal amplitude

- ✓ The experimental natural frequency occur at 37Hz with resonant horizontal amplitude of $3.84*10^{-5}$m, whereas using impedance function method superposition approach occur at 23.5Hz with $8.45*10^{-6}$m and $8.26*10^{-6}$m for undamped and damped natural frequency respectively.

Rocking (Angular) amplitude for effective height (d) =0.9144m (d/D=0.75)

From the analysis of Figure 4.28 to 4.30 represents the of value of the angular amplitude for effective embedment depth (d) of 0.9144m for different eccentric moments (0.09605Nm,0.19323Nm and 0.28928Nm) and for excitation frequency range of 10-60Hz.

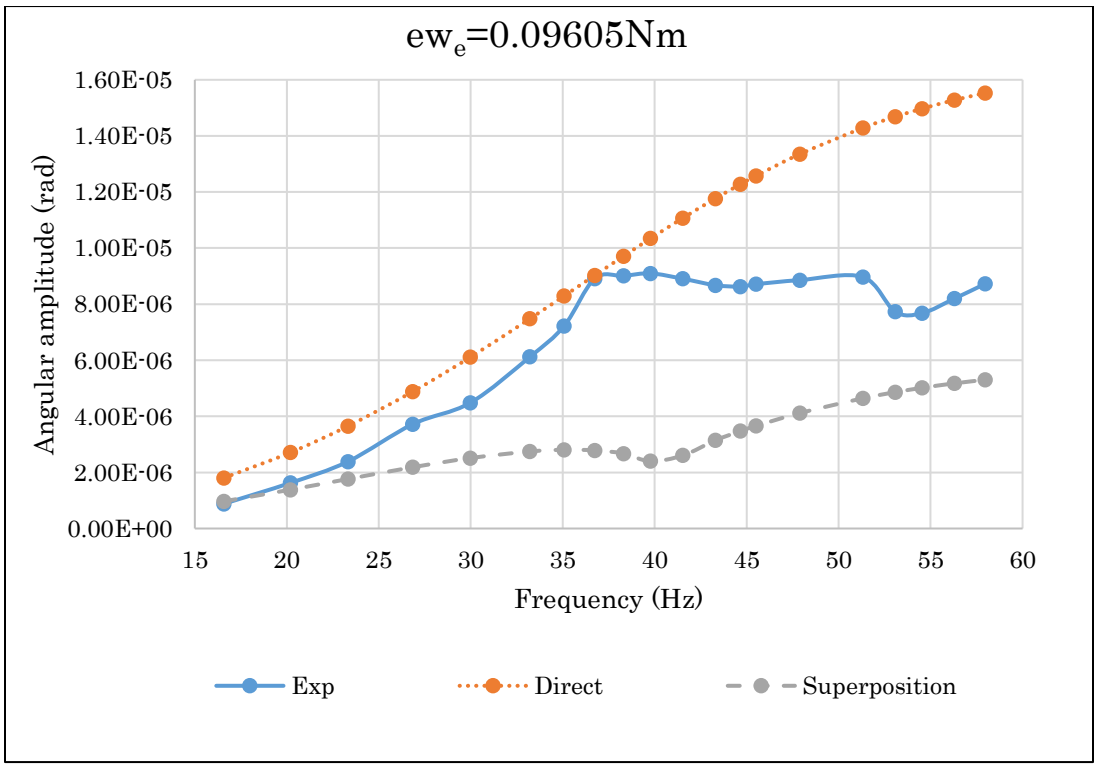

(a)

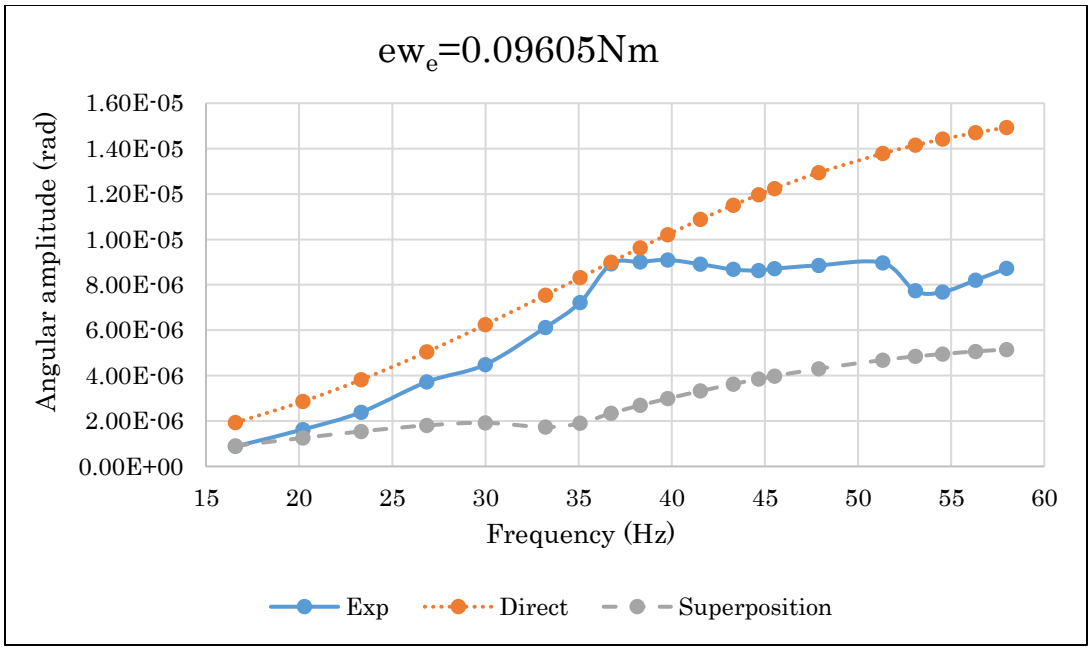

(b)

Figure 4.28 Embedded angular amplitude (a) undamped natural frequency (b) damped natural frequency, ew$_e$=0.09605Nm and d=0.9144m

Observations from Figure 4.28 for angular amplitude

- ✓ The experimental natural frequency occur at 45.5Hz with resonant angular amplitude of 8.7*10^{-6}rad, whereas using impedance function method for super-position approach occur at 35Hz with 2.786*10^{-6} and 30Hz with 1.92*10^{-6}rad for undamped and damped natural frequency respectively.

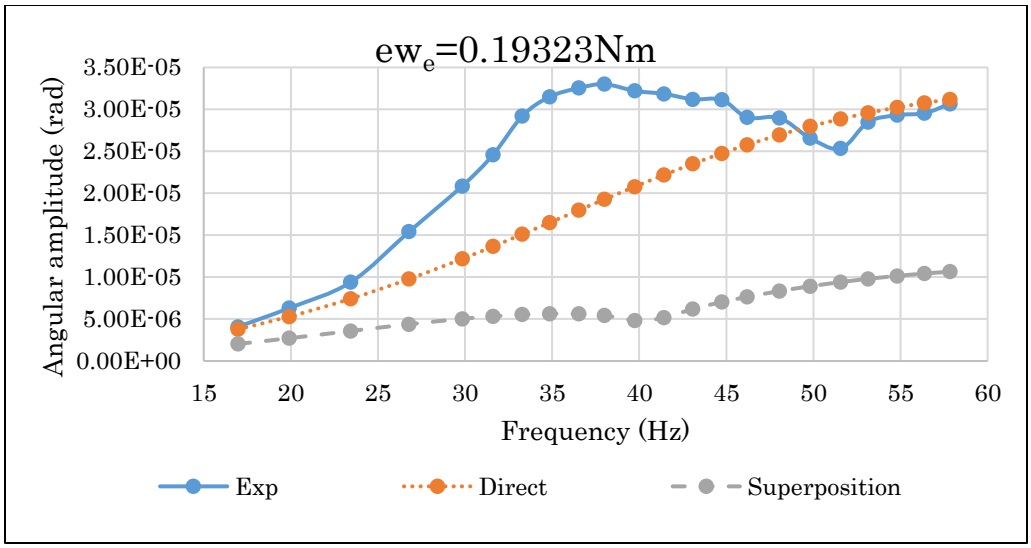

(a)

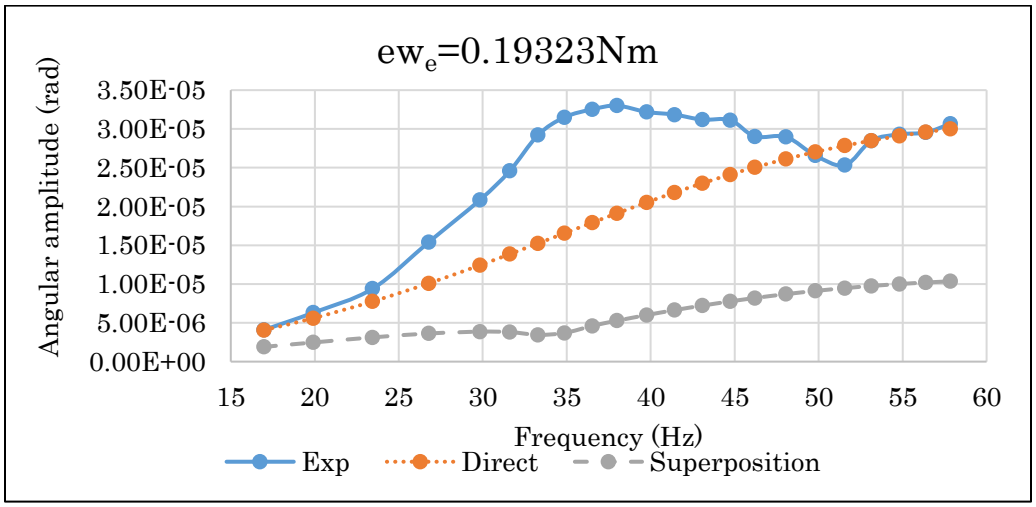

(b)

Figure 4.29 Embedded angular amplitude (a) undamped natural frequency (b) damped natural frequency, ew$_e$=0.19323Nm and d=0.9144m

Observations from Figure 4.29 for angular amplitude

- ✓ The experimental natural frequency occur at 38Hz with resonant angular amplitude of $3.3*10^{-5}$rad, whereas using impedance function method for super-position approach occur at 35Hz with $5.64*10^{-6}$ and 30Hz with $3.86*10^{-6}$rad for undamped and damped natural frequency respectively.

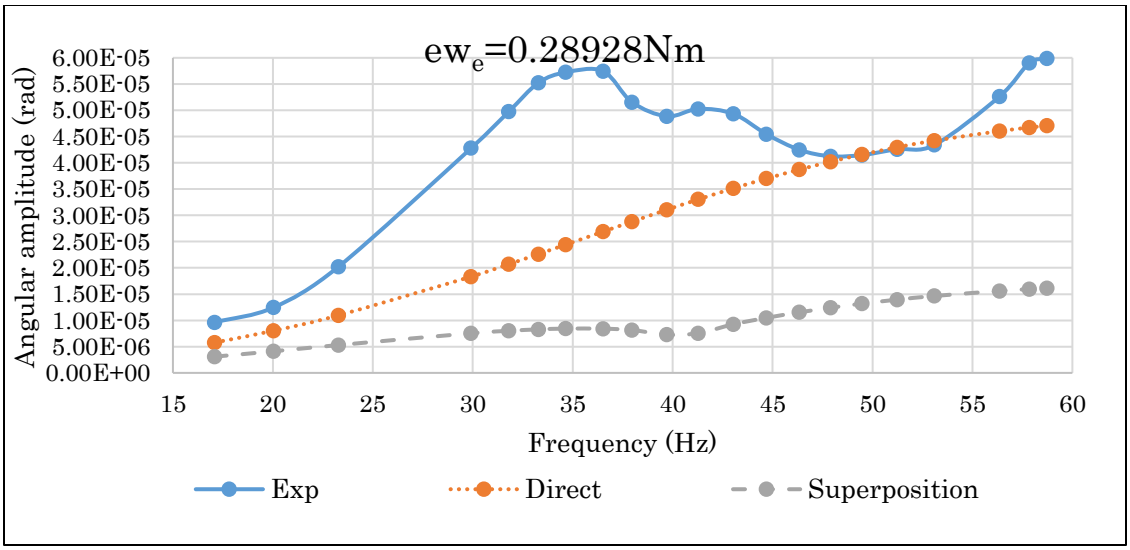

(a)

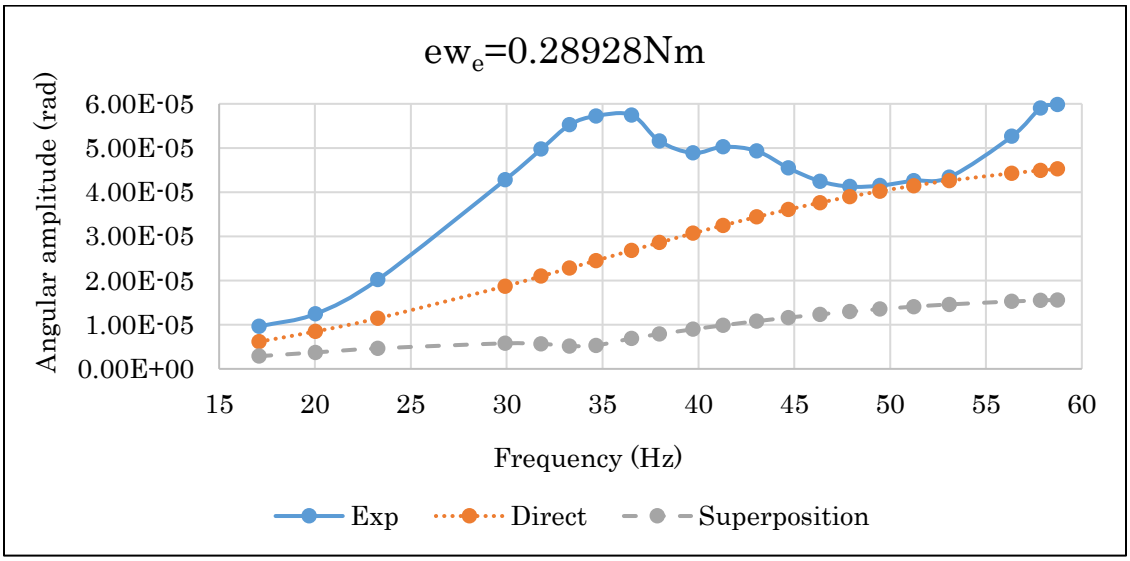

(b)

Figure 4.30 Embedded angular amplitude (a) undamped natural frequency (b) damped natural frequency, ew$_e$=0.28928Nm and d=0.9144m

Observations from Figure 4.30 for angular amplitude

✓ The experimental natural frequency occur at 36.5Hz with resonant angular amplitude of 5.75*10^{-5}rad, whereas using impedance function method for superposition approach method occur at 34.6Hz with 8.42*10^{-6} and 30Hz with 5.78*10^{-6}rad for undamped and damped natural frequency respectively.

Overall observation from Figure 4.25-4.30

The resonant frequency has shifted to the left in the case of the superposition method with respect to the experimental value while these difference is significant and the graph is not smooth it shows fluctuating trend it is the shortcoming of this method. In the direct approach method no clear peak is observed despite the variation of excitation frequency. Direct approach is relatively better than Superposition approach method in estimating experimental resonant horizontal and angular amplitude. The actual damping is so high that the experimental amplitude is very small.

The difference between the two methods should be important in surface where the foundation is near the surface, where the damping and stiffness are small and the vibration amplitude is high enough.

5 CONCLUSIONS AND RECOMMENDATIONS

5.1 CONCLUSIONS

The main aim of this study has been concentrated around the sensitivity and comparative study of coupled horizontal and rocking vibration of block machine foundation to compute angular and horizontal amplitude by applying direct method which considers the combined effect of force and moment without simplifications. while superposition method uses simple superposition of the contributions of the separate actions of force and moment. The sensitivity study is carried out for reciprocating compressor resting on block foundation of different size resting on clay, gravel and sand are considered. The values of translational and rotational amplitude corresponding to their natural frequencies and damping ratios are presented. For the comparative study the horizontal and angular amplitudes are compared with field tests measured by (Beredugo, 1971 and Beredugo and Novak1972) for surface and embedded block foundations are considered. Based on the results obtained, the following conclusions are drawn:

From comparative study

1. For surface foundation the theory predicts the experimental natural frequency with good agreement and percentage error of -3.17% to -20.91% for horizontal and angular amplitude.
2. Direct approach method gives better than superposition approach method in predicting horizontal resonant amplitude. Whereas superposition approach method gives better results than direct approach method in predicting angular resonant amplitude for the range of frequency considered but both of them overestimates angular and horizontal amplitude for surface foundation because of the stiffness is over estimated and the actual damping is much larger than estimated by the impedance function method developed by Gazetas (Gazetas G. , 1991) it is not the shortcoming of the two approaches.

3. When the eccentric moment increases the percentage error decreases for the direct and superposition methods in predicting experimental results in surface foundation.
4. For embedded footings horizontal and angular resonant amplitudes both theories underestimated because of high damping and stiffness values of impedance function method.

From sensitivity study

1. For damped natural Frequency when the aspect ratio (L/B) increases horizontal and angular amplitude increases whereas damping ratio decreases due to high damping ratio.
2. For undamped natural frequency, horizontal and angular amplitude and frequency ratio (ω/ω_n) decreases when the aspect ratio (L/B) increases.
3. For both damped and undamped natural frequency as the embedment ratio increases angular and horizontal amplitude decreases.

5.2 RECOMMENDATIONS

- Further study needs to be conducted on non-homogenous soil strata.
- Many more experimental data needs be analyzed to develop rational correction factors for impedance function which may be used by a practicing engineer.

6 REFERENCES

ACI. (2011). *Foundations for dynamic equipment.* American concrete institute.

Beredugo. (1971). vibrations of embedded symmetric footings. London, Western ontario, canada (Digitized Phd thesis).

Beredugo, Y. 0. and Novak, M. (1972). Coupled Horizontal and Rocking Vibration of . *Canadian Geotechnical Journal*, 477-497.

Bhatia, K. (2008). Foundations for industrial machines & earthquake effects. *ISET Journal of Earthquake Technology*.

Braja M. Das and G. V. Ramana. (2011). *Principles of soil dynamics.* Cengage Learning.

Briaud, j.-L. (2013). *Geotechnical Engineering:Unsaturated and Saturated soils.* Hoboken, New Jersey: John Wiley and sons,Inc.

F.E. Richart,J.R Hall & R.D.Woods. (1970). *Vibrations of soils and foundations.* new jersey: prentice-hall.

Fry, Z. (1963). *Development and evaluation of soil bearing capacity foundations of structures.* Vicksburg,mississipi: ENGINEERS, U.S. Army Engineer Waterways Experiment Station.

Gazetas, G. (1983). Analysis of machine foundation vibrations, state of art. Soil dyn. *International Conference on Soil Dyn.& earthquake eng.* (pp. 2-42). Southampton: CML Publications.

Gazetas, G. (1991). Formulas and charts for impedances of surface and embedded foundations. *j.Geotech. Engrg (ASCE)*, 1363-1381.

George Gazetas and Kenneth H. Stokoe. (1991). Free Vibration OF Embedded Foundations:. *J. Geotech Engrg,ASCE, 117*, pp. 1382-1401.

Hongchun. (2018). *Concrete Foundations for turbine generators Analysis design and construction.* Reston, Virginia: American Society of Civil Engineers.

Hongjuan Chen,Rul Sun,Xiaoming YUAN and Jianyi ZHANG. (2008). Variability of Nonlinear Dynamic Shear Modulus and Damping Ratio of soils. *World Conference on Earthquake Engineering.* Beijing,China.

Kramer, L. (1996). *Geotechnical Earthquake engineering.* New jersey: Prentice-Hall.

Mandal A. ,Baidya D.k and Roy D. (2012). Dynamic Response of the Foundations Resting on a two-layered soil underlain by a rigid layer. *Geotechnical Geol Eng, 30*, 775-786.

Manyando, George M. S. and Prakash, Shamsher,. (1991). On Predictions and Performance of Machine Foundations. International coferences on recent advance in geotechnical earthquake engineering.

Nii, Y. (1987). Experimental half-space dynamic stifness. *journal of Geotechnical Engineering*, 1359-1373.

Prakash, S. (1981). *soil dynamics.* New York: McGraw-Hill.

Ricardo Dobry, George Gazetas and kenneth H.stoke. (1986). Dynamic response of arbitrarily shaped foundation:experimental verification. *Journal of Geotechnical Engineering,ASCE, 112*.

S.Prakash and V.Puri. (1995). Coupled Horizontal and Rocking Vibration of block foundations. *International conferences on Recent advances in Geotechnical Earthquake Engineering and soil Dynamics.* St.Louis Missouri.

Saran, S. (2014). *Soil dynamics and machine foundation.* India: Galgotia printing press.

Shamsher Prakash and Vijay K. Puri. (2006). Foundations for vibrating machines. *Journal of Structural Engineering*(special issue), 1-39.

Smoltczyk, U. (2002). *Geotechnical Engineering Handbook.* Berlin.

Srinivasulu.P and Vaidyanathan.C.V. (1990). *Handbook of machine foundations.* New-Delhi: Mc-graw-hill.

Suresh Arya, Michael O'Neill and George Pincus. (1984). *Design of structures and Foundations for Vibrating Machines.* Houston: Gulf Publishing company.

Veletsos.A.S andVerbic.B. (1973). Vibration of viscoelastic foundations. *Earthquake engineering and structural dynamics, 2*, 87-102.

Verruijt, A. (2008). *soil dynamics.* netherlands.

Villaverde, R. (2009). *Fundamental Concepts of Earthquake Engineering.* New York: Taylor & Francis Group, LLC.

Vivek P and P.Ghosh. (2012). Dynamic Interaction of Two Nearby Machine Foundations on Homogeneous soil. *ASCE*, 21-30.

Worku, A. (2012). An Analytical Solution Procedure for Dynamic Analysis of Soil-Structure Systems Subjected to Periodic Loading. *Electronic Journal of Geotechnical Engineering*, 3835-3852.

Worku, A. (2016). An analytical method of dynamic analysis of block machine foundations using impedance functions. *unpublished manuscript*, 1-19.

Appendix-A

Table A-1. Dynamic stiffnesses and dashpot coefficients for arbitrarily shaped foundations on Surface of Homogenous Half-Space. (Gazetas G. , 1991)

Vibration mode (1)	Static stiffness,K (2)	Dynamic stiffness coefficient,k (3)	Radiation dashpot coefficient,C (4)
$Vertical\ (z)$	$k_z = \left[\frac{2GL}{1-v}\right](0.73 + 1.54x^{0.75})\ with\ x = A_b/4L^2$	$K_z = kz\left(\frac{L}{B}, v, ao\right)\ is\ plotted\ in\ A1(a)$	$C_z = (\rho V_{La} A_b).\overline{c_z}$ where, $\overline{C_z} = \overline{c_z}\left(\frac{L}{b}; a_o\right)$ plotted in A1(c)
$Horizontal\ (y)$ (Lateral direction)	$k_y = \left[\frac{2GL}{2-v}\right](2 + 2.5x^{0.85})$	$K_y = ky\left(\frac{L}{B}, v, ao\right)$ $is\ plotted\ in$ $A1(b)$	$C_y = (\rho V_s A_b).\overline{c_y}$ where $\overline{C_y} = \overline{c_y}\left(\frac{L}{b}; a_o\right)$ is plotted in A1(d)
$Horizontal\ (x)$ (Longitudinal direction)	$k_x = k_y - [0.2/(0.75 - v)]GL[1 - (B/L)]$	$k_x = 1$	$C_x = \rho V_s A_b$
$Rocking\ (rx)(about\ the\ longitudinal\ x, axis)$	$K_{rx} = \left[\frac{G}{1-v}\right] {I_{bx}}^{0.75}\left({L}/{B}\right)^{0.25} * [2.4 + 0.5(B/L)]$	$Krx = 1 - 0.20a_o$	$C_{rx} = (\rho V_{La} \mathrm{I_{bx}}).\overline{c_{rx}}, where$ $\overline{C_{rx}} = \overline{c_{rx}}\left(\frac{L}{b}; a_o\right)$ is plotted in A1(e)
$Rocking\ (ry)(about\ the\ lateral\ y, axis$	$K_{ry} = \left[3G/(1-v) Iby^{0.75}\left(\frac{L}{B}\right)^{0.15}\right]$	$v < 0.40; K_{ry} \cong 1 - 0.26a_o$ $v \cong 0.50; K_{ry} \cong 1 - 0.26a_o\left(\frac{L}{B}\right)^{0.30}$	$C_{ry} = (\rho V_{La} \mathrm{I_{by}}).\overline{c_{ry}}$ $where$ $\overline{C_{ry}} = \overline{c_{ry}}\left(\frac{L}{b}; a_o\right)$ is plotted in A1(f)

$Torsion\ (t)$	$K_t = 3.5GI_{bz}\left(\frac{B}{L}\right)^{0.4}\left({}^{I_{bz}}/_{B^4}\right)^{0.3}$	$K_t = 1 - 0.14a_o$	$Ct = (\rho V_s \mathrm{I_{bz}}).\bar{c_t}\ where\ \bar{C_t} = \bar{c_t}\left(\frac{L}{b}; a_o\right)$ is plotted in A1(g)

Table A-2. Dynamic stiffnesses and dashpot coefficients for arbitrarily shaped foundations Embedded in Half-Space with Arbitrary basemat Shape. (Gazetas G. , 1991)

Vibration mode (1)	Static stiffness,K (2)	Dynamic stiffness coefficient,k (3)	Radiation dashpot coefficient,C (4)
$Vertical\ (z)$	$k_{z,emb} = k_z\left[1 + \left(\frac{1}{21}\right)\left(\frac{D}{B}\right)(1 + 1.3x)\right]*$ $\left[1 + 0.2\left(\frac{Aw}{Ab}\right)^{\frac{2}{3}}\right]\ where$ $k_z \equiv k_{z,surface}\ is\ obtained\ from\ table\ 1.$ $A_w = actual\ sidewall\ soil\ contact\ area; for\ constant\ effective\ contact\ height\ , d, along\ the\ perimeter: A_w = (d) * (perimeter)\ with\ ;$ $x = A_b/4L^2$	$(v \leq 0.40)$: $fully\ embedded:$ $k_{z,emb} \cong k_z\left[1 - 0.09\left(\frac{D}{B}\right)^{\frac{3}{4}} a_o^2\right]$ $in\ a\ trench: k_{z,tre} =$ $k_z\left[1 + 0.09\left(\frac{D}{B}\right)^{\frac{3}{4}} a_o^2\right]$ $(v \approx 0.48)$: $fully\ embedded: with\ \frac{L}{B} = 1 - 2$	$C_{z,emb} \cong c_z + \rho v_s A_w\ where\ c_z = c_{z,surface}$ is obtained from $Table\ 1\ and\ the\ associated\ chart$ of Fig. A1 .

		$k_{z,emb} \cong k_z\left[1-0.09\left(\frac{D}{B}\right)^{\frac{3}{4}} a_o^2\right]$ *fully embedded: with* $\frac{L}{B}>3$ $k_{z,emb} \cong k_z\left[1-0.35\left(\frac{D}{B}\right)^{\frac{1}{2}} a_o^{3.5}\right]$ $k_{z,tre} \cong k_z$, *where* $k_z \equiv k_{z,surf}$ *from Table* 1.	
Horizontal (y) (Lateral direction) *Horizontal* (x) (Longitudinal direction)	$k_{y,emb} = k_y\left[1+0.15\left(\frac{D}{B}\right)^{0.5}\right] * \left\{1+0.52\left[\left(\frac{h}{B}\right)\left(\frac{A_w}{L^2}\right)\right]^{0.4}\right\}$ $k_{x,emb} = k_x.\left(\frac{k_{y,emb}}{k_y}\right)$ *where,* $k_y = k_{y,surface}$ *and* $k_x = k_{x,surface}$ *are obtained from table* 1.	*All* v, *Partially embedded: interpolate* K_y, *emb and* K_x, *emb can be estimated interms of* L/B , D/B , *and* d/B *for each value of* a_o *from the plots in Fig.* $A2$	$C_{y,emb} = c_y + 4\rho V_s Bd + 4\rho V_{La} Ld$ $C_{x,emb} = c_x + 4\rho V_{La} Bd + 4\rho V_s Ld$ Where $c_y \equiv C_{y,surface}$ *and* $c_x \equiv c_{x,surface}$ *are obtained from Table* $A1$ *and the* associated chart of Fig. A1 $C_x = \rho V_s A_b$
Rocking (rx) (*about the longitudinal* x, *axis*)	$K_{rx,emb} = k_{rx}\left\{1+1.26\left(\frac{d}{B}\right) * \left[1+\left(\frac{d}{B}\right)\left(\frac{d}{D}\right)^{-0.2}\left(\frac{B}{L}\right)^{0.5}\right]\right\}$	$K_{rx,emb} \cong K_{rx}$	$C_{rx,emb} = C_{rx} + \rho I_{bx}\left(\frac{d}{B}\right)\left\{V_{La}\left(\frac{d^2}{B^2}\right) +3v_s + v_s * \left(\frac{B}{L}\right)\left[1+\left(\frac{d^2}{B^2}\right)\right]\right\}\eta_{rx}$

Rocking (ry) (about the lateral y, axis) *Swaying − rocking (x − ry)(y − rx)*	$K_{ry,emb} = k_{ry}\left\{1 + 0.92\left(\frac{d}{L}\right)^{0.6} * \left[1.5 + \left(\frac{d}{L}\right)^{1.9}\left(\frac{d}{L}\right)^{-0.6}\right]\right\}$ Where $k_{rx} \equiv k_{rx}, surface$ *and* $k_{ry} \equiv k_{ry,surface}$ are obtained from Table 1 $K_{x-ry} \cong \left(\frac{1}{3}\right) dK_{x,emb}$ $K_{y-rx} \cong \left(\frac{1}{3}\right) dK_{y,emb}$	$K_{ry,emb} \cong K_{ry}$ $K_{x-ry} \cong K_{y-rx} \cong 1$	*where*, $\eta_{rx} = 0.25 + 0.65\sqrt{a_o}\left(\frac{d}{D}\right)^{-\frac{a_o}{2}}\left(\frac{D}{B}\right)^{-\frac{1}{4}}$ $C_{ry,emb}$ *is similarly evaluated from* C_{ry} *after replacing* x *with* y *, and interchanging* B with L foregoing two expressions . in both cases $a_o = \frac{\omega B}{V_s}$. $C_{x-ry,emb} = \left(\frac{1}{3}\right) dC_{x,emb}$ $C_{y-rx,emb} = \left(\frac{1}{3}\right) dC_{y,emb}$
Torsion (t)	$K_{t,emb} = K_t . \Gamma_w . \Gamma_{tre}$ *where* $K_t \cong K_{t,surface}$ *is obtained from Table* 1. $\Gamma_w = 1 + 0.4\left(\frac{D}{d}\right)^{0.5}\left(\frac{j_s}{j_r}\right)\left(\frac{B}{D}\right)^{0.6}$ $\Gamma_{tre} = 1 + 0.5\left(\frac{D}{B}\right)^{0.1}\left(\frac{B^4}{I_{bz}}\right)^{0.13}$ $J_s = \left(\frac{4}{3}\right) d(B^3 + L^3) + 4BLd(L + B)$ $j_r = \left(\frac{4}{3}\right) BL(B^2 + L^2)$	$K_{t,emb} = K_{t,surface}$	$C_{t,emb} = C_t + 4\rho d\left[\left(\frac{1}{3}\right) V_{la}(L^3 + B^3) + V_s BL(L + B)\right]\eta_t$ *where* $C_t \equiv C_{t,surface}$ *is obtained from Table A*1 *and* Fig. A1. $\eta_t = \left(\frac{d}{D}\right)^{-0.5} . a_o^2 / \left[a_o^2 + \left(\frac{1}{2}\right)\left(\frac{L}{B}\right)^{-1.5}\right]$

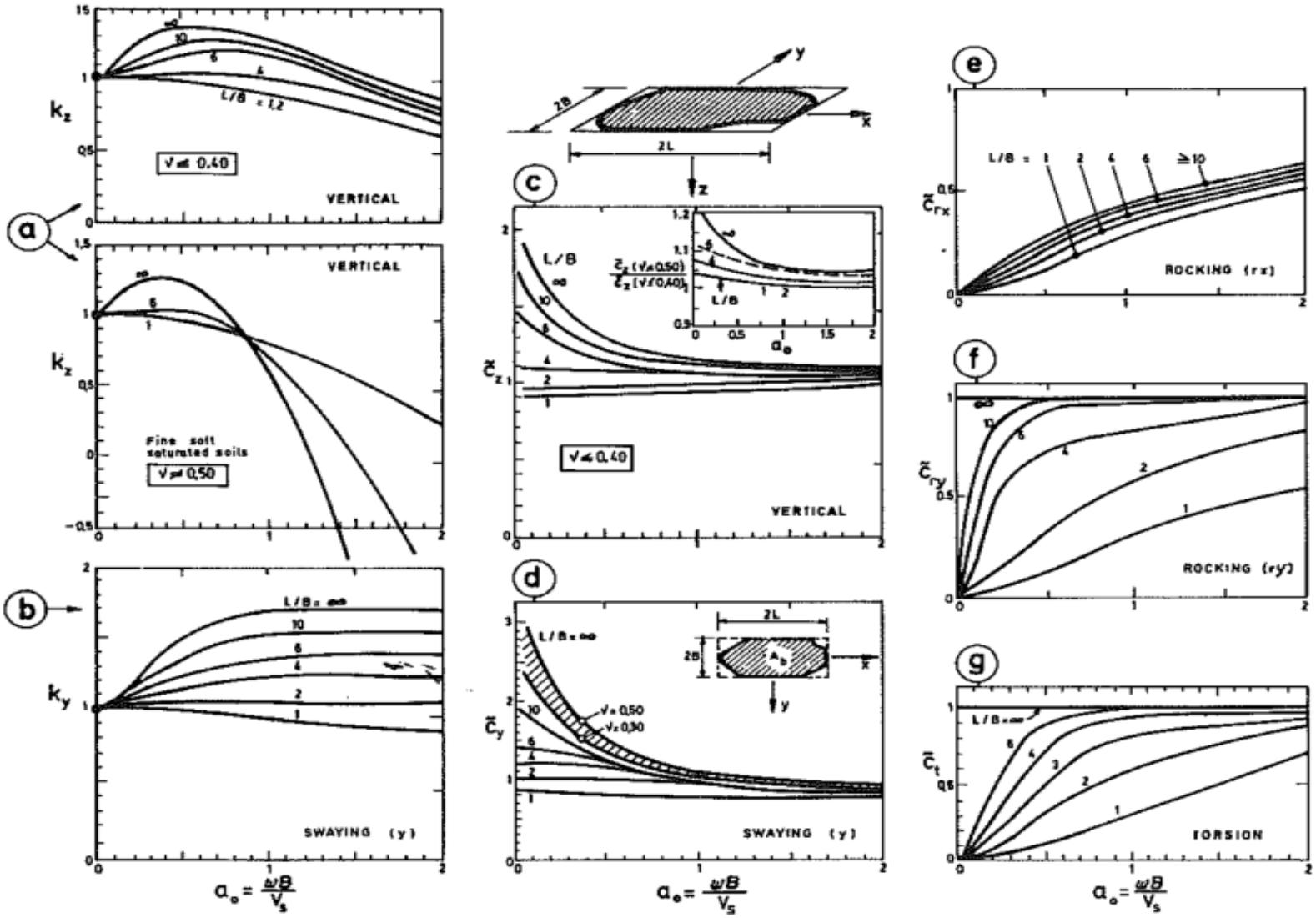

Figure A-1 Dimensionless graphs for determining dynamic stiffness and damping coefficients of surface foundations (Gazetas G. , 1991)

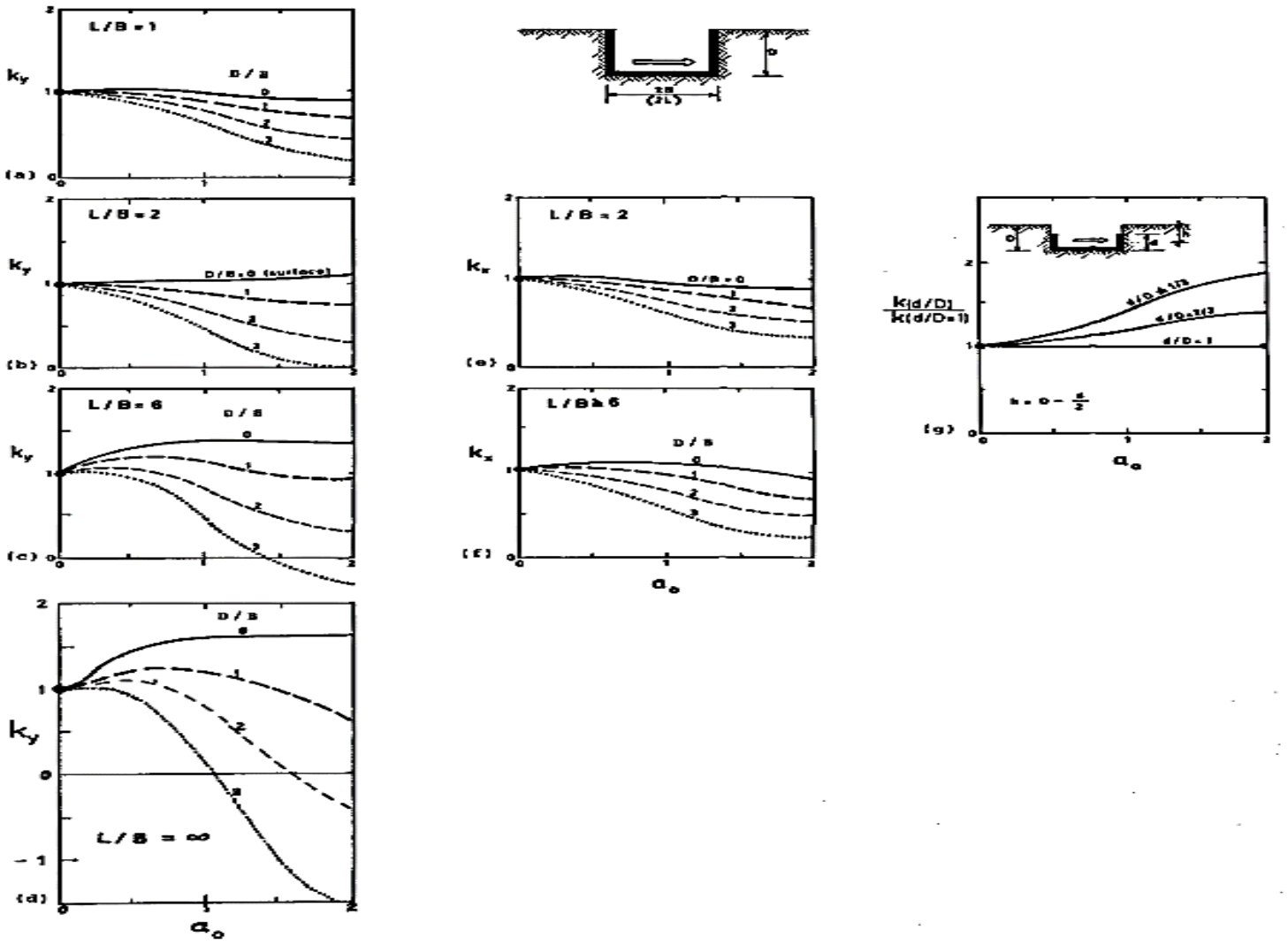

Fig A2 Dimensionless Graphs for Determining Dynamic Stiffness Coefficients of Fully and Partially Embedded Foundations (Gazetas G. , 1991)

Appendix-B

Parametric results for Firm clay and dense gravel

Soil type clay

Undamped natural frequency

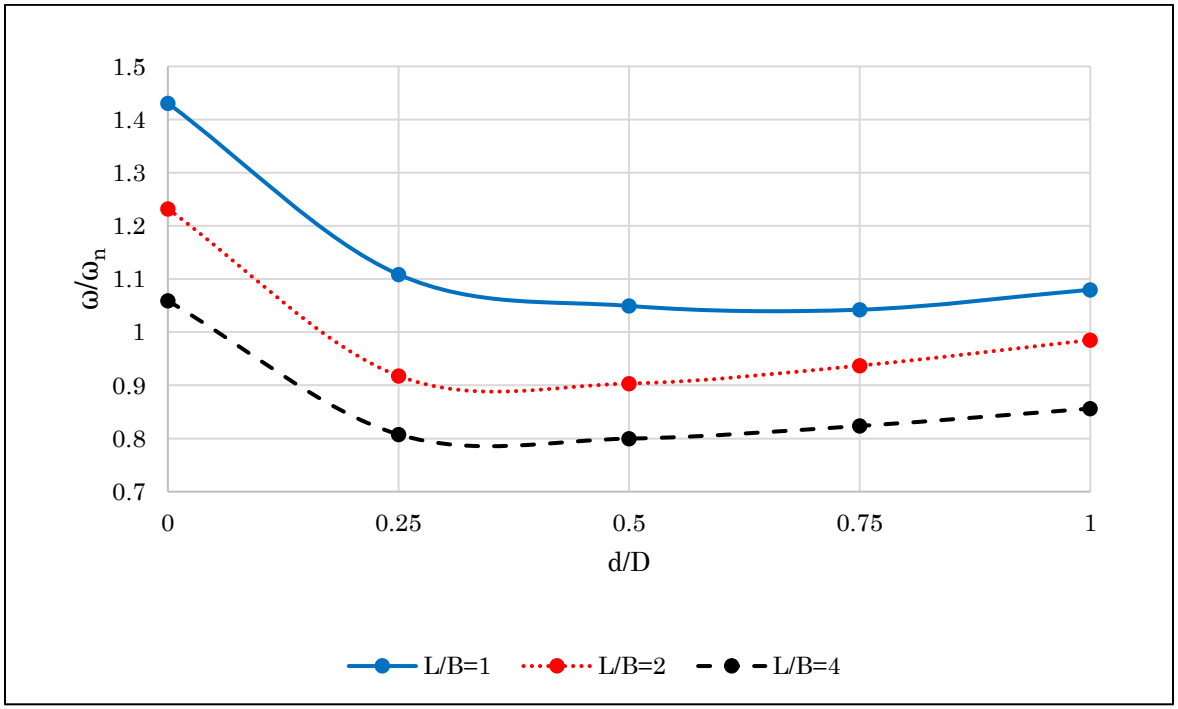

Figure B1 - effect of aspect ratio and embedment ratio on frequency ratio utilizing undamped natural frequency for Clay

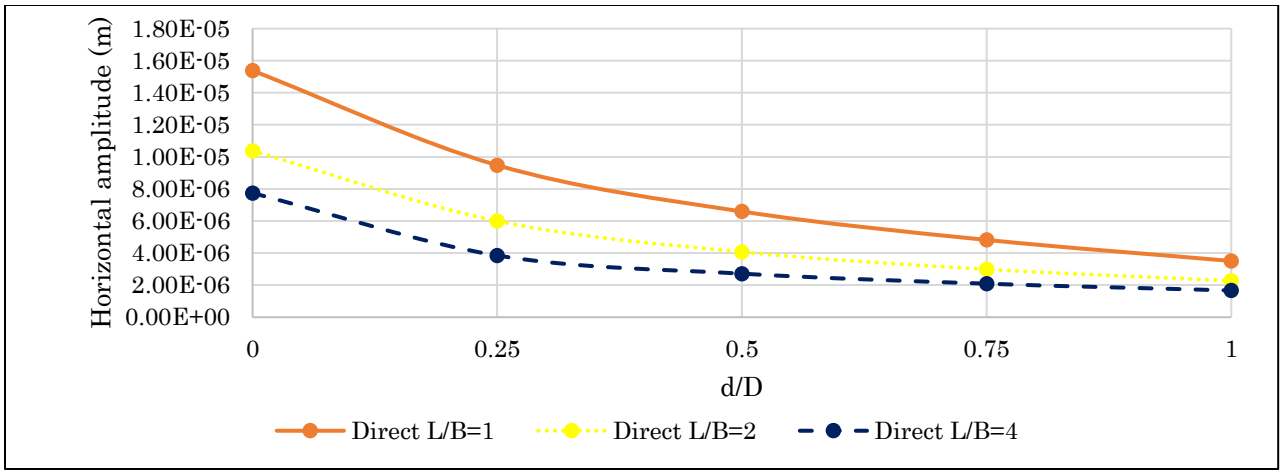

(a)

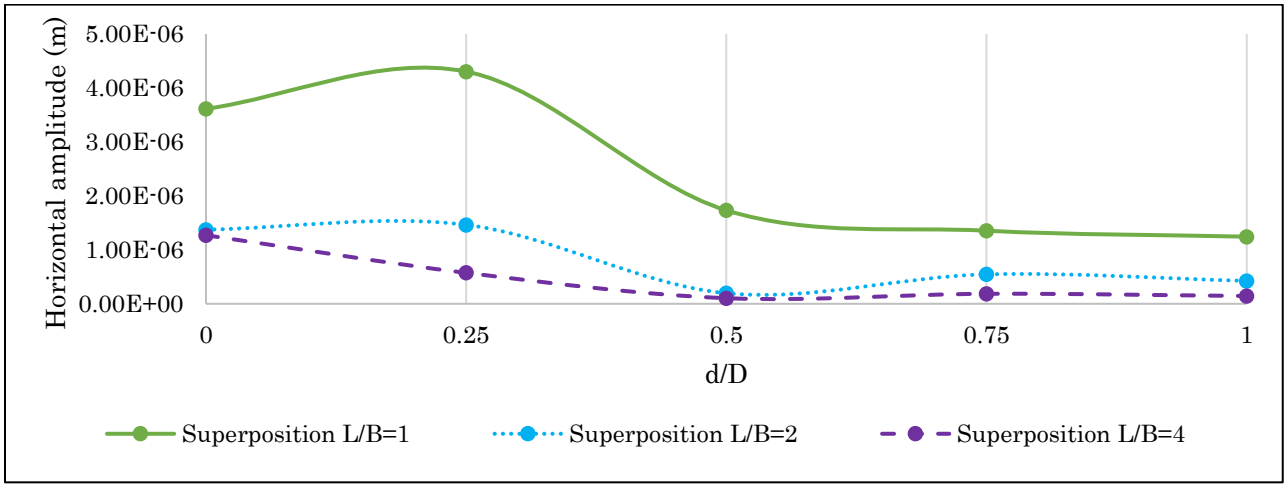

(b)

Figure B2 - effect of aspect ratio and embedment ratio on horizontal amplitude utilizing undamped natural frequency and (a) Direct method (b) Superposition approach method for Clay

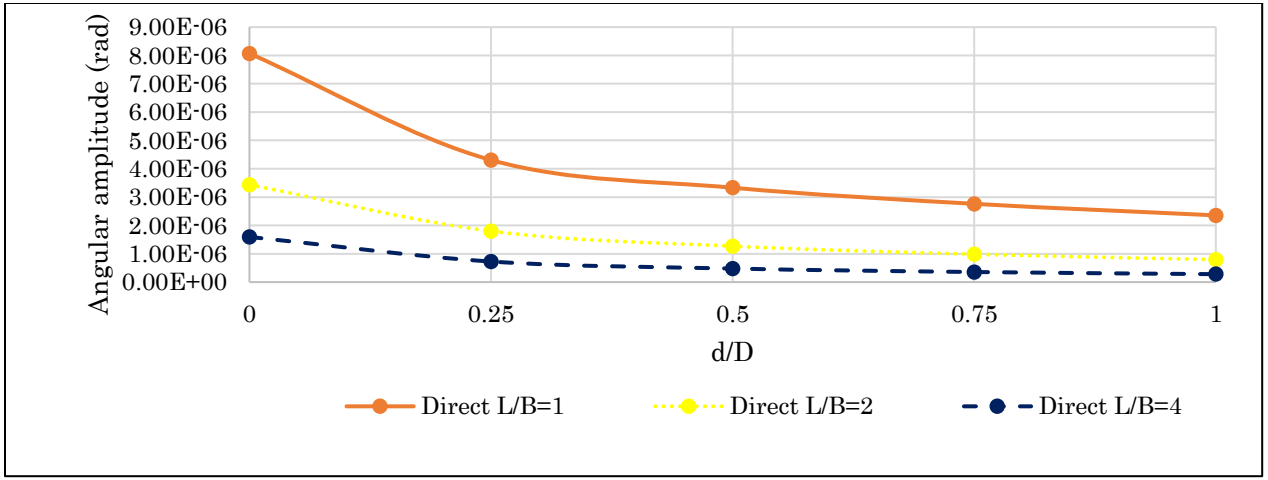

(a)

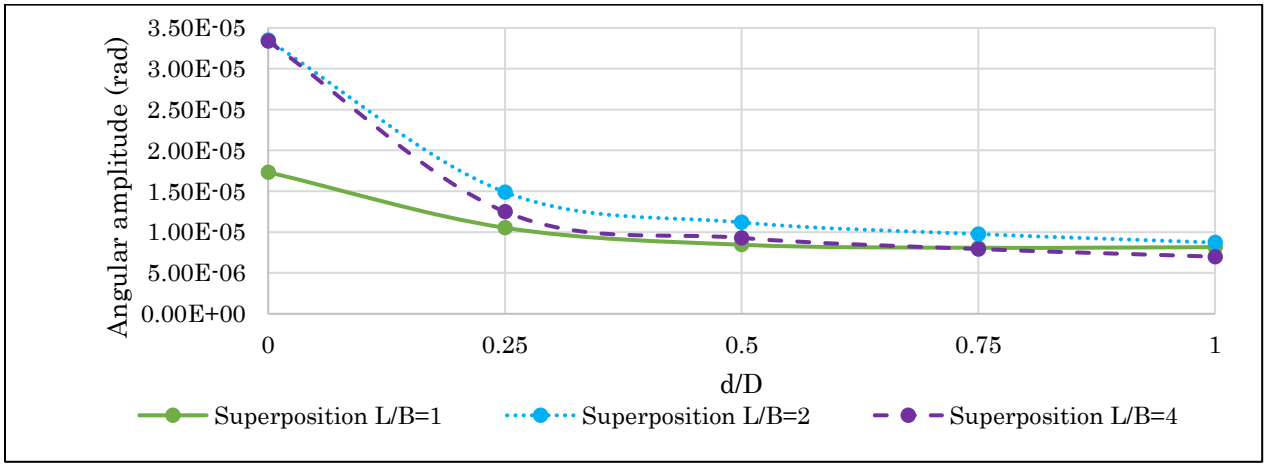

(b)

Figure B3 - effect of aspect ratio and embedment ratio on Angular amplitude utilizing undamped natural frequency and (a) Direct method (b) Superposition approach method for Clay

Damped natural frequency

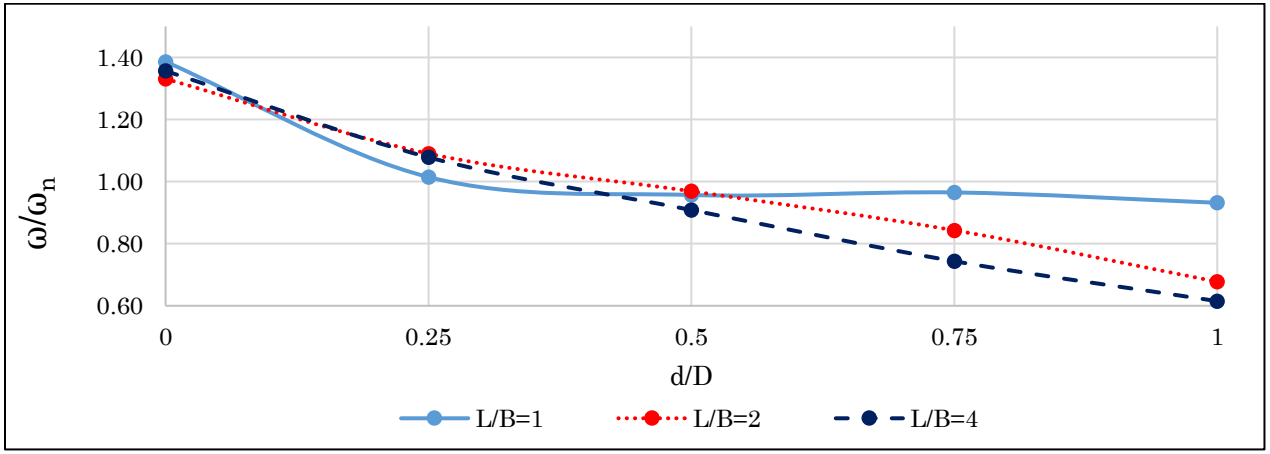

Figure B4 - effect of aspect ratio and embedment ratio on frequency ratio utilizing damped natural frequency for Clay

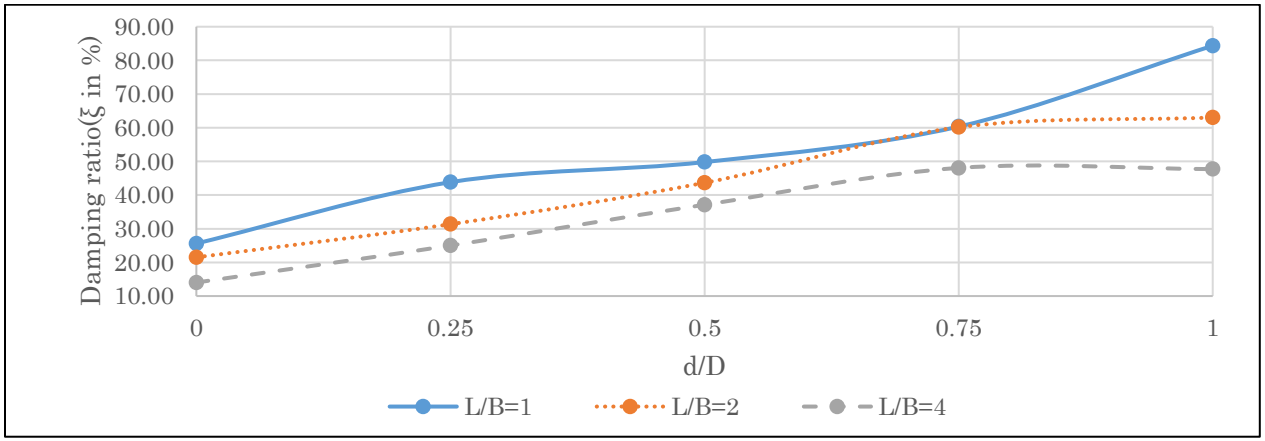

Figure B5 - effect of aspect ratio and embedment ratio on damping ratio utilizing damped natural frequency for Clay

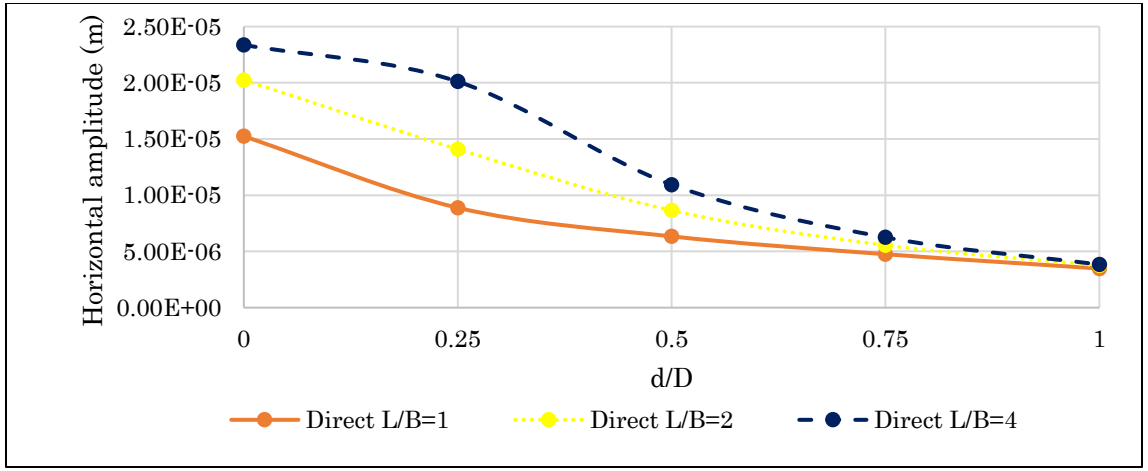

(a)

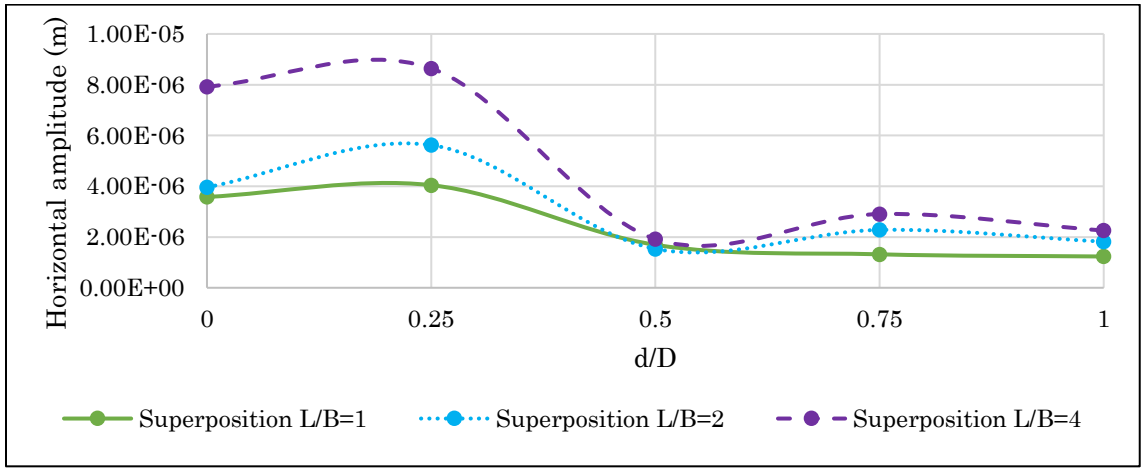

(b)

Figure B6 - effect of aspect ratio and embedment ratio on horizontal amplitude utilizing damped natural frequency and (a) Direct method (b) Superposition approach method for Clay

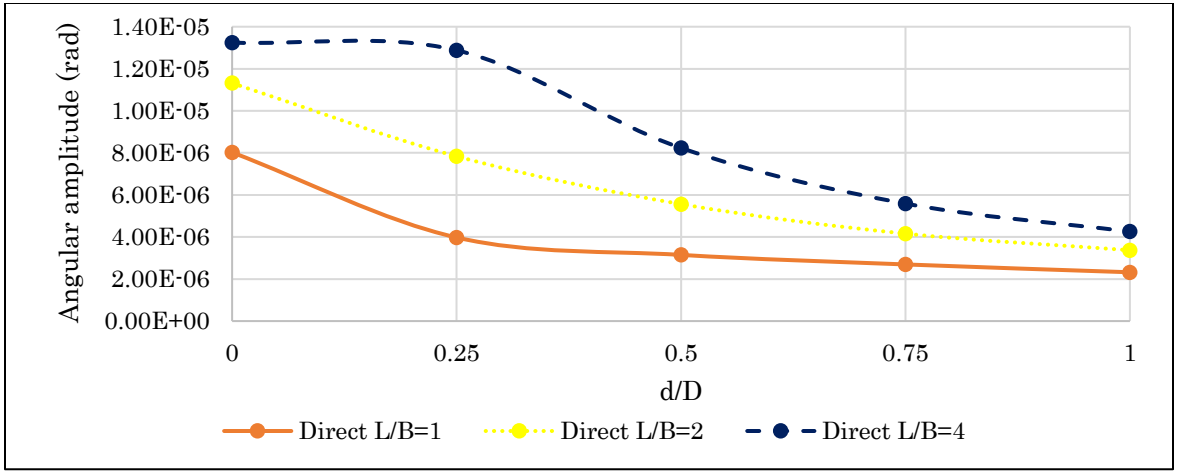

(a)

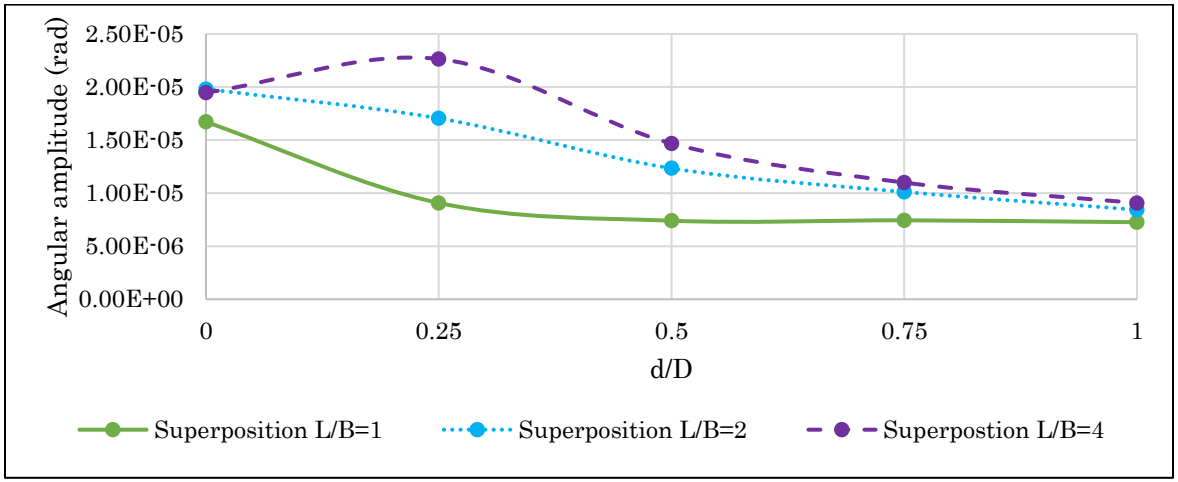

(b)

Figure B7 - effect of aspect ratio and embedment ratio on Angular amplitude utilizing damped natural frequency and (a) Direct method (b) Superposition approach method for Clay

Soil type Gravel

Undamped natural frequency

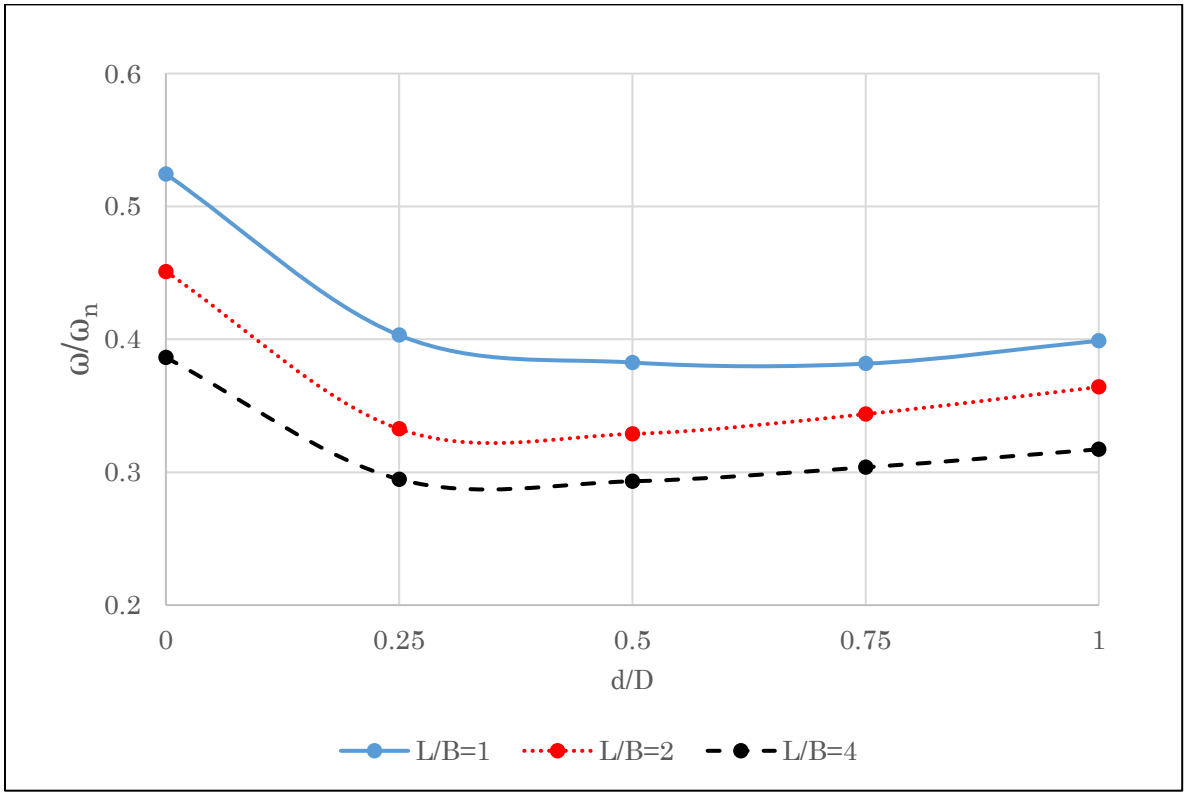

Figure B8 - effect of aspect ratio and embedment ratio on frequency ratio utilizing undamped natural frequency for Gravel

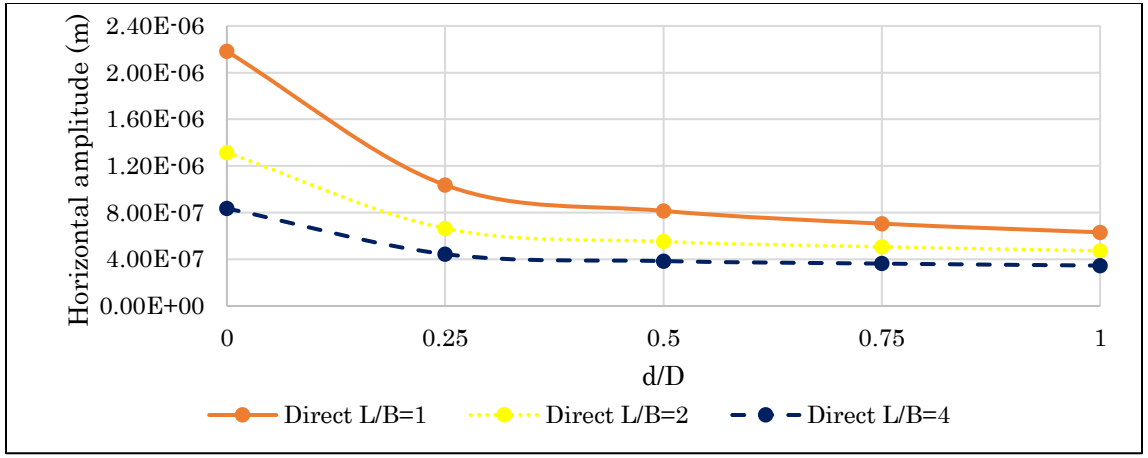

(a)

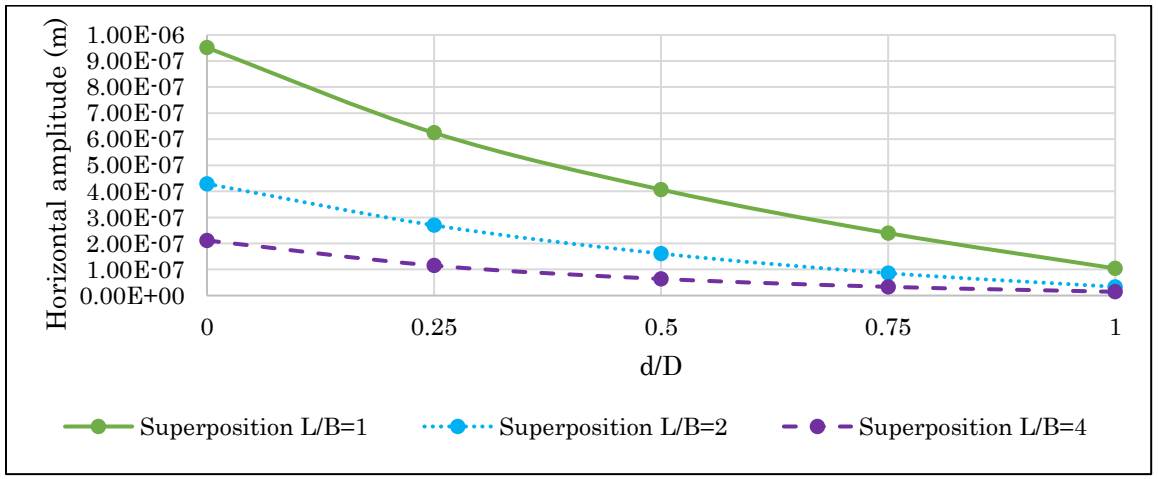

(b)

Figure B9 - effect of aspect ratio and embedment ratio on horizontal amplitude utilizing undamped natural frequency and (a) Direct method (b) Superposition approach method for Gravel

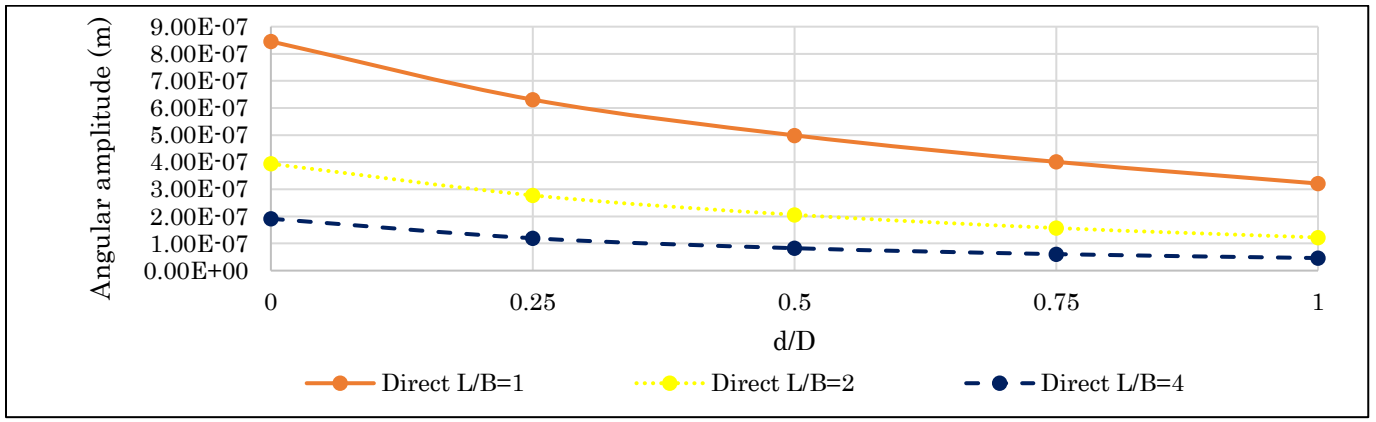

(a)

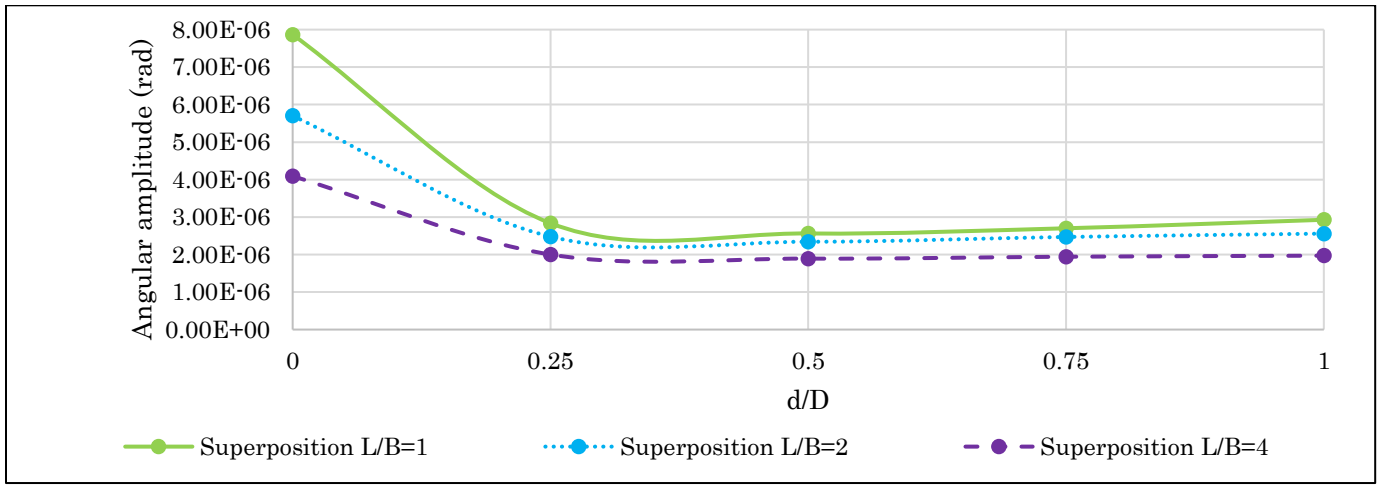

(b)

Figure B10 - effect of aspect ratio and embedment ratio on Angular amplitude utilizing undamped natural frequency and (a) Direct method (b) Superposition approach method for Gravel

Damped natural frequency

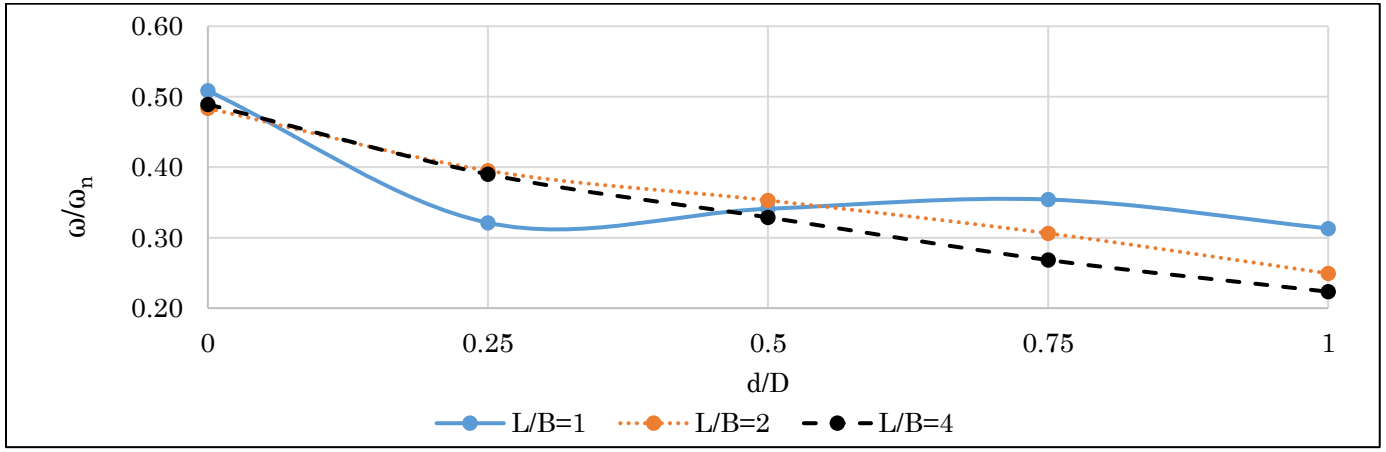

Figure B11 - effect of aspect ratio and embedment ratio on frequency ratio utilizing damped natural frequency for Gravel

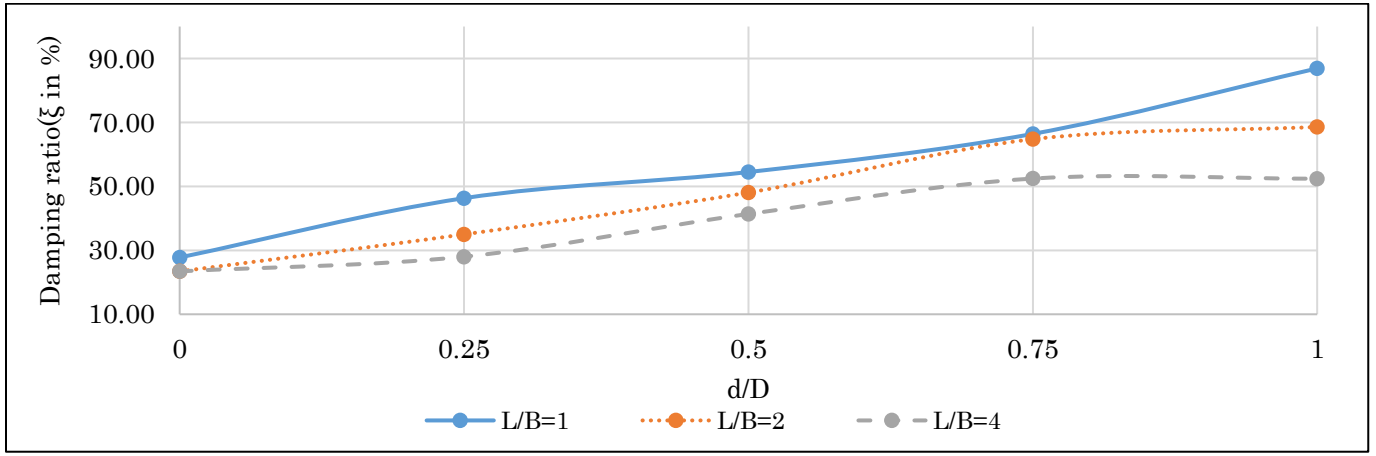

Figure B12 - effect of aspect ratio and embedment ratio on damping ratio utilizing damped natural frequency for Gravel

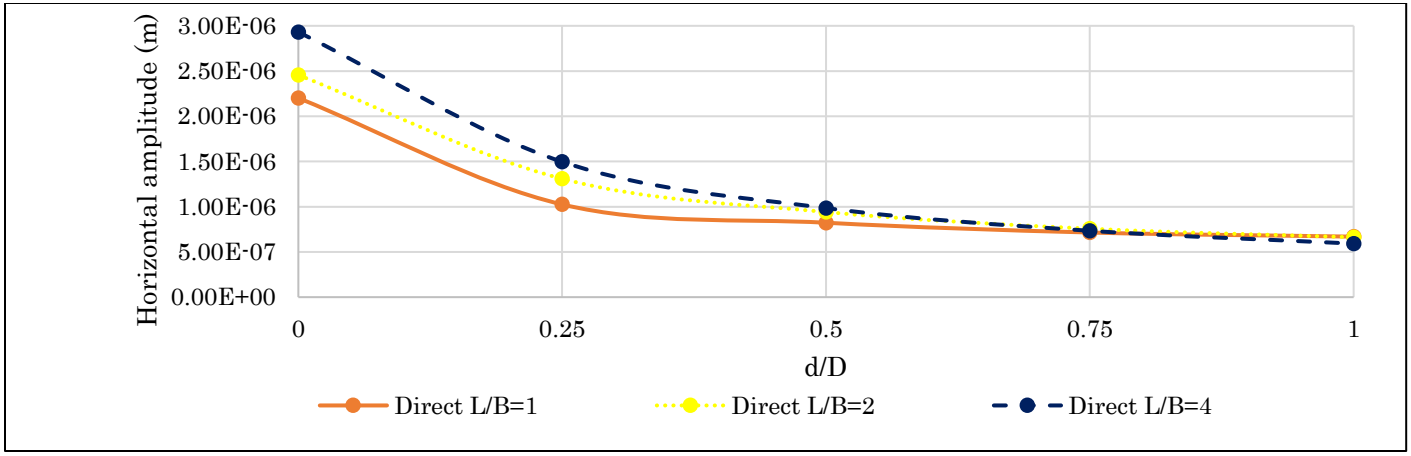

(a)

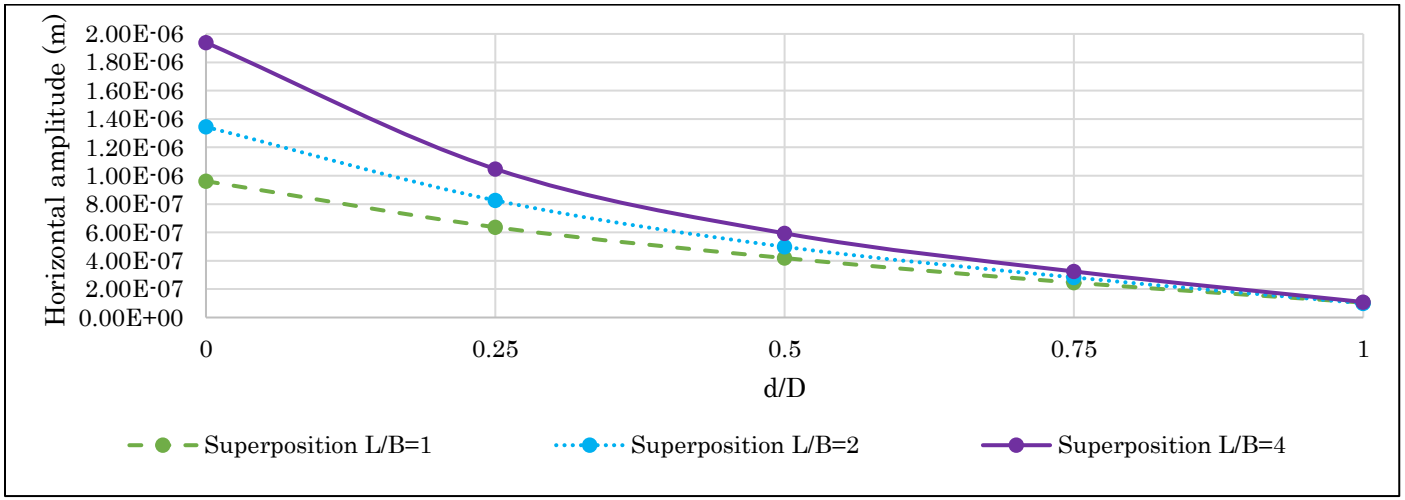

(b)

Figure B13 - effect of aspect ratio and embedment ratio on horizontal amplitude utilizing damped natural frequency and (a) Direct method (b) Superposition approach method for Gravel

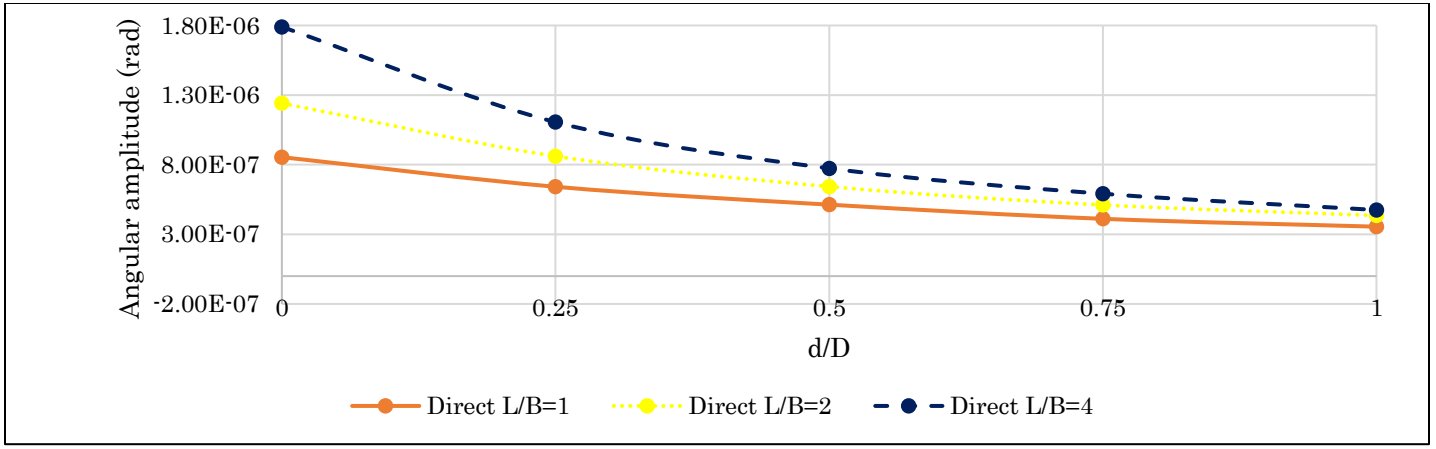

(a)

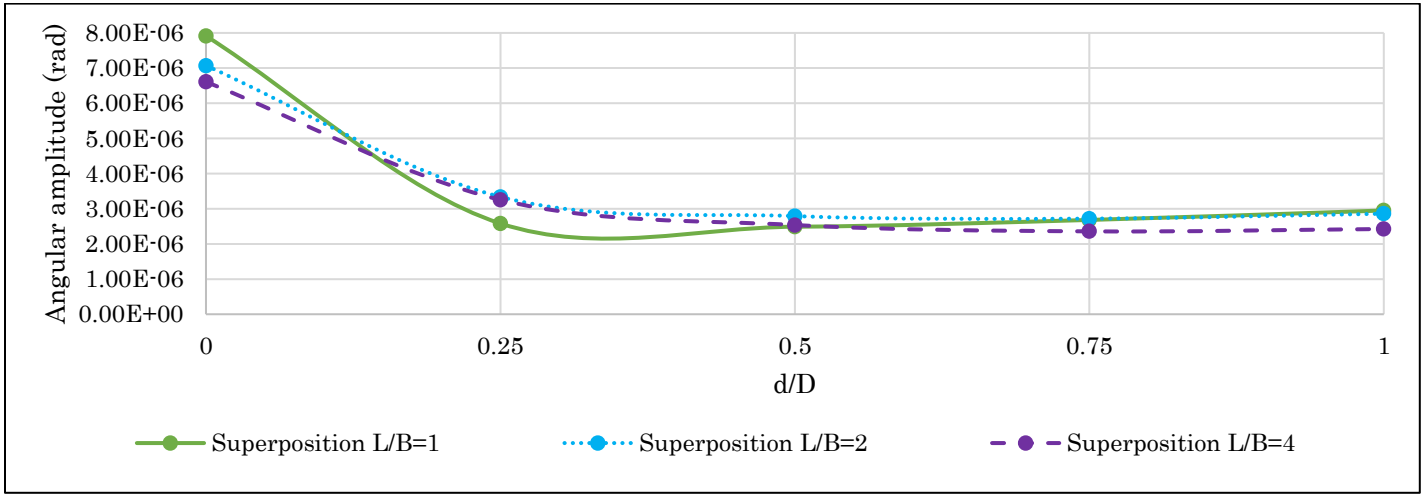

(b)

Figure B14 - effect of aspect ratio and embedment ratio on Angular amplitude utilizing damped natural frequency and (a) Direct method (b) Superposition approach method for Gravel